NASA CR-166,104

NASA CONTRACTOR REPORT 166104

APPLICATION OF ACTIVE CONTROL TECHNOLOGY TO THE A-10 AIRCRAFT

IRVING ROSS and RALPH EDSON

Contract NAS1-17068
June 1983

National Aeronautics and
Space Administration

Langley Research Center
Hampton, Virginia 23665

TABLE OF CONTENTS

Paragraph No.	Title	Page No.
1.0	SUMMARY	1
2.0	INTRODUCTION	3
3.0	SYMBOLS	5
4.0	DYNAMIC ANALYSIS OF ALTERNATE ACTIVE CONTROL LANDING GEAR	15
4.1	Introduction	15
4.2	Discussion of Concept	15
4.3	Dynamic Simulation Math Model	19
4.4	Transient Response Results	29
4.4.1	Landing Impact	30
4.4.2	Runway Disturbances	38
4.5	Failure Detection Scheme	46
4.6	Reliability Assessment	49
5.0	DYNAMIC ANALYSIS OF ACTIVE CONTROL LANDING GEAR	55
5.1	Introduction	55
5.2	Concept Description	56
5.3	Dynamic Simulation Math Models	56
5.3.1	Nonlinear Model	56
5.3.2	Linear Model	70
5.4	Correlation of Linear and Nonlinear Models	75
5.5	Loop Compensation	80
5.6	Transient Response Results	89
5.6.1	Landing Impacts	89
5.6.2	Runway Disturbances	98
5.7	Failure Detection and Redundancy Management	109

TABLE OF CONTENTS

Paragraph No.	Title	Page No.
6.0	APPLICATION PROGRAM.....	113
6.1	Statement of Work.....	113
6.1.1	System Sizing and Analysis.....	113
6.1.1.1	Control Laws.....	113
6.1.1.2	Nonlinear Analysis.....	113
6.1.1.3	Simulated Drop Tests.....	115
6.1.1.4	Simulated Landings and Takeoffs.....	115
6.1.2	System Analysis.....	115
6.1.2.1	ACLG Logic Analysis.....	115
6.1.2.2	Redundancy Management Analysis.....	115
6.1.2.3	A-10 Aircraft Taxi Analysis.....	116
6.1.3	Three Stage Servovalve Design and Development.....	116
6.1.3.1	Servovalve Detailed Sizing Analysis.....	116
6.1.3.2	Three Stage Servovalve Design and Development.....	116
6.1.4	Nose and Main ACLG Design and Fabrication.....	117
6.1.5	Electronic Controller Design and Development.....	117
6.1.6	ACLG Drop Tests.....	121
6.1.7	ACLG Shaker Test.....	119
6.1.8	Simulated Taxi Tests.....	119
6.1.9	A-10 Aircraft Taxi Tests.....	119
6.2	Schedule.....	119
7.0	CONCLUSIONS.....	121
8.0	REFERENCES.....	122

LIST OF FIGURES

Figure No.	Title	Page No.
4-1	Load-Stroke Curves.....	18
4-2	Schematic of Active Control Landing Gear Alternate Concept.....	21
4-3	Loop Closure Schematic with Servovalve Dynamics, Alternate Concept.....	26
4-4	Schematic of Servovalve Second Stage Valve and Power Valve, Alternate Concept.....	28
4-5	Impact Landing, Modified Gear, Passive Case (Alternate Concept).....	31
4-6	Impact Landing, Modified Gear, Passive Case (Alternate Concept).....	32
4-7	Impact Landing, Modified Gear, Passive Case (Alternate Concept).....	33
4-8	Impact Landing, Modified Gear, Active Case (Alternate Concept).....	34
4-9	Impact Landing, Gear, Active Case (Alternate Concept).....	35
4-10	Impact Landing, Modified Gear, Active.....	36
4-11	Impact Landing, Modified Gear, Active Case (Alternate Concept).....	37
4-12	Runway Disturbance, Modified Gear, Passive Case.....	39
4-13	Runway Disturbance, Modified Gear, Passive Case.....	40
4-14	Runway Disturbance, Modified Gear, Active Case (Alternate Concept).....	41
4-15	Runway Disturbance, Modified Gear, Active Case (Alternate Concept).....	42

LIST OF FIGURES

Figure No.	Title	Page No.
4-16	Runway Disturbance, Modified Gear, Active Case (Alternate Concept).....	43
4-17	Runway Disturbance, Modified Gear, Active Case (Alternate Concept).....	44
4-18	Runway Disturbance, Modified Gear, Active Case (Alternate Concept).....	45
4-19	Alternate Controller.....	47
4-20	System Schematic.....	51
4-21	Reliability Block Diagram.....	54
5-1	Schematic of Active Control Landing Gear System.....	59
5-2	Forces Acting on the Airplane Mass.....	60
5-3	Inner Loop Schematic.....	64
5-4	Power Valve.....	66
5-5	Outer Loop Closure and Compensation Schematic.....	67
5-6	Linear Model Block Diagram.....	74
5-7	Open Loop Frequency Response, No Compensation.....	76
5-8	Open Loop Frequency Response, No Compensation.....	77
5-9	Open Loop Nyquist Diagram From Nonlinear Model.....	78
5-10	Open Loop Nyquist Diagram From Linear Model.....	79
5-11	Frequency Response of Compensation (Amplitude).....	81

LIST OF FIGURES

Figure No.	Title	Page No.
5-12	Frequency Response of Compensation (Phase)	82
5-13	Nyquist Plot of Compensation	83
5-14	System Nyquist Plot (Notch Only)	84
5-15	System Nyquist Plot (Notch and Lead/Lag)	85
5-16	Impact Landing, Active Gear (Notch Only)	87
5-17	Impact Landing, Active Gear (Notch and Lead/Lag)	88
5-18	Impact Landing, Passive Gear	90
5-19	Impact Landing, Passive Gear	91
5-20	Impact Landing, Passive Gear	92
5-21	Impact Landing, Active Gear	93
5-22	Impact Landing, Active Gear	94
5-23	Impact Landing, Active Gear	95
5-24	Impact Landing, Active Gear	96
5-25	Impact Landing, Active Gear	97
5-26	Runway Disturbance	100
5-27	Runway Disturbance, Passive Gear	101
5-28	Runway Disturbance, Passive Gear	102
5-29	Runway Disturbance, Passive Gear	103
5-30	Runway Disturbance, Active Gear	104
5-31	Runway Disturbance, Active Gear	105
5-32	Runway Disturbance, Active Gear, Active Case	106
5-33	Runway Disturbance, Active Gear	107
5-34	Runway Disturbance, Active Gear	108
5-35	Controller Original Concept	110
6-1	Program Plan	114

LIST OF FIGURES

Figure No.	Title	Page No.
6-2	Landing Gear Alternate Concept.....	118
6-3	Program Schedule.....	120

LIST OF TABLES

Table No.	Title	Page No.
4-1	Reliability Trade Study.....	52
4-2	Component Failure Rates.....	53

1.0 SUMMARY

This report describes two concepts which reduce the A-10 aircraft's wing/gear interface forces as a result of applying active control technology to the main landing gear.

In the first concept, referred to as the "alternate concept" a servovalve in a closed pressure control loop configuration effectively varies the size of the third stage spool valve orifice which is embedded in the strut. This action allows the internal energy in the strut to shunt hydraulic flow around the metering orifice. The command signal to the loop is reference strut pressure which is compared to the measured strut pressure, the difference being the loop error. Thus, the loop effectively varies the spool valve orifice size to maintain the strut pressure, and therefore minimizes the wing/gear interface force referenced.

The second concept is referred to as the "original concept," and the electronic controller for this concept was developed under NASA contracts NAS1-14459 and NAS1-16420 and the concept is described in detail in References 1, 2, and 3. As in the previous designs, the controller continuously compares the kinetic energy with the work potential of the gear until the work potential exceeds the kinetic energy. The wing/gear interface force present at this condition becomes the command force to a servo loop which maintains the wing/gear interface force at this level by providing a signal to an electrohydraulic servovalve to port flow into or out of the landing gear.

Analytical results indicate that the original concept reduces the wing/gear interface force by 32% on landing impact and by 43% on rollout over a Class I repaired bomb crater while the alternate concept reduces the wing/gear interface force by 12% on landing impact and by 36% on rollout over a similar irregularity.

Failure detection and redundancy management means were developed for both the alternate and original concepts in order to insure that upon the occurrence of a failure, reversion to a passive configuration will take place.

A reliability analysis was performed for the alternate configuration and the results indicate that the reliability of the active gear is almost the same as that for the unmodified passive gear.

A program plan, statement of work, and schedule are also presented for application of the alternate concept active landing gear system to the A-10 aircraft. The implementation can be accomplished in 24 months.

2.0 INTRODUCTION

HR Textron Inc. (HR) was retained under NASA contract NAS 1-17068 to apply active control technology to the to the main landing gear on the A-10 aircraft.

The purpose of this study was to determine to what extent the application of active control technology to the A-10 main landing gear would reduce the loads transmitted to the airframe, relative to those occuring with the original passive gear system, during landing impact and rollout over simulated hastily repaired bomb-damage craters.

The active control landing gear concepts which have exhibited significant reductions in loads transmitted to the airframe are presented in this report. The concepts are as follows:

The first concept is referred to as the "alternate concept." In the alternate concept a three stage servovalve is placed in parallel with the metering orificies, and a pressure control loop is tied around the servovalve. The internal energy in the landing gear strut is used to propel the hydraulic fluid through the third stage spool valve. The command signal to the loop is referenced strut pressure which is compared to the measured strut pressure, the difference being loop error. Thus the loop effectively varies the third stage spool valve orifice size to maintain the strut limit pressure which in turn minimizes the wing/gear interface force. The alternate concept can be implemented to enhance landing gear performance with no impact on the aircraft's aerodynamic and mission performance, and a

very minimal impact on the aircraft's reliability and maintainability.

The second concept is referred to as the "original concept." The electronic controller for this concept was developed under NASA Contract NAS1-14459 and modified under NASA Contract NAS1-16420 and a detailed description of the concept and controller is contained in References 1, 2, and 3. In the original concept for the impact phase of the landing the controller continuously compares the kinetic energy of the aircraft with the work potential of the landing gear strut until the work potential exceeds the kinetic energy. The wing/gear interface force present at this condition becomes the command force to the servoloop which maintains the wing/gear interface force at this level by providing a signal to the servovalve to port flow into or out of the landing gear. Subsequent to the impact phase, the controller linearly transitions the command force to zero for the rollout phase. During rollout the controller maintains the command force within design tolerances about zero.

For both concepts defined above, the control laws and system gains were determined for stable and reliable operation of the A-10 aircaft main landing gear. Nonlinear dynamic analyses were conducted to simulate landing impact and rollout over a repaired runway.

Also included in this report is a program plan, statement of work, and schedule for implementing the alternate concept active control landing gears on the A-10 aircraft.

3.0 SYMBOLS

AH — area of hole in shock strut plate, .001665 m^2(2.580 in^2)

AMV — effective area of ends of metering valve (alternate concept), .000381 m^2(.591 in^2)

AO — area of orifice in shock strut orifice plate, = AH - AP

AO23 — rebound orifice area, .0000516 m^2(.080 in^2) for strut extending, .0001897 in^2(.294 in^2) for strut retracting

AP — landing gear metering pin area in plane of shock strut plate, m^2(in^2)

APV — effective area of power valve, .0006452 m^2(1.107 in^2)

A1 — shock strut hydraulic area (piston area), .01142 m^2 (17.71 in^2)

A2 — shock strut pneumatic area (cylinder area), .00713 m^2 (11.05 in^2)

A3 — annular area in shock strut between piston and cylinder walls, .00228 m^2 (3.53 in^2)

ATIRE — constant in tire deflection force equation, 1.0

BMV — viscous damping coefficient on metering valve (alternate concept), 0. N-sec/m (0. lbf-sec/in)

CD discharge coefficient for spool/sleeve valve orifices, 0.611

CDO discharge coefficient for shock strut metering orifice, 0.65

CDO23 discharge coefficient for rebound orifice, .70 for strut extending, .75 for strut retracting

CO orifice coefficient for shock strut orifice

$= CDO \cdot AO \sqrt{2g_c/\rho}$, $m^4 sec^{-1} N^{1/2} (in^3/sec/psi^{1/2})$

CO23 Orifice coefficient for rebound orifice

$= CDO23 \cdot AO23 \sqrt{2g_c/\rho}$, $m^4 sec^{-1} N^{1/2} (in^3/sec/psi^{1/2})$

CPPV Linearized orifice coefficient for power valve

$= -\frac{\partial QPV}{\partial P_1}$ $3.16 \times 10^{-11} m^5 . N^{-1} . sec^{-1}$ $(0.01334\ in^3/sec/psi)$

CPO linearized orifice coefficient for shock strut orifice

$= \frac{\partial Qo}{\partial (P1-P2)} = CO/(2\sqrt{P_1-P_2})$, $2.139 \times 10^{-9} m^5 . N^{-1} . sec^{-1}$ $(0.9\ in^3/sec/psi)$

CQPV linearized orifice coefficient for power valve

$= \frac{\partial QPV}{\partial XPV} = CPV\sqrt{(P_S-P_R)/2}$, $8.61 m^2/sec$ $(13{,}340\ in^3/sec/in)$

CQSV linearized orifice coefficient for servovalve second stage

$= \frac{\partial QSV}{\partial XSV} = CSV \sqrt{(PS-PR)/2}$, .538 m^2/sec(833.5 in^3/sec/in)

CPV orifice coefficient for power valve

$= CD \cdot WPV \sqrt{2g_c/\rho}$, $m^3 sec^{-1} N^{-1/2} (in^3/sec/lbf^{1/2})$

CSV orifice coefficient for servovalve second stage

$= CD \cdot WSV \sqrt{2g_c/\rho}$, $m^3 \cdot sec^{-1} \cdot N^{-1/2}$ $(in^3/(in\ lbf^{1/2}))$

DSV servovalve second stage spool diameter, .00508 m(.200 in), (.00476m(.1875 in), alternate concept

f coulomb friction between shock strut piston and cylinder, 222.N (50.lbf)

FA vertical force exerted on shock strut by the runway surface, N (lbf)

FACC Force as measured by upper mass accelerometer =

$M \frac{d^2 XWG}{dt^2}$, N(lbf)

FL lift force per gear, N(lbf)

FLIM limit force, N (lbf)

f_{mv} coulomb friction on metering valve (alternate concept), 44.5 N(10.lbf)

FOMV spring preload on metering valve, for XMV = 0 (alternate concept), 89.0 N(20.blf)

FWG wing-gear interface force, N (lbf)

g acceleration due to gravity, 9.81m/sec^2(386.in/sec^2)

g_c gravitational acceleration constant

1 kg m N^{-1} sec^{-2}(12 slug in lbf^{-1} sec^{-2})

i_1 input signal to electronic compensation networks, A

i_2 output signal from electronic compensation networks, or input signal to active control servovalve, (±0.050 A maximum)

KA amplifier gain in active control loop, 0.0216 A/V, (0.0104 A/V, alternate concept)

KF position feedback gain in strut position control loop, 563 V/m (14.29V/in)

KFB servo loop postion feedback gain, 1141. V/m(28.98 v/in), (281. v/m (7.14 v/in), alternate concept)

K_{FDGE} fraction of total strut stroke assumed available when computing impact phase force, 1.0

KFWD forward path gain, .000725 v/v (.0100 v/v, alternate concept)

KMV spring rate on metering valve, alternate concept, 3500.N/m(20.0 lbf/in)

KP1 pressure transducer gain, alternate concept, .0001450 v/n/m^2(1.00v/psi)

KSV position gain of two-stage servovalve in active control loop, .0254 m/A (1.00 in/A), (.0254 m/A(1.00/A), alternate concept)

KT linearized tire force constant, 1277. kN/m(7290.lbf/in)

KTIRE constant in tire deflection force equation 1277.1 kN/m (7290 lbf/in)

KX gain in strut position control loop, 1.0 m/m (1.0 in/in)

M mass of airplane per gear, 7827. kg (44.7 lbf-sec^2/in)

MC mass of upper portion of landing gear (cylinder plus orifice plate attachment, 0. kg (0. slugs)

ML mass of lower portion of landing gear (piston plus tire), 152. kg (10.42 slugs = .868 lbf . sec^2/in = 335. lbm)

MMV mass of metering valve, alternate concept, .1751 kg (.001 lbf-sec^2/in)

MU = $M + M_c$, total upper mass per gear, 7827. kg (536. slugs = 44.7 lbf. sec^2/in = 17254. lbm)

PLIM command limit pressure, alternate concept, N/m^2(psi)

PS hydraulic supply pressure, 2.07×10^7 N/m^2 (3000 . psi), (6.90×10^6 N/m^2(1000.psi), alternate concept)

PR hydraulic return pressure, 0.0 N/m^2 (0.0 psi)

P1 hydraulic pressure in shock strut piston, N/m^2 (psi)

P1DED pressure transducer hysteresis, alternate concept, 3.45×10^5 N/m^2(50.psi)

P1M output signal from pressure transducer, alternate concept, N/m^2(psi)

P2 gas pressure in shock strut cylinder, N/m^2 (psi)

$P2_i$ gas pressure at charging condition, 2.65×10^6 N/m^2(384.psi), (4.83×10^6 N/m^2 (700. psi), alternate concept)

P3 pressure in volume betweeen walls of shock strut piston and cylinder, N/m^2 (psi)

QMV flow through metering valve, alternate concept, m^3/sec (cis)

QO flow rate through shock strut orifice from piston to cylinder, m^3/sec (in^3/sec)

QPV flow rate from power valve to shock strut cylinder, m^3/sec (in^3/sec)

Q1 flow rate through power valve from supply pressure to the shock strut piston, m^3/sec (in^3/sec)

Q3 flow rate through power valve from shock strut piston to return pressure, m^3/sec (in^3/sec)

R_s	the slope of the limit force with respect to time during transition phase, 444800. N/sec (100000. lbf/sec)
S	LaPlace operator, sec^{-1}
t	time, sec
V	velocity, m/sec (in/sec)
VBIAS	voltage bias, -6.48 V (-1.00 V, alternate concept)
V_s	sink rate, m/sec (in/sec)
V_{tr}	transition velocity, m/sec (in/sec)
V1	hydraulic volume in shock strut upper cylinder and lines up to the power valve $m^3(in^3)$
$V1_i$	total volume of oil in shock strut upper cylinder for fully extended gear, .00455 m^3 (278. in^3)
V2g	gas volume, $m^3(in^3)$
$V2g_i$	gas volume at charging condition, .00391 m^3 (238.5 in^3), (.00590 m^3 (360. in^3), alternate concept)
$V2_i$	total volume in shock strut lower cylinder that oil plus gas can occupy for fully extended gear, $m^3(in^3)$
V2o	oil volume in shock strut lower cylinder,$m^3(in^3)$

V3	shock strut rebound volume m^3 (in^3)
$V3_i$	shock strut rebound volume for fully extended gear, 0. m^3(0. in^3)
WMV	total window width of metering valve orifice, alternate concept, .0947 m (3.73 in)
WPV	total window width of power valve orifices, .0897 m (3.53 in)
WSV	total window width of servovalve second stage orifices, alternate concept, .00582 m (.229 in)
XA	displacement of lower mass of shock strut or axle, m (in), positive upwards as shown in Figure 4-2
XSCMD	commanded position of shock strut, -.1905 m (-7.50 in)
XG	ground level displacement, m (in), positive upwards as shown in Figure 4-2
XMV	metering valve displacement, alternate concept, m(in)
XPV	power valve displacement, m (in)
XS	shock strut stroke, m(in) X_S = 0 fully extended, X_S = 0.381 m (-15.00 in) fully compressed
XSV	servovalve second stage spool displacment, m (in)

XWG — displacement of wing gear interface, m (in), positive upwards as shown in Figure 4-2

β — bulk modulus of hydraulic fluid, 8.27×10^8 N/m^2 (1.2×10^5 psi)

γ — ratio of specific heat of gas at constant pressure to that at constant volume, 1.4

ρ — mass density of hydraulic fluid, 833. kg/m^3 (.000936 slugs/in^3 = 0.0301 lbm/in^3)

ωF — corner frequency of compensation in strut position feedback loop, 10.0 sec^{-1}

$\omega C1$ — natural frequency in numerator of compensation notch, 628. sec^{-1}

$\omega C2$ — natural frequency in denominator of compensation notch, 628. sec^{-1}

$\omega C3$ — corner frequency in compensation lead-lag, 129.7 sec^{-1}

$\omega C4$ — corner frequency in compensation lead-lag, 1297. sec^{-1}

ω_{sv} — natural frequency of two-stage servovalve transfer function, 1073. sec^{-1}, (1600. sec^{-1}, alternate concept)

ζ_{sv} — damping coefficient of two-stage servovalve transfer function, 0.855, (1.50, alternate concept)

ζ_{C1} — damping coefficient in numerator of compensation notch, 0.1

ζ_{C2} damping coefficient in denominator of compensation notch, 5.0

Subscripts:

i initial conditions before impact

im impact phase

max maximum value

min minimum value

r rollout phase

tr transition phase

Miscellaneous:

d( ) indicates the differential of a variable

Δ( ) indicates difference or change in a variable

(•), (••), (•••) dots indicate differentiation with respect to time

4.0 DYNAMIC ANALYSIS OF THE ALTERNATE ACTIVE CONTROL LANDING GEAR CONCEPT

4.1 Introduction

The original active control concept utilizes a high flow, high response electrohydraulic servovalve to meter fluid into or out of the landing gear shock strut cylinder from external hydraulic supply and return sources in order to minimize the transient forces transmitted to the wing/aircraft structure through the gear. This concept (described in Section 5.0) typically requires a hydraulic power source consisting of high flow pumps and/or accumulators. An alternate concept for actively controlling the landing gear which does not have this requirement and is much simpler to implement, is addressed in this section.

4.2 Discussion of Concept

The alternate active control landing gear configuration is achieved by two modifications of the existing gear. First, the strut gas volume at precharge is increased to the maximum feasible without major redesign. This allows lowering of the spring rate of the strut and provides a larger available stroke. Second, a valve is added which bypasses the normal metering orifice, which remains unchanged. Unlike the original active control concept discussed in Section 5.0, no net fluid is added to or taken out of the strut cylinders to or from any external hydraulic supply or return sources. Thus, the oil and gas in the gear constitute a closed system, similar to the passive gear case. The main difference functionally is the ability to actively control the metering orifice. To preserve

the rebound damping of the strut, this valve will be driven closed during the rebound phase.

The metering valve is controlled by upper strut pressure, and could conceivably be either mechanical, operating as a pressure relief valve, or electronically controlled by a pressure transducer signal. The latter approach was used for the analyses herein. The valve represents the final stage of a three-stage electrohydraulic servo control loop. The servo loop consists of a commanded limit pressure (input) which is compared with the actual hydraulic pressure in the upper cylinder of the gear as measured by the pressure transducer. This error signal drives a two-stage electrohydraulic servovalve, which meters fluid to the ends of the metering valve, which, in turn, meters the fluid in the strut. Thus, the only external hydraulic power supply required is that necessary to drive the two-stage servovalve, which consists of a nozzle-flapper first stage driving a spool/sleeve second stage. The two-stage valve used for this application has a rated flow of 1.3 gmp at 1000 psi pressure drop. The no-load open-loop gain of the servo loop is sized at 62.8 sec^{-1}. Also, the system gains KP1, KFWD, and KFB are sized such that the equivalent of approximately 200 psi of presssure error signal will statically cause full scale displacement of the metering valve, or .28 inches.

The landing gear gas charging pressure and volume were also modified for the alternate concept. The charging pressure was changed from 384 psi to 700 psi and the gas charging volume was changed from 238.5 in^3 to 360 in^3. As indicated earlier, this allows lowering the spring rate of the strut and provides a larger available stroke.

The forces in a shock strut are due to two effects. First, there is a force resulting from forcing the oil in the strut through the metering orifice. This force is a function of strut stroke and rate of stroke. The second force is due to compression of gas in the strut and is a function of strut position. The first force may be controlled, within limits, by varying the metering orifice; however, it cannot be made lower than the second force. To absorb the kinetic energy of the airplane with the least force, this limit force should be applied over a length of strut travel which is limited by the strut position where the static force due to gas compression exceeds the limit force.

The limit force is sensed by measuring the oil pressure in the strut upstream of the metering orifice. When this pressure exceeds the desired limit pressure, the metering valve is opened to attempt to maintain limit pressure. If the pressure falls below the limit pressure, the valve is then closed.

A value of limit pressure must be selected which will result in the lowest peak pressure (and force) in the strut. This value is a function of the touchdown kinetic energy in the case of a landing, or of aircraft velocity and aircraft dynamics in the case of runway irregularities.

Figure 4-1 illustrates the strut force due to position for various values of initial gas volume and pressure. Superimposed on the graph are curves of strut stroke and limit force required to absorb the kinetic energy of the airplane at various input velocities. These curves neglect tire deflection and aircraft lift. From these curves it is evident that at best the

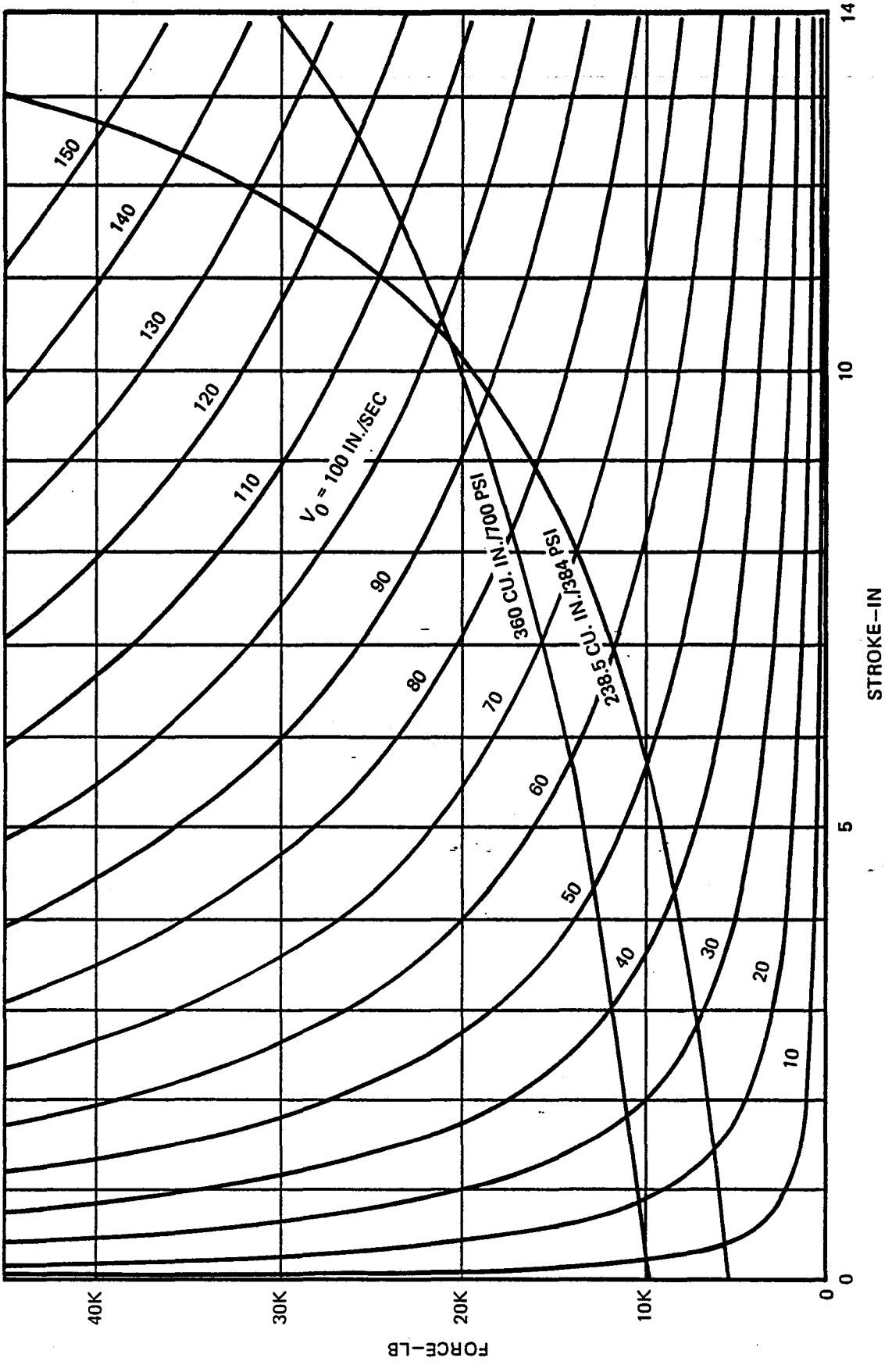

FIGURE 4-1. LOAD-STROKE CURVES

present passive gear could only limit wing/gear force to 123.7 KN (27,800 lbs) with a stroke of 79.39 cm. (11.57 ins.) if it were 100% efficient. The actual peak load with the present arrangement approaches 153.5 KN (34,500 lbs). Increasing the gas volume to 5900 cc. (360 cu. ins) and the precharge to 4826 KPa would reduce this optimum peak to 107.7 KN (24,200 lb) with a 31.9 cm. (12.56 in) stroke at best. If it is attempted to lower the limit force below this value, all the kinetic energy will not be absorbed before the strut reaches the point where its static force exceeds the commanded limit force and the strut force will rise regardless of how far the metering orifice is opened. Thus, the intersection of the gas curve with the various sink rate curves represents the lowest limit force that one could hope to achieve from the particular sink rate. Also, it is evident from the curves that the gear with the modified gas charging pressure and volume has a greater potential for reducing the landing impact forces for the high sink rate cases.

In the case of a runway irregularity, the onset of the rise is usually rapid enough so that the upper mass does not have time to significantly respond, and therefore the entire height of the irregularity must be absorbed by strut and tire deflection. Thus the strut must be precharged with enough pressure to allow this stroke.

4.3 Dynamic Simulation Math Model

The main analytical tool used in the study of the alternate concept was the nonlinear model. A linear model was not used because of the difficulty in linearizing the flow through the metering valve, which is highly nonlinear.

Dynamic Equations

Figure 4-2 shows a schematic of the active control landing gear system (without loop closure and controller electronics) for reference in writing the dynamic equations. A force balance on the airplane mass including the upper portion of the landing gear shock strut gives

$$MU \frac{d^2XWG}{dt^2} = P1(A1-AP) + P2 \cdot AP - P3 \cdot A3 - MU \cdot g + FL \pm f \qquad (1)$$

A force balance on the lower portion of the shock strut (piston and tire) gives

$$ML \frac{d^2XA}{dt^2} = - P1(A1-AH) - P2 \cdot AH + P3 \cdot A3 - ML \cdot g + FA \pm f \qquad (2)$$

where the tire force is

$$FA = \begin{cases} KTIRE(XA - XG)^{ATIRE} & \text{for } XA > XG \\ 0 & \text{for } XA < XG \end{cases} \qquad (3)$$

The force transmitted through the wing/gear interface structure is of interest, and is determined by performing a force balance on the airplane mass not including the upper portion of the shock strut. Referring to Figure 5-2,

$$M \frac{d^2XWG}{dt^2} = FWG + FL - M \cdot g = FACC \qquad (4)$$

The wing/gear interface force (FWG) is calculated from this equation, where $\ddot{X}WG$ is obtained from equation (1).

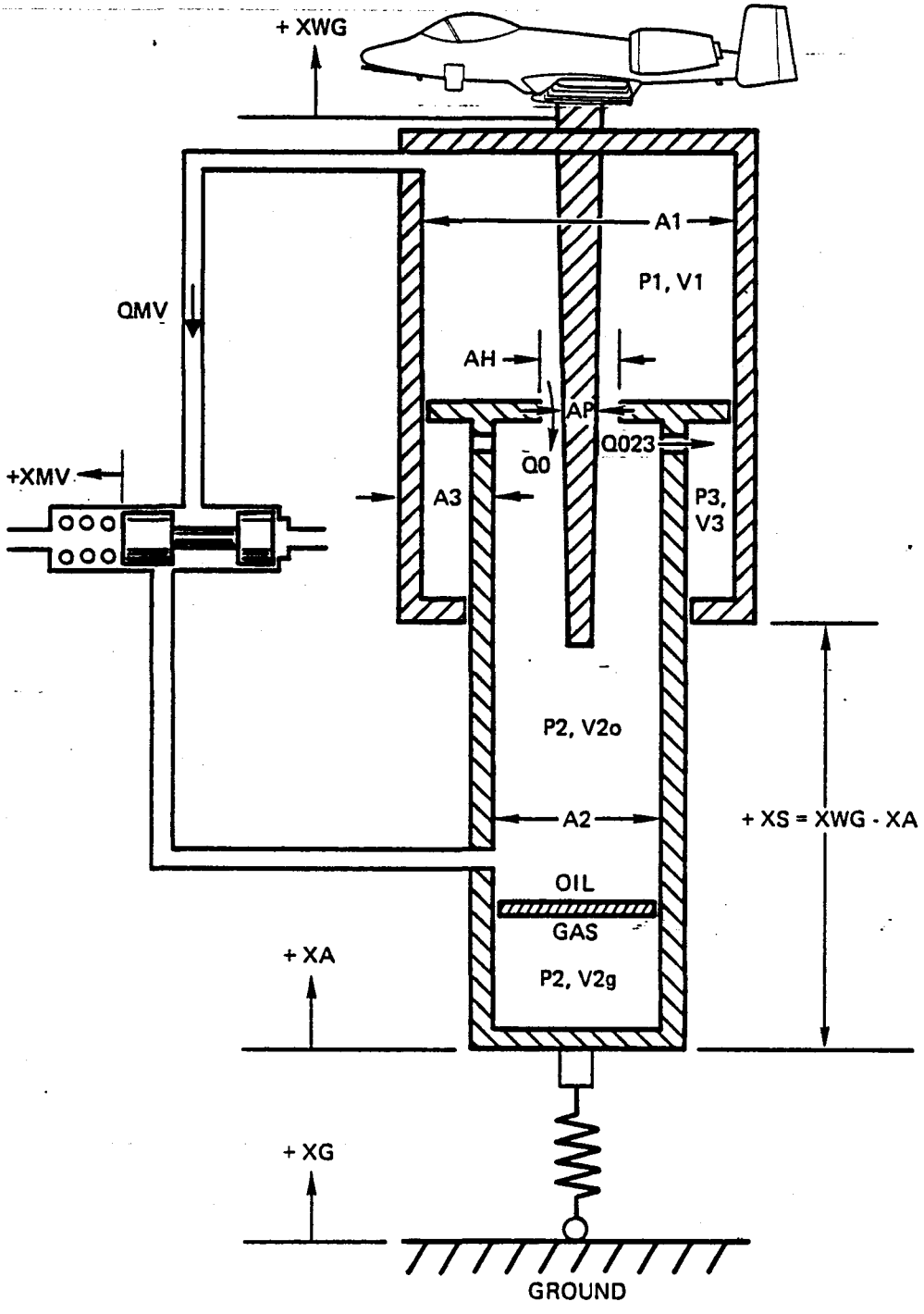

FIGURE 4-2. SCHEMATIC OF ACTIVE CONTROL LANDING GEAR, ALTERNATE CONCEPT

The pressure-volume relationships for the oil and gas in the shock strut are derived in the following manner. Referring to Figure 4-2, conservation of mass applied to the oil in the upper chamber (volume V1) gives

$$\frac{V1}{\beta}\frac{dP1}{dt} = - QO - QMV - (A1 - AP)\frac{dXS}{dt} \tag{5}$$

where

$$V1 = V1_i + A1 \cdot XS + VPIN \tag{6}$$

and where VPIN is described later.
For the oil in the rebound chamber (volume V3), conservation of mass gives

$$\frac{V3}{\beta}\frac{dP3}{dt} = QO23 + A3\frac{dXS}{dt} \tag{7}$$

where

$$V3 = V3_i - A3 \cdot XS \tag{8}$$

To avoid ending up with a differential equation for the rebound pressure P3, which typically occupies a relatively small oil volume, the compressibility effect in equation (7) is neglected, thus, equation (7) becomes

$$QO23 = - A3\frac{dXS}{dt} \tag{9}$$

For the oil portion in the lower strut (volume V2o), conservation of mass gives

$$\frac{V2o}{\beta}\frac{dP2}{dt} = QO - QO23 + \frac{dV2g}{dt} - AP\frac{dXS}{dt} \tag{10}$$

where

$$V2o = V2_i - V2g - VPIN - A3 \cdot XS \tag{11}$$

Note that the volume V20 is written to include the volume of oil in the rebound chamber. This is to compensate for the fact that the oil compressibility in the rebound chamber was neglected in equations (9). The last VPIN represents the volume of oil displaced in the lower chamber (from the fully-extended strut condition) by the metering pin or tube which protrudes through the hole in the shock strut plate, as a function of the stroke. For gears with tapered metering pins (as shown in Figure 4-2), where the pin cross sectional area at the hole is a function of stroke,

$$VPIN = - \int_o^{XS} AP \cdot dXS \tag{12}$$

Note that the fully extended reference condition is defined at XS = 0. The minus sign is due to the fact that xs becomes more negative as the strut collapses. The equation thus produces positive values for VPIN, as desired. For gears with constant area metering tubes (as in the A-10 landing gear), VPIN is simply equal to - AP • XS.

For the gas portion in the lower cylinder, assuming an isentropic process,

$$P2 \cdot V2g^{\gamma} = \text{constant} \tag{13}$$

Thus,

$$\frac{dP2}{P2} + \gamma \frac{dV2g}{V2g} = 0$$

$$dV2g = -\frac{1}{\gamma} \frac{V2g}{P2} dP2 \tag{14}$$

where

$$V2g = V2g_i (P2_i/P2)^{1/\gamma} \tag{15}$$

Substituting equations (9) and (14) into equation (10):

$$\left(\frac{V2o}{\beta} + \frac{1}{\gamma} \frac{V2g}{P2}\right) \frac{dP2}{dt} = QO + QMV + (A3 - AP) \frac{dXS}{dt} \tag{16}$$

The pressures P1 and P2 are determined from the differential equations (5) and (16), respectively. Since oil compressibility in volume V3 is neglected, the pressure P3 is determined algebraically as follows: From the orifice flow equation,

$$QO23 = CO23(P2-P3)/\sqrt{|P2-P3|} \tag{17}$$

or,

$$P3 = P2 - \frac{QO23\ |QO23|}{CO23^2} \tag{18}$$

The flow rate through the metering orifice is

$$QO = CO(P1-P2)/\sqrt{|P1-P2|} \tag{19}$$

Figure 4-3 shows a schematic of the outer loop closure along with the inner servo loop up to the point of second stage spool position. The outer loop closure is comprised of a preset command limit pressure signal and a feedback pressure signal obtained from a pressure transducer mounted in the landing gear upper cylinder. Note that dynamic compensation is not required. The inner servo loop is comprised of a servoamplifier driving a two-stage electrohydraulic servovalve which drives the metering valve, which has electrical position feedback to the servoamplifier input.

The two-stage servovalve consists of a first stage electrical torque motor-driven flapper nozzle valve driving a second stage four-way spool valve.

As indicated in Figure 4-3, the dynamics of the two stage servovalve are simulated by relating input torque motor current to output spool position using a second order differential equations, which has been broken down so that the nonlinear effect of second stage saturation is simulated by limiting spool displacement, and first stage flapper saturation is simulated by limiting second stage spool velocity. The effects of a static null bias in spool position and servovalve hysteresis are also simulated.

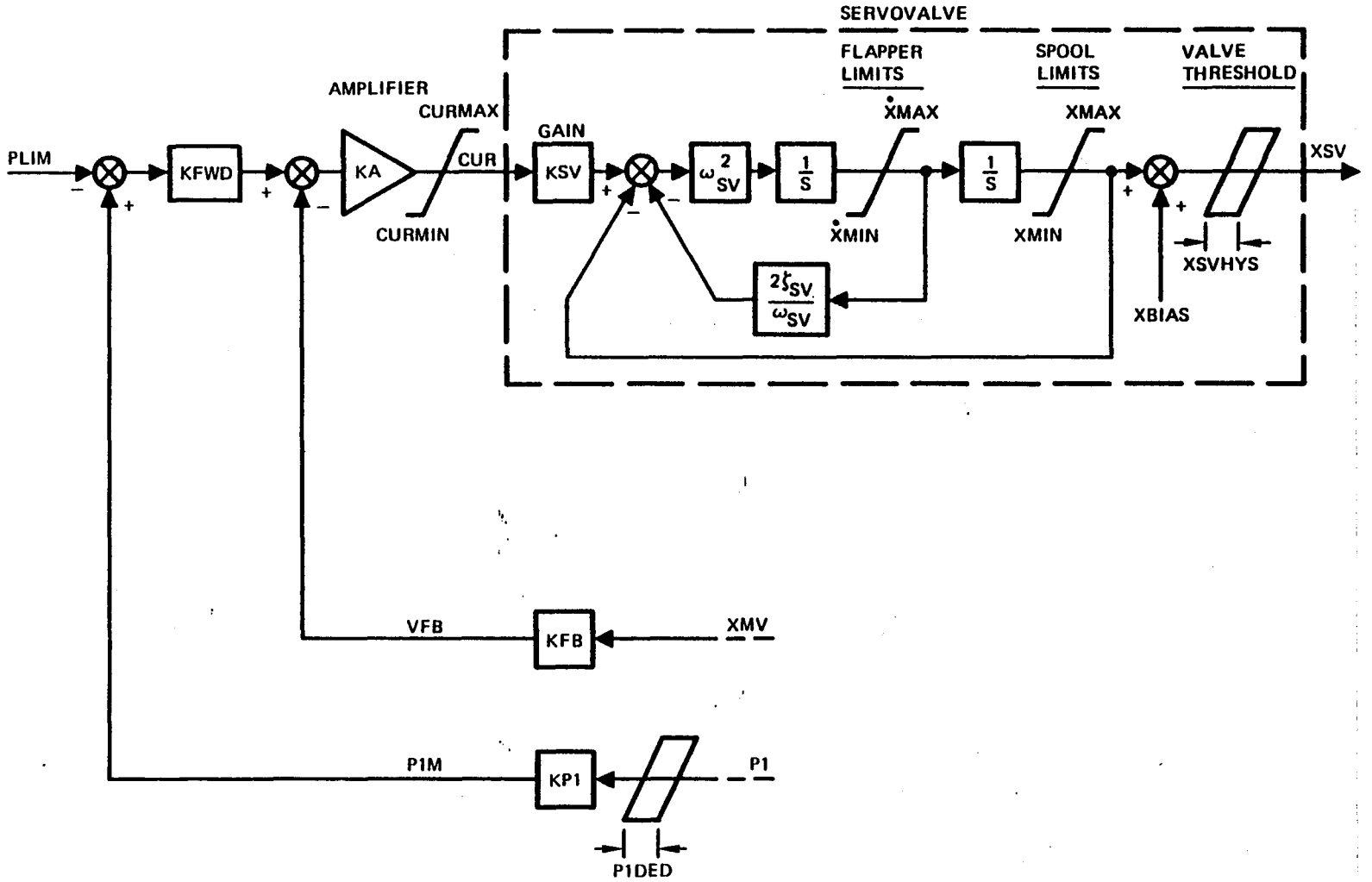

FIGURE 4-3. LOOP CLOSURE SCHEMATIC WITH SERVOVALVE DYNAMICS, ALTERNATE CONCEPT

Figure 4-4 shows a hydraulic schematic of the servovalve second stage valve driving the metering valve. The potentiometer on the metering valve is not shown. The equation of motion for the metering valve is:

$$MMV \frac{d^2XMV}{dt^2} = AMV(PC1 - PC2) - KMV \cdot XMV - FOMV - BMV \frac{dXMV}{dt} \pm f_{MV} \tag{20}$$

Conservation of mass applied to the oil in the control volumes between the second stage servovalve and the end of the metering valve gives:

$$\frac{VC1}{\beta} \frac{dPC1}{dt} = QNET1 - AMV \frac{dXMV}{dt} \tag{21}$$

$$\frac{VC2}{\beta} \frac{dPC2}{dt} = QNET2 + AMV \frac{dXMV}{dt} \tag{22}$$

where

$$VC1 = VC1_i + AMV \cdot XMV \tag{23}$$

$$VC2 = VC2_i - AMV \cdot XMV \tag{24}$$

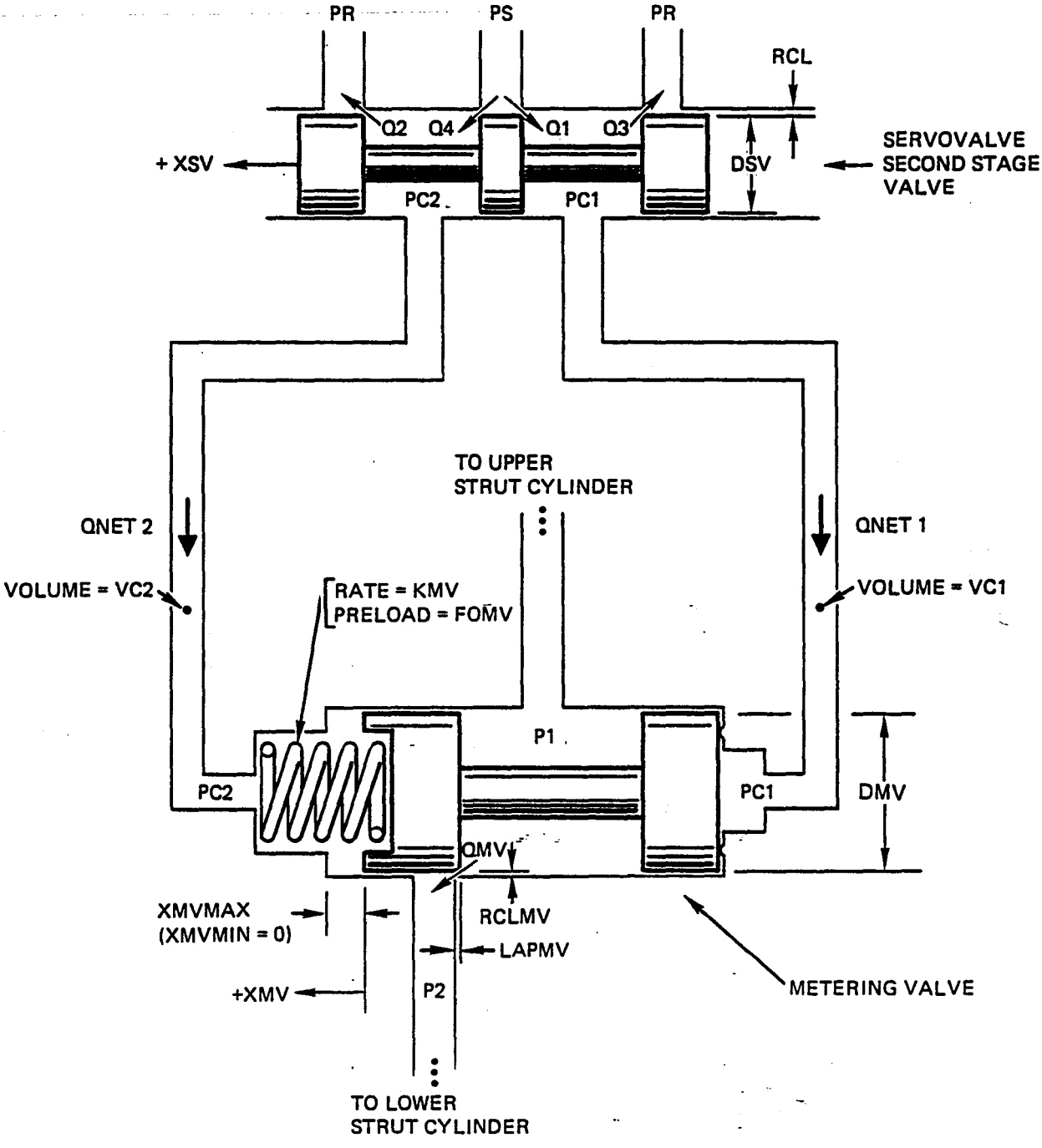

FIGURE 4-4. SCHEMATIC OF SERVOVALVE SECOND STAGE VALVE AND THE METERING VALVE, ALTERNATE CONCEPT

The flows through the spool/sleeve orifices of the second stage servovalve and the metering valve are calculated as a function of the spool displacements, the cylinder pressures, and the supply and return pressures, fluid properties, and the spool/sleeve geometry (i.e., window widths, window lengths, spool/sleeve clearance, spool diameter, overlap and/or underlap lengths). The method utilizes sharp-edge orifice equations and equations for flow between concentric cylinders, with entrance region effects taken into account. Reynolds number effects (i.e., laminar, transitional, and turbulent flow considerations) are accounted for.

4.4 Transient Response Results

The nonlinear model was used to simulate vertical drop landings and rollouts over runway disturbances using the alternate active control concept on the A-10 main landing gear. Since a modified version of the gear was used for the alternate concept, the passive gear cases were re-run with the modification incorporated in order to obtain a fair baseline for comparison in evaluating the effectiveness of the alternate active control concept.

4.4.1 Landing Impact

The conditions for the vertical drop case are as follows:

a. The sink rate prior to impact is 2.54 m/sec (100 in/sec).

b. The lift equals airplane weight of 7827 Kg. (17,254 lbs.) (per gear) prior to and up to the point of impact, then lift is linearly reduced to 10 percent of airplane weight during the first second after impact, and lift is held constant at ten percent thereafter.

c. The ground level remains constant.

The command limit pressure was preset to a value of 1216 psi. Figures 4-5 through 4-7 show the resultant transients for the passive gear. Figures 4-8 through 4-11 show the results for the active control case. The active control reduces the peak force 22 percent below the modified gear passive case, and 14 percent below the original gear passive case from Section 5.6.1. Note that the modified gear leaves the ground for a short duration after impact for both the passive and active cases, whereas the original unmodified passive gear did not. (See Figure 5-19.)

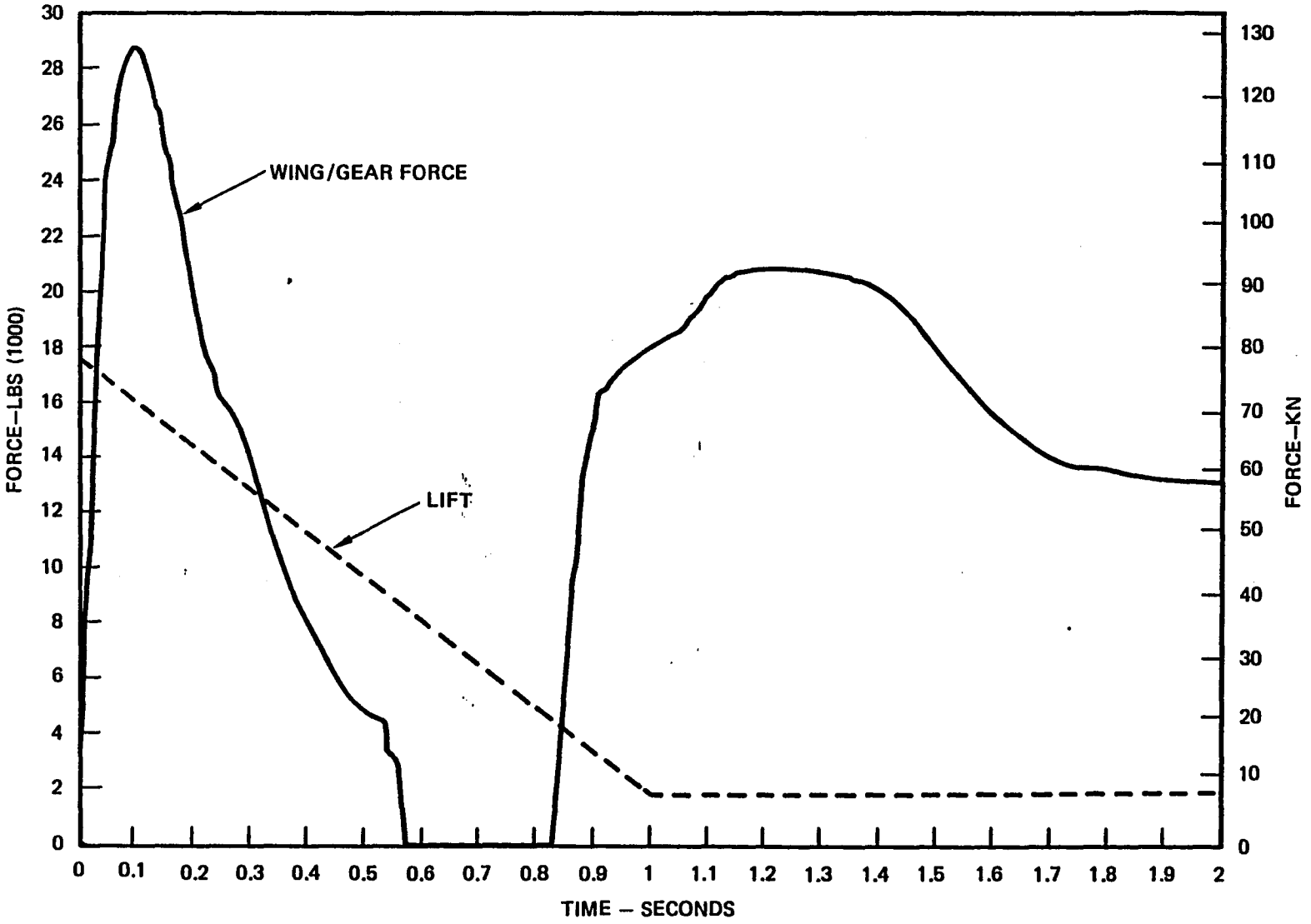

FIGURE 4-5. IMPACT LANDING, MODIFIED GEAR, PASSIVE CASE (ALTERNATE CONCEPT)

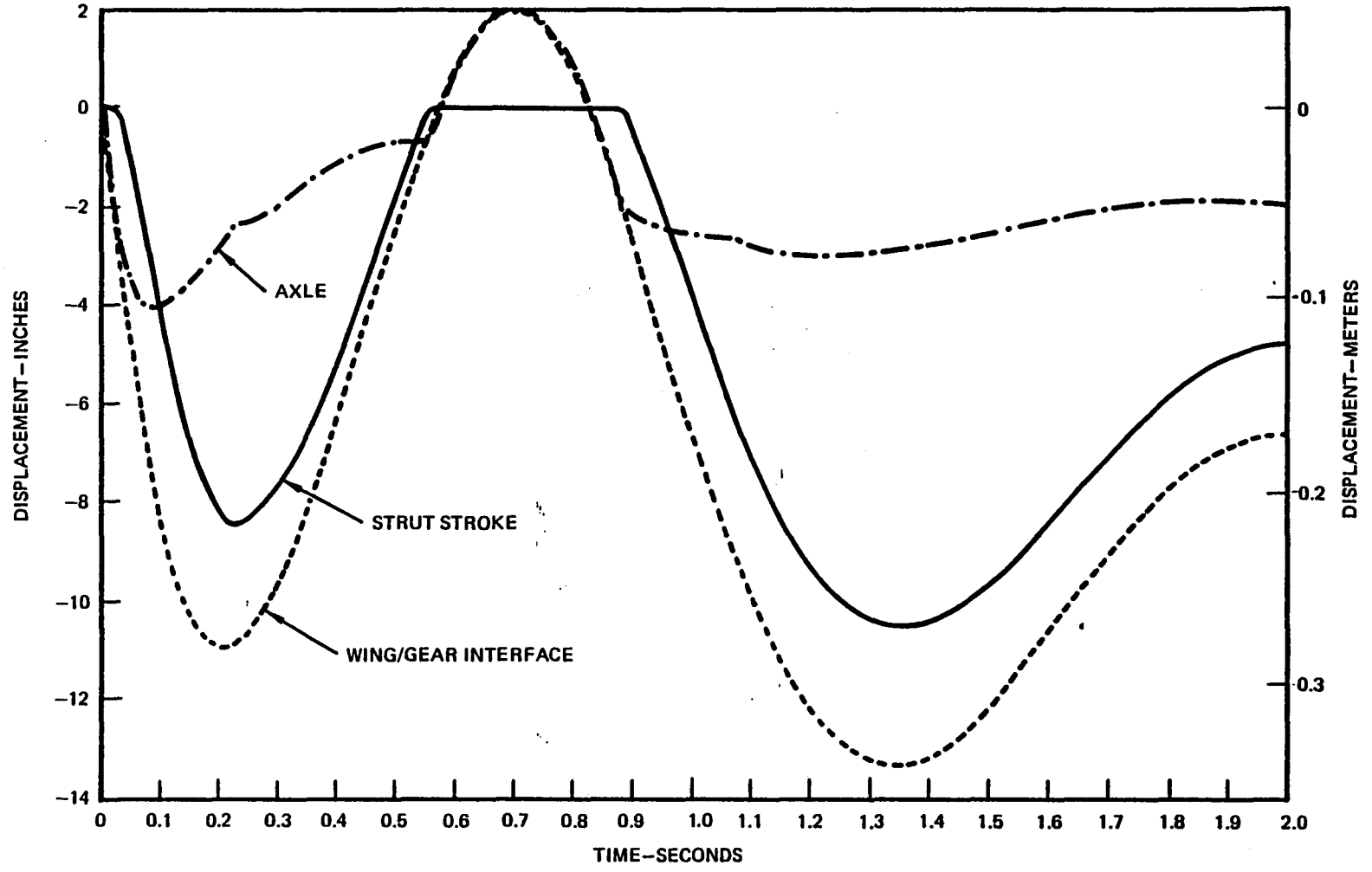

FIGURE 4-6. IMPACT LANDING, MODIFIED GEAR, PASSIVE CASE (ALTERNATE CONCEPT)

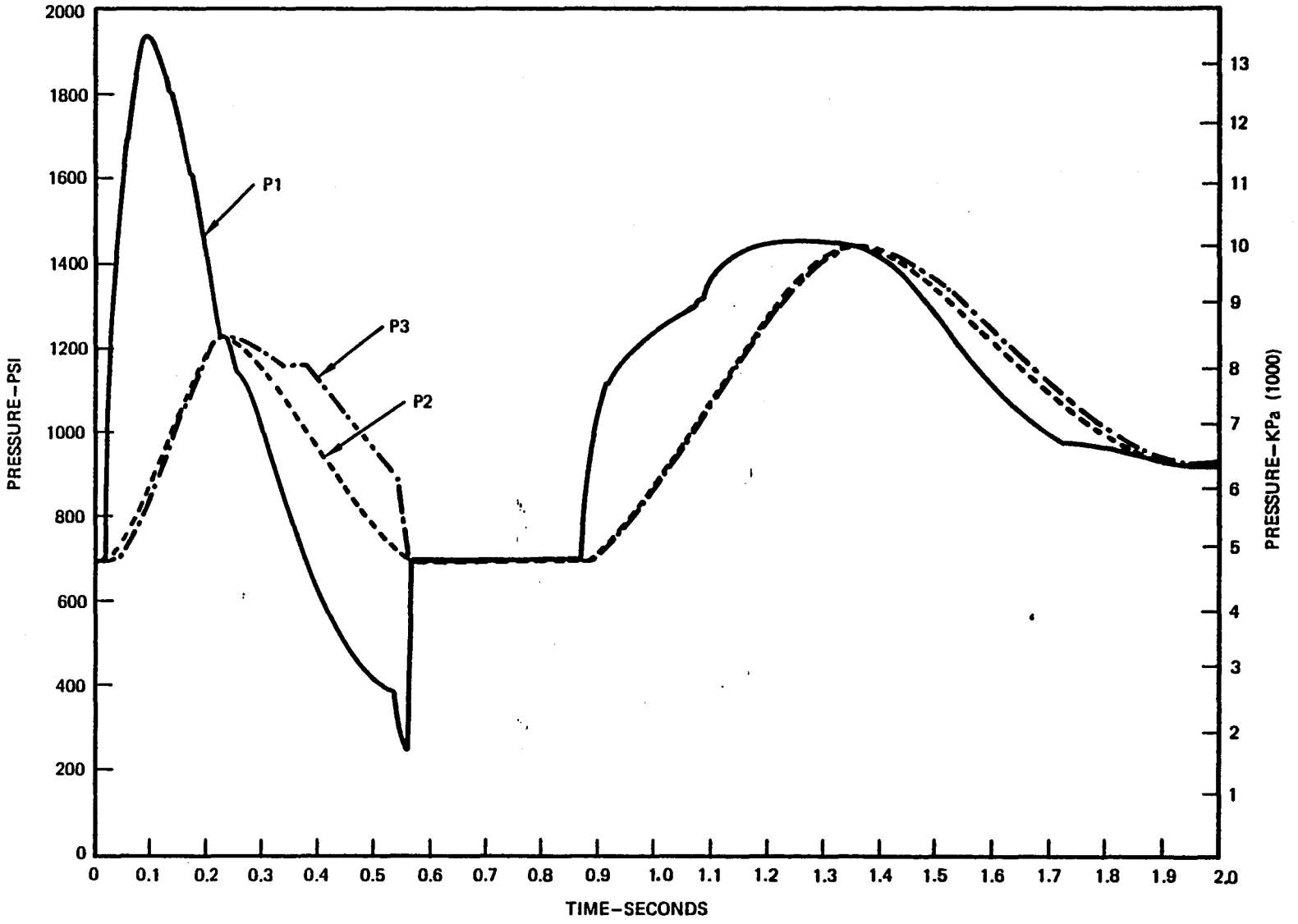

FIGURE 4-7. IMPACT LANDING,MODIFIED GEAR, PASSIVE CASE (ALTERNATE CONCEPT)

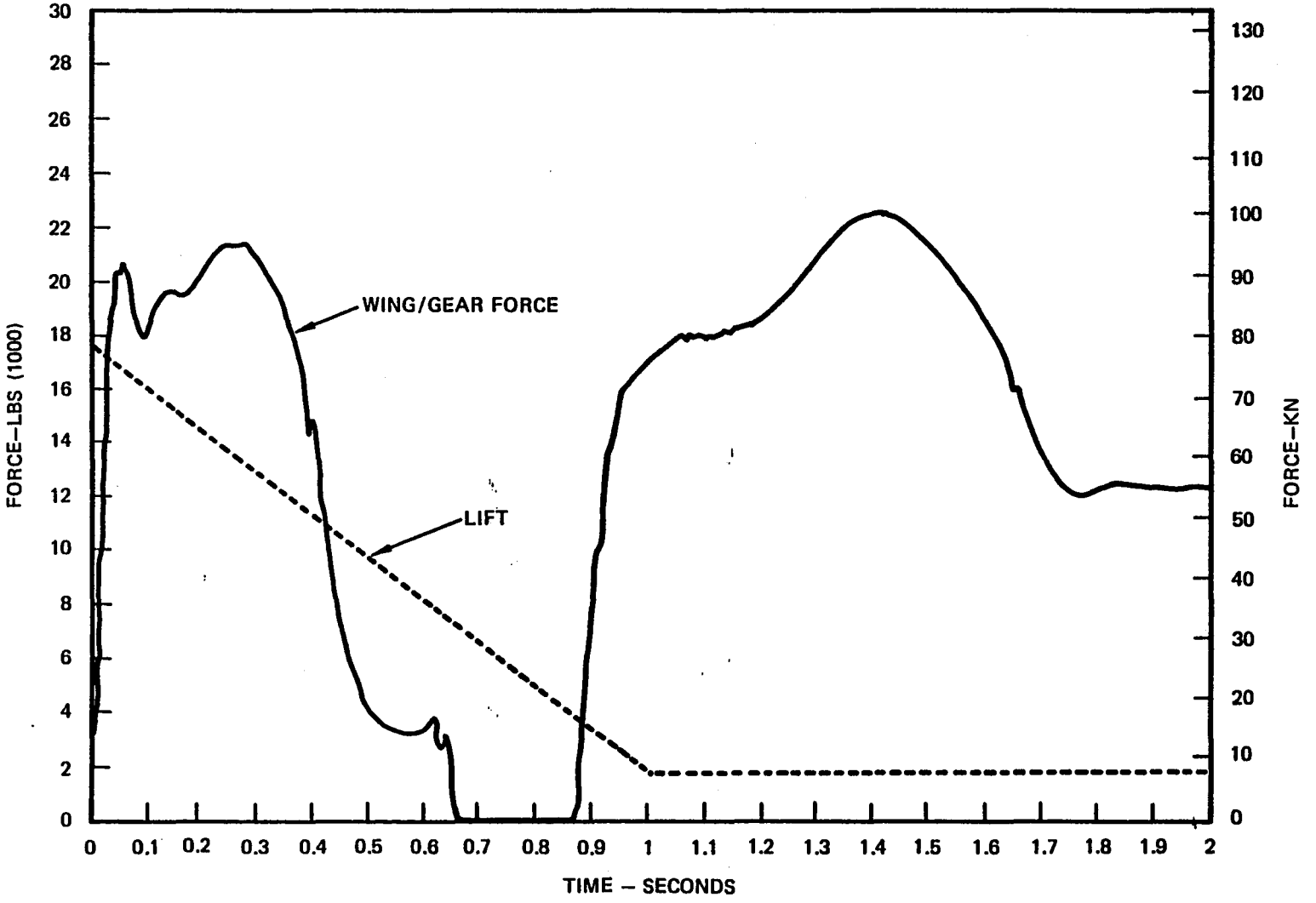

FIGURE 4-8. IMPACT LANDING, MODIFIED GEAR, ACTIVE CASE (ALTERNATE CONCEPT)

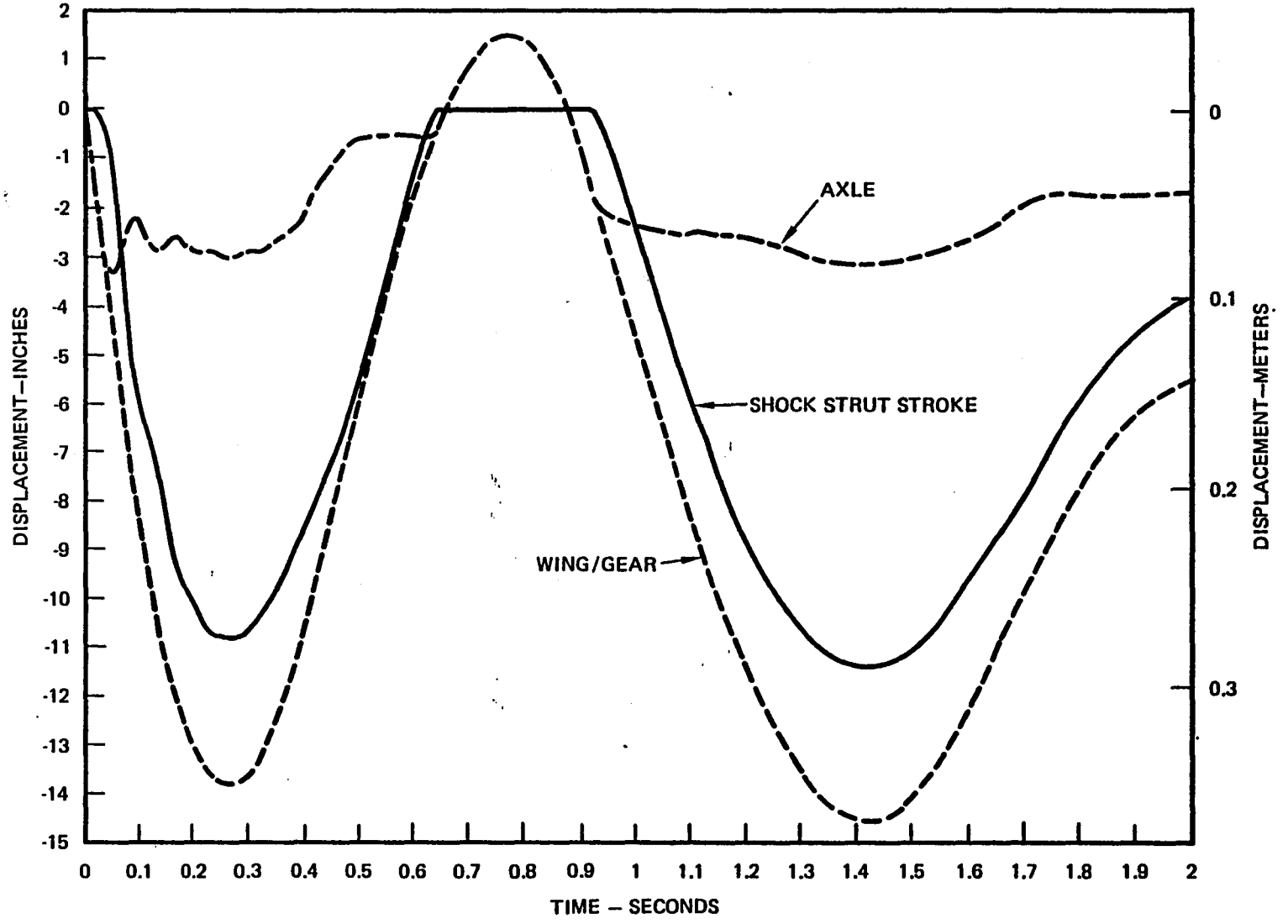

FIGURE 4-9. IMPACT LANDING, MODIFIED GEAR, ACTIVE CASE (ALTERNATE CONCEPT)

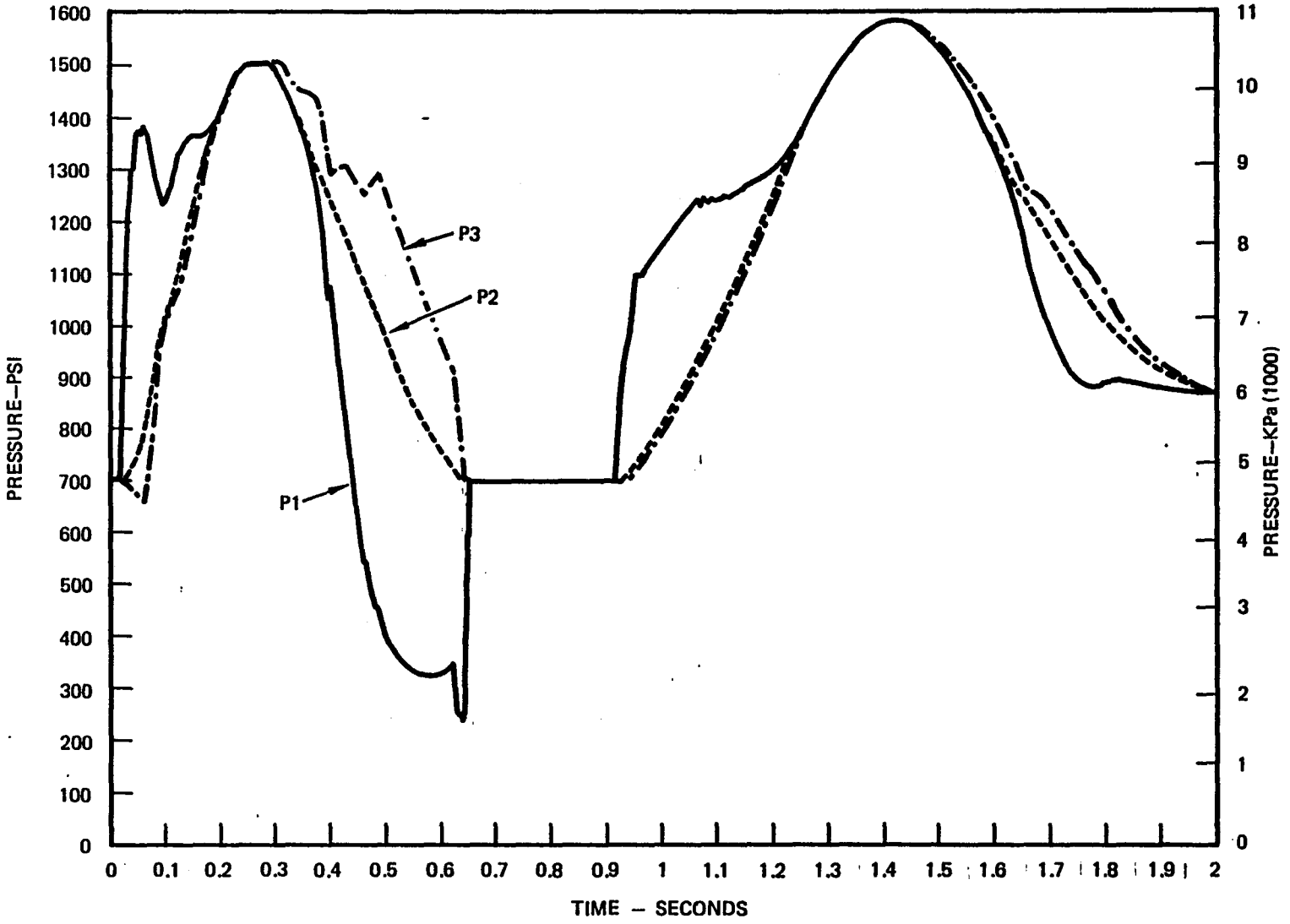

FIGURE 4-10. IMPACT LANDING, MODIFIED GEAR, ACTIVE CASE (ALTERNATE CONCEPT)

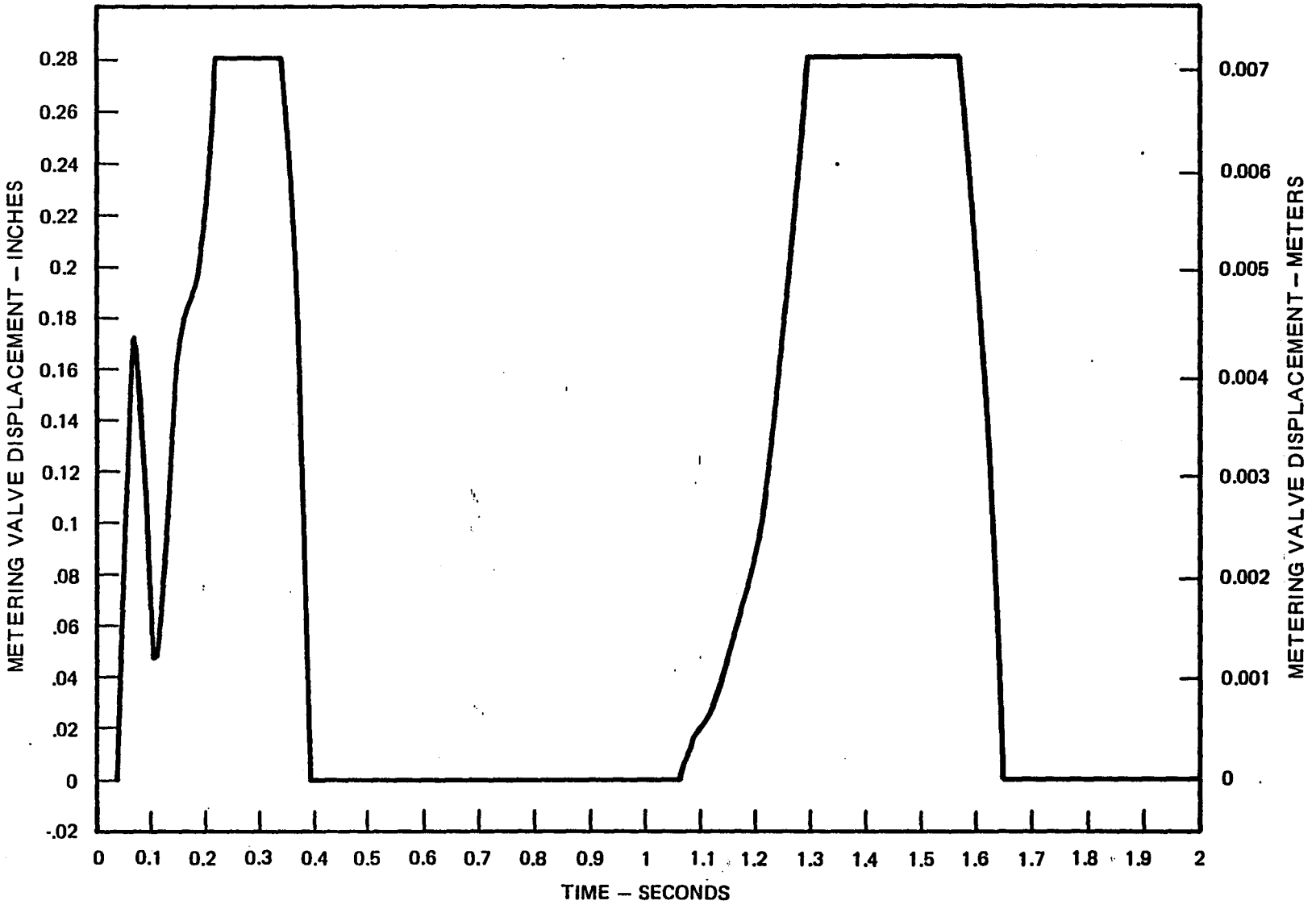

FIGURE 4-11. IMPACT LANDING, MODIFIED GEAR, ACTIVE CASE (ALTERNATE CONCEPT)

4.4.2 Runway Disturbances

Simulation of aircraft rollout over a runway disturbance (subsequent to an impact landing) was accomplished using the nonlinear vertical drop model. Initial conditions are calculated assuming the aircraft is in contact with the ground and the landing gear has reached an equilibrium condition in supporting the aircraft weight minus its lift. Assuming some horizontal speed for the aircraft, actual physical changes in ground level can be represented as transient changes which can be input to the nonlinear model. For this case a Class I repaired bomb crater constituted the runway disturbance. A diagram of a repaired bomb crater is shown in Figure 5-26. The horizontal speed of the aircraft was assumed to be 51.8 m/sec (170 ft/sec). The lift is set to 10 percent of the aircraft weight (per gear) throughout the transient.

The command limit pressure was preset to a value of 1216 psi, which is the equilibrium pressure that would exist in the strut when the airplane had zero lift. Figures 4-12 through 4-14 show the results for the passive gear. Figures 4-15 through 4-18 show the results for the active gear. The active control reduces the peak force 36 percent below the modified gear passive case and 39 percent below the original gear passive case from Section 5.6.2.

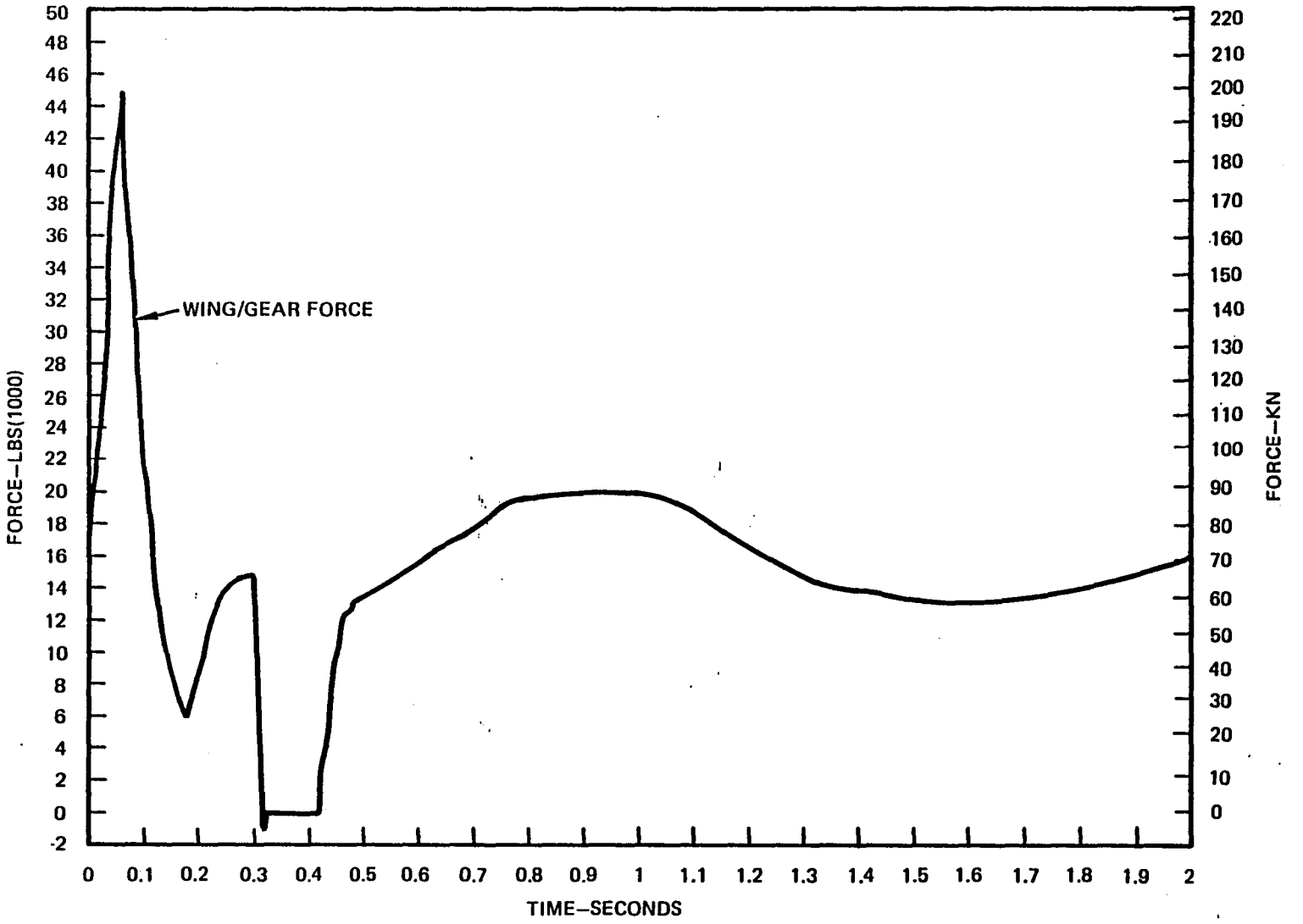

FIGURE 4-12. RUNWAY DISTRUBANCE, MODIFIED GEAR, PASSIVE CASE

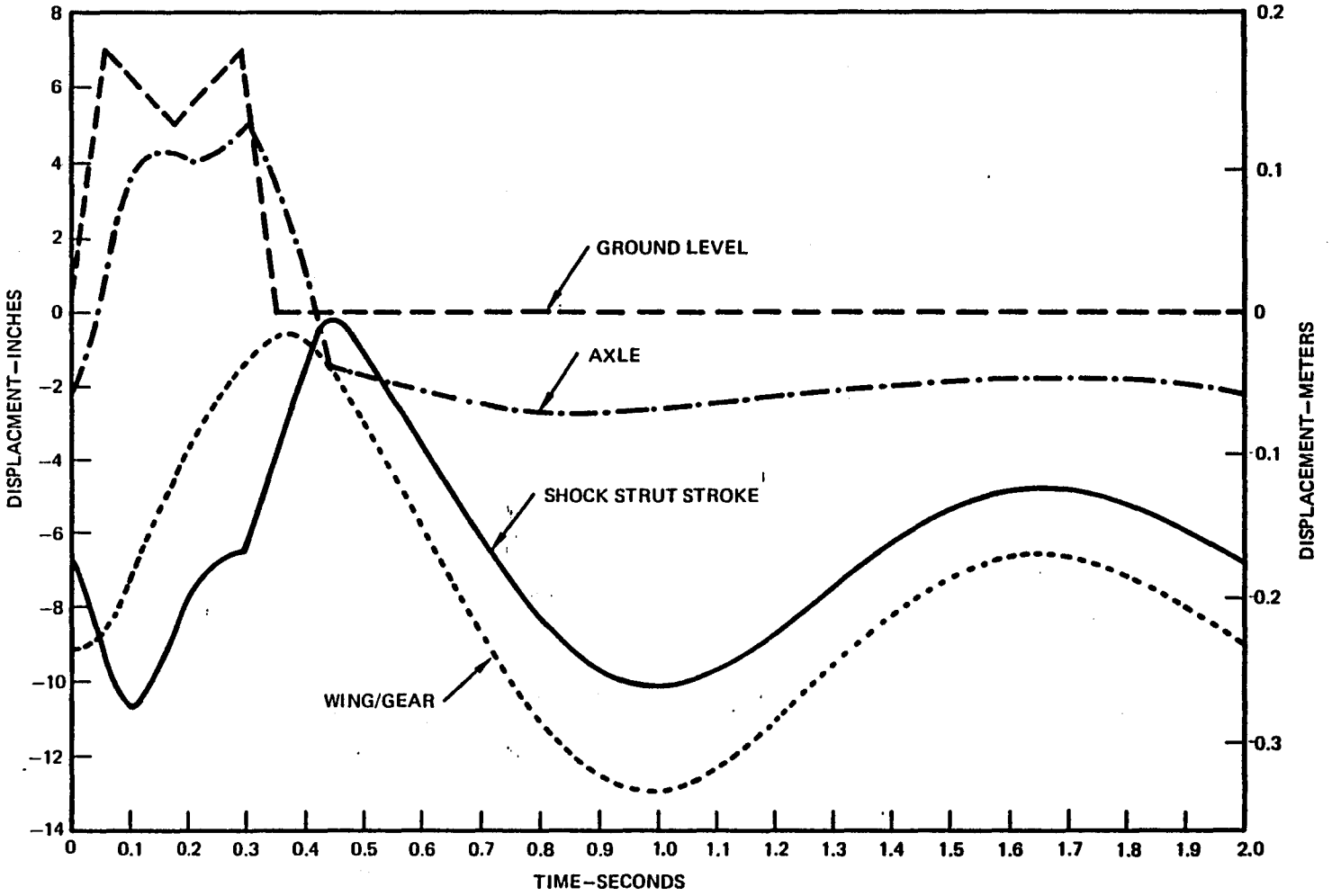

FIGURE 4-13. RUNWAY DISTURBANCE, MODIFIED GEAR, PASSIVE CASE

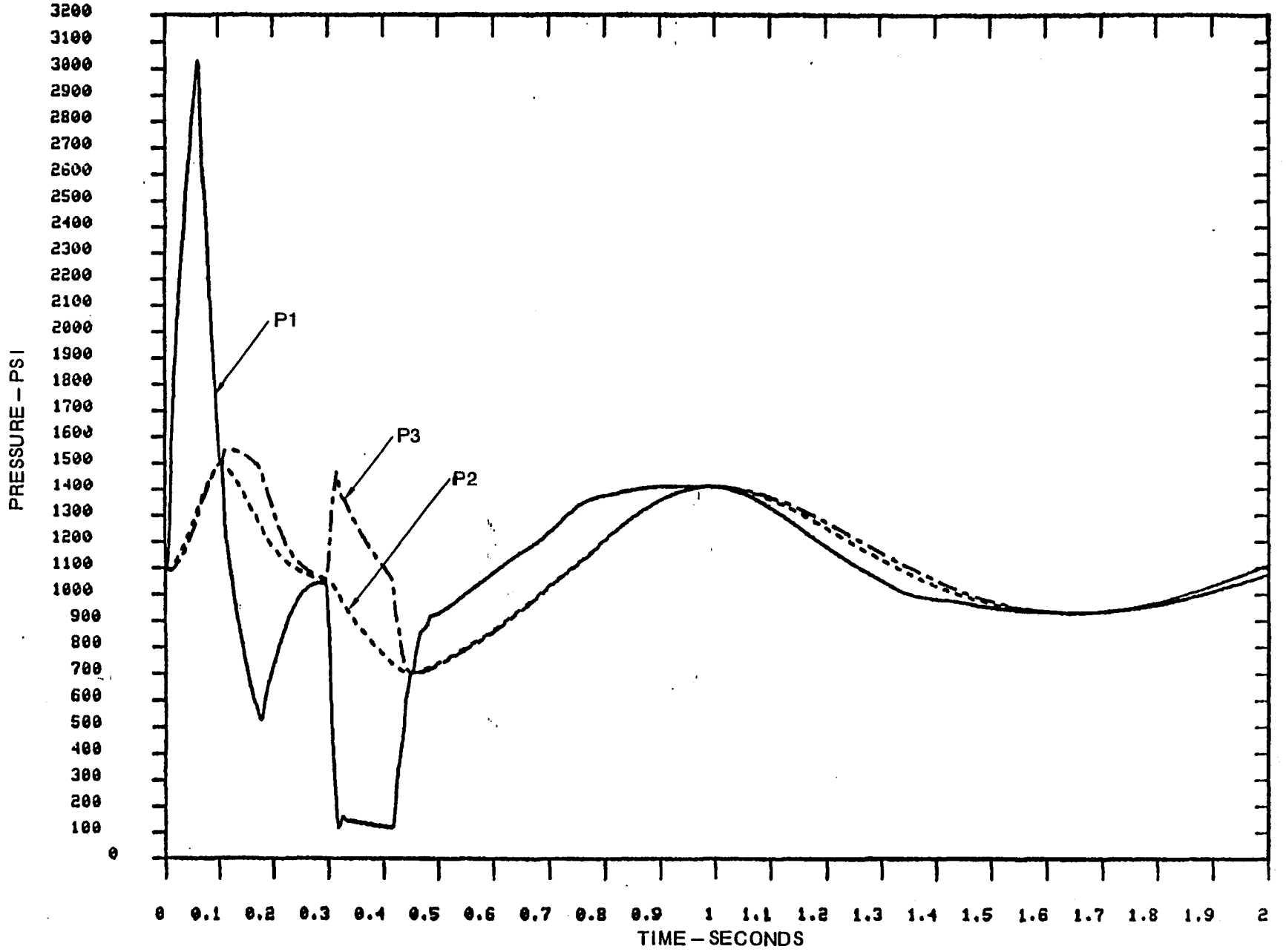

FIGURE 4-14. RUNWAY DISTURBANCE, MODIFIED GEAR, PASSIVE CASE (ALTERNATE CONCEPT)

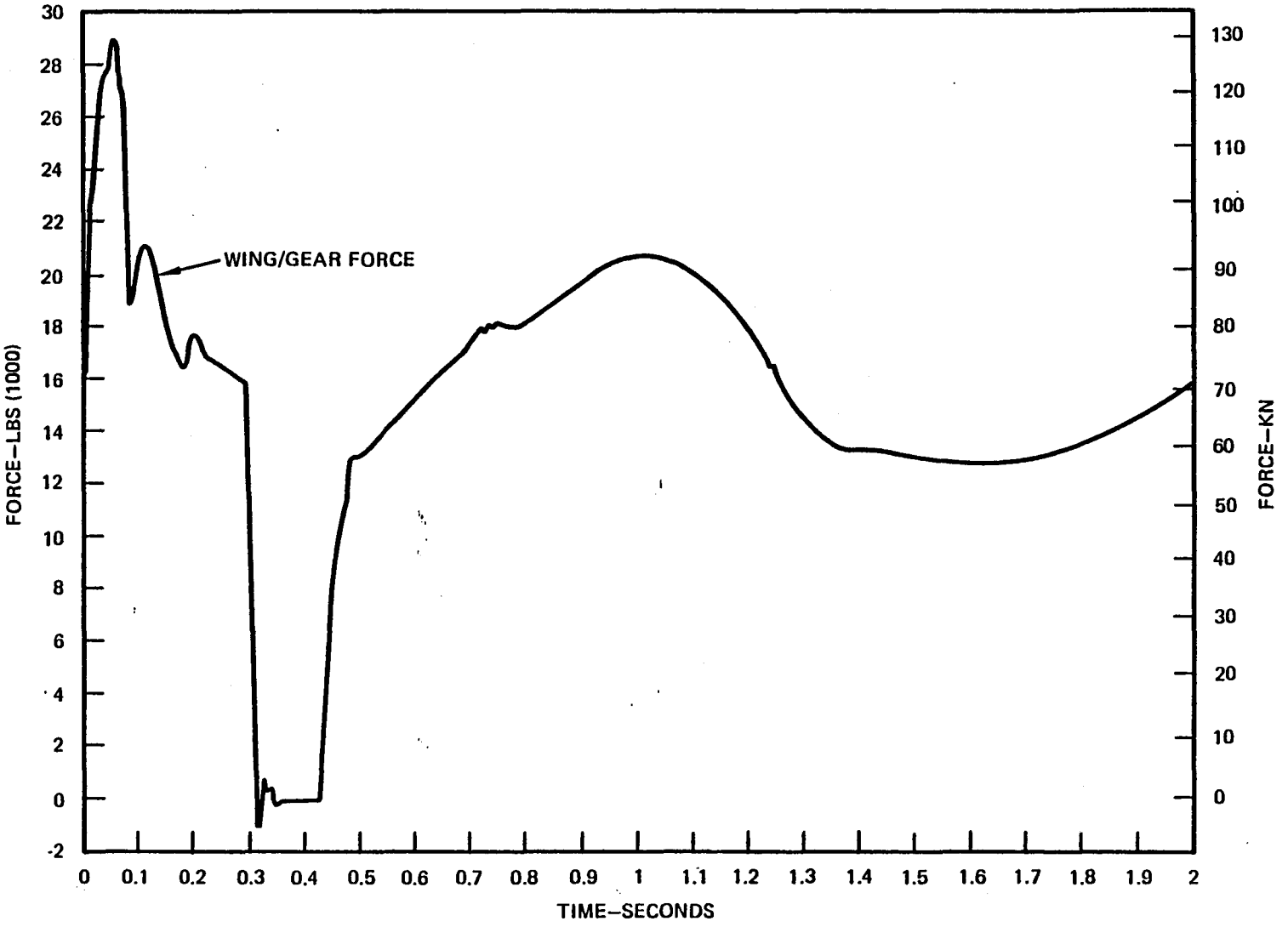

FIGURE 4-15. RUNWAY DISTURBANCE, MODIFIED GEAR, ACTIVE CASE (ALTERNATE CONCEPT)

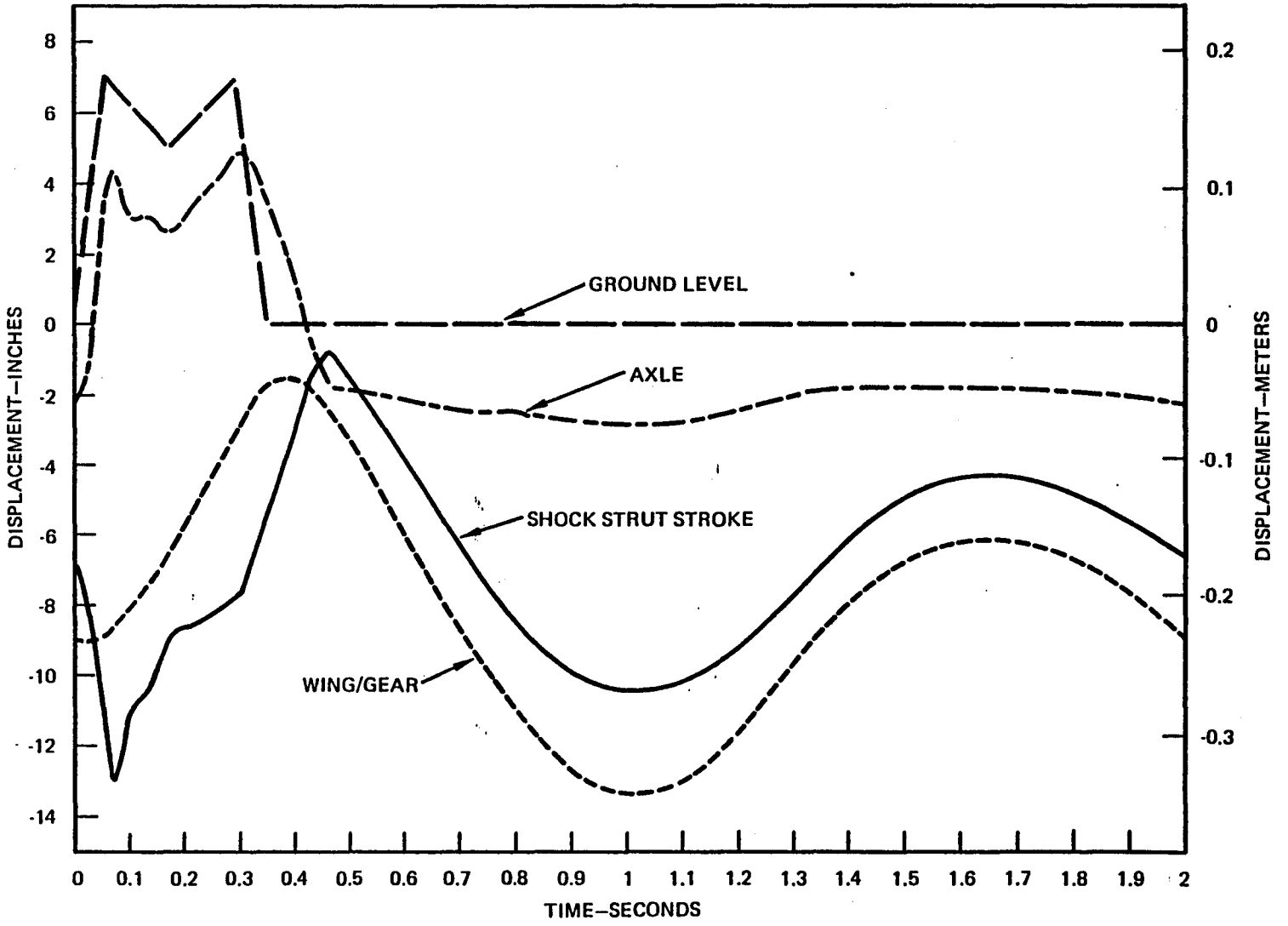

FIGURE 4-16. RUNWAY DISTRUBANCE, MODIFIED GEAR, ACTIVE CASE (ALTERNATE CONCEPT)

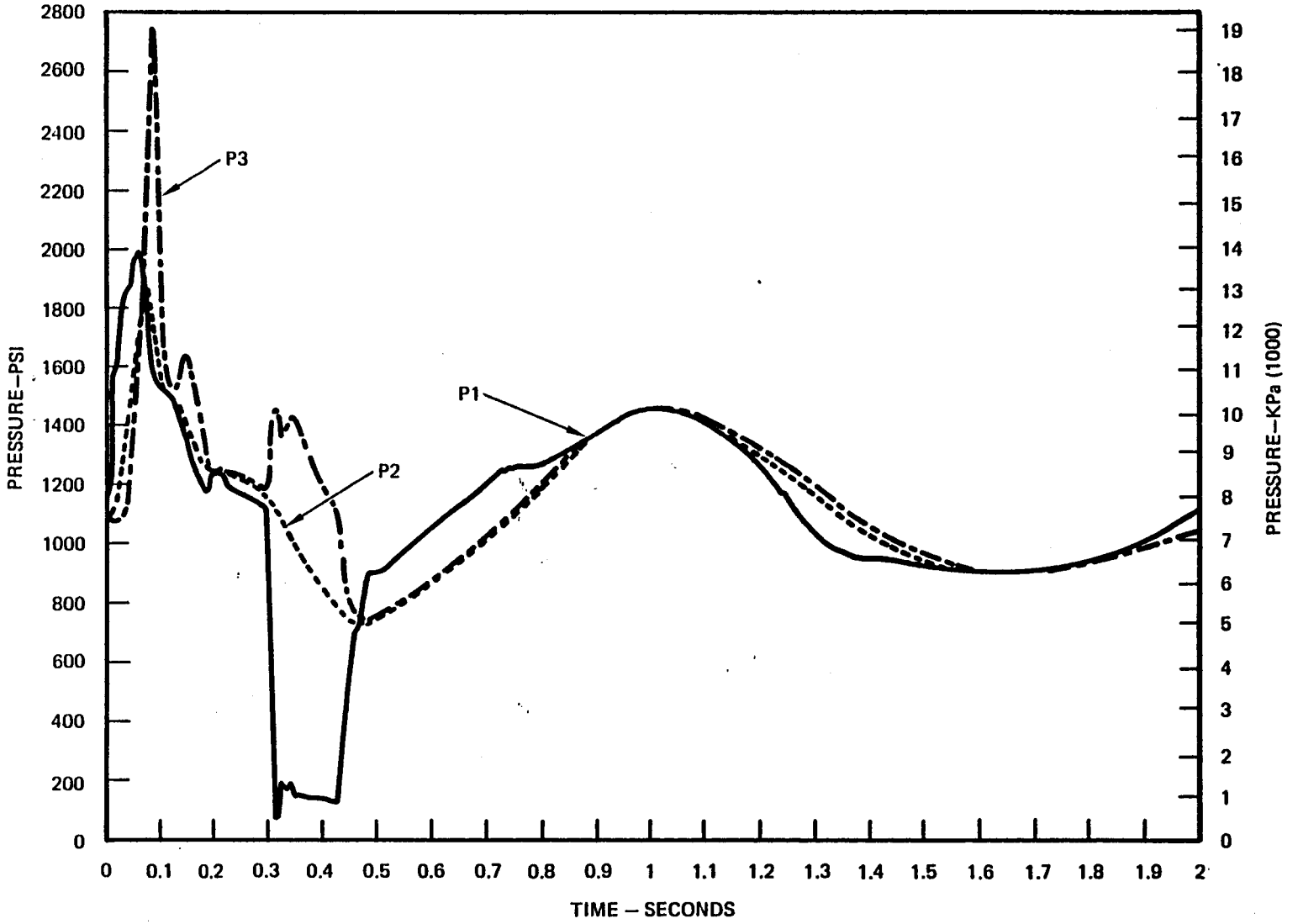

FIGURE 4-17. RUNWAY DISTURBANCE, MODIFIED GEAR, ACTIVE CASE (ALTERNATE CONCEPT)

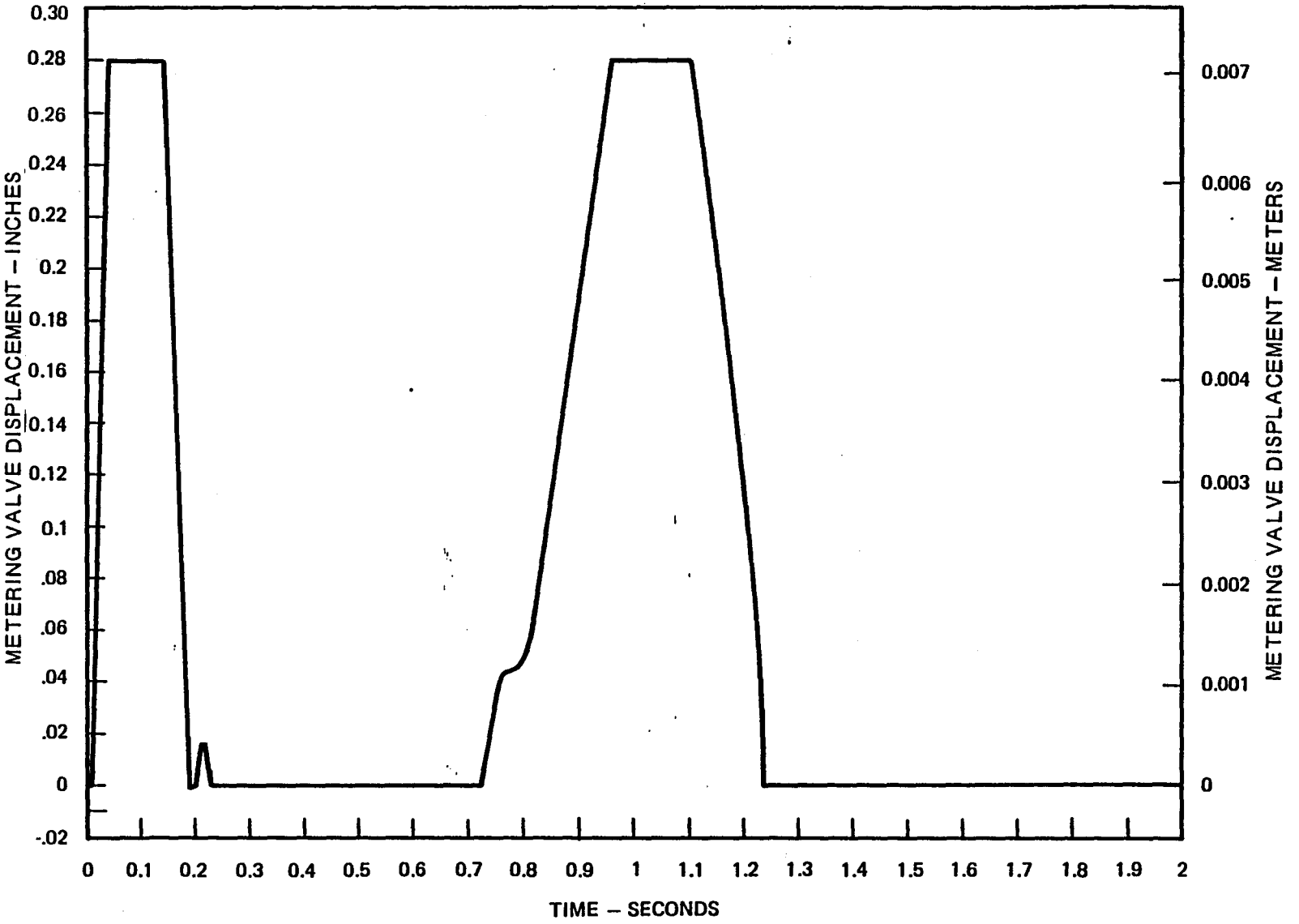

FIGURE 4-18. RUNWAY DISTURBANCE, MODIFIED GEAR, ACTIVE CASE (ALTERNATE CONCEPT)

4.5 Failure Detection Scheme

The object of the failure detection scheme is to assure that all failures will be detected and the system will revert to the passive mode.

Two parallel paths exist which have three detection points as shown on Figure 4-19. One path is the control path which includes one of the microprocessors, the servoamp, servovalve and the strut. The other path contains a model of the servoamp and servovalve and the other microprocessor. The model path includes a parallel pressure feedback path from one of the two pressure sensors. The three detection points are as follows:

a. Dual cross monitoring microprocessors
b. Model of the servovalve
c. Servovalve open coil monitor

The dual microprocessors constitute the only place where cross comparison exists. The microprocessors are synchronized and have a continuous bit-by-bit comparison, and any difference will cause a failure signal through the logic driver (LD) to the dual gates. This will initiate the reversion to the passive mode. The microprocessors also perform the failure detection function for the sensors. The sensors are all dual and each sensor feeds into the separate multiplexer (MUX) analog to digital (A/D) blocks. The MUX A/D's transmit the sensor information to both microprocessors. Each microprocessor processes the signal, determining if the sensor has failed and also calculates the average value between the dual sensors. The average value is used in calculating the command. Again, a failure signal to the dual gates will cause the system to revert to the passive mode.

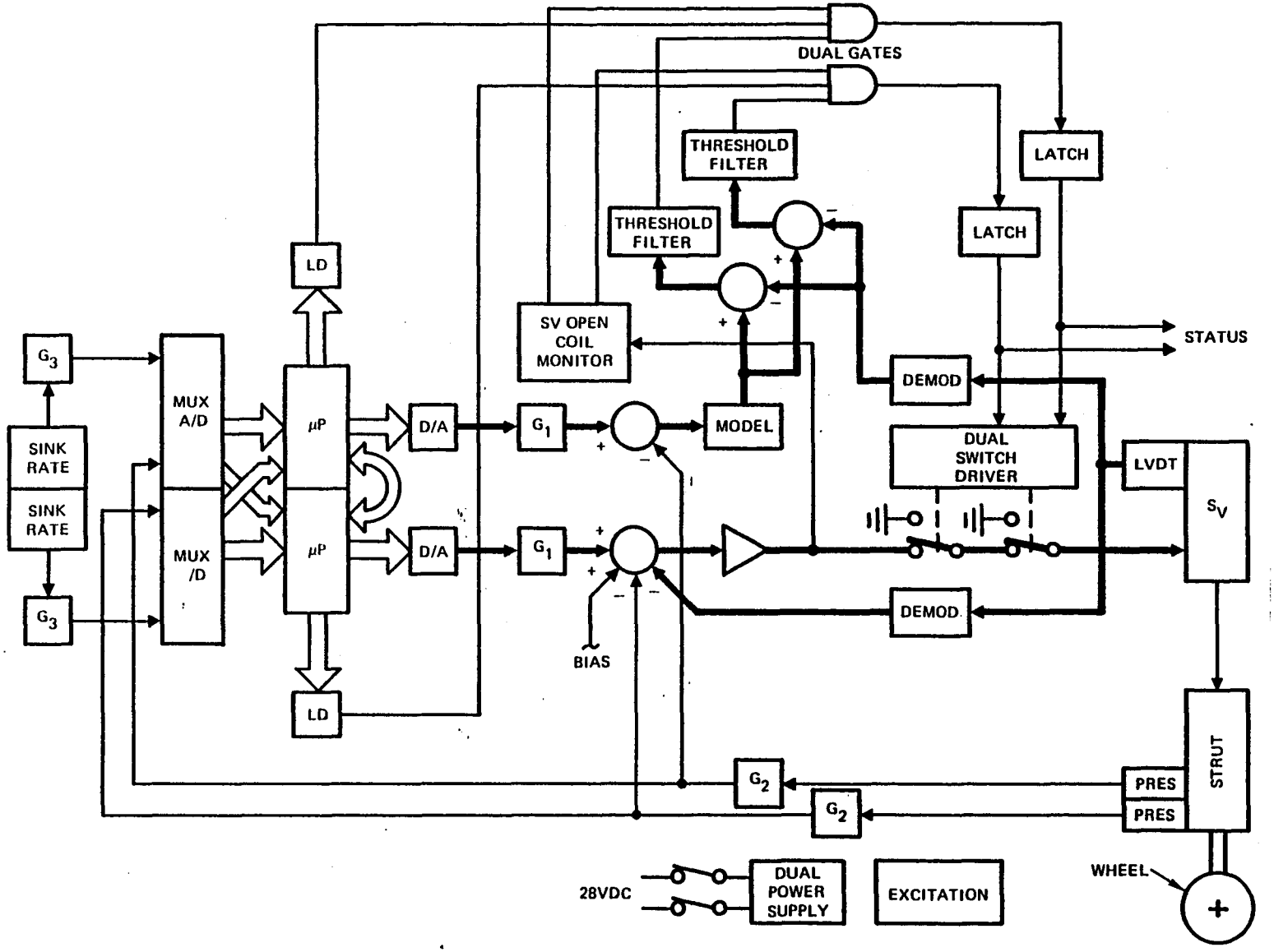

FIGURE 4-19. ALTERNATE CONTROLLER

The servovalve third stage has an LVDT to provide a signal proportional to its position and this signal is used in the feedback loop; it is also used to compare with the output of the model. Any failure of any component between the microprocessor and the servovalve LVDT will cause a disagreement between the model and the demodulated LVDT signal and a failure signal will be generated. A threshold and a filter are used to prevent nuisance trips.

It is noted that a pressure-sensor failure will be detected by both the model and the microprocessor.

The servovalve open coil monitor is used to detect a servovalve coil failure. During the pre-touchdown mode, the servovalve is approximately at the zero current position. A failure of the coil would not cause a significant change in servovalve position and the model would not detect the failure, therefore the open coil monitor is used. An open coil will be detected and a failure signal generated. This failure signal causes reversion to the passive mode and provides an indication supplied to the flight crew.

Both the second and third stage spools are spring loaded in the direction to block the cylinder port so that the gear reverts to the passive mode in the event of a power failure.

The system is mechanized so that the gates are normally high. If any signal into the gate goes low, a failure signal will be transmitted. The dual power supplies will be mechanized such that each gate is powered by a different supply. A failure of a power supply will therefore cause the system to revert to the passive mode.

The reversion to the passive mode is accomplished by the use of a biased torque motor, and a spring bias on the second and third stage spool. Either electric or hydraulic failure will result in the third stage spool going to the closed (blocked) position. This is accomplished by use of the dual switch driver in the servovalve command. On failure, the switch will open, thus opening the coil and the bias will cause the third stage spool to move in the proper direction, blocking the strut cylinder.

4.6 Reliability Assessment

The alternate concept active control landing gear incorporates a failure detection system which provides assurance that the gear will revert to the passive mode upon the occurrence of a failure, the passive mode being the unmodified configuration of the gear.

A previous reliability study on the A-10 landing gears has produced numbers for the catastrophic failure mode and these numbers will be used for comparison. It should be noted that the reliability numbers are those for the entire aircraft even though the report, in general, has concentrated on the main gear.

A system schematic with the items numbers is shown in Figure 4-20. A summary of the reliability numbers for this system is shown in Tables 4-1 and 4-2.

A block diagram of the system for a catastropic failure is shown in Figure 4-21. All items not included do not cause a catastropic failure and only fail to passive.

The total failure rate (FR) is computed as follows:

$$FR = [(9) + (11) + (18) + (19)]^2 + (SV)\ \text{hardover}$$

$$+ (3\text{rd Stage})\ \text{stuck} + (\text{spring})\ \text{fracture} + (\text{gear \& tire})$$

The items are as follows:

	$\lambda \times 10^{-6}$
(9) Gate	.304
(11) Latch	.30
(18) Comparator	.264
(19) SW Driver	.13
	$.998 \times 10^{-6}$ or 9.96×10^{-13}
SV Hardover	$10 \times 10^{-6}(.05)$ $.50 \times 10^{-6}$
3rd Stage	$1. \times 10^{14}$
Spring	.05
Sub-total	$.55 \times 10^{-6}$
Three Per Aircraft	1.65×10^{-6}
Gear & Tire	5912.1×10^{-6}
Total	5913.75×10^{-6} Failures/HR
MTBF	169.10 HR

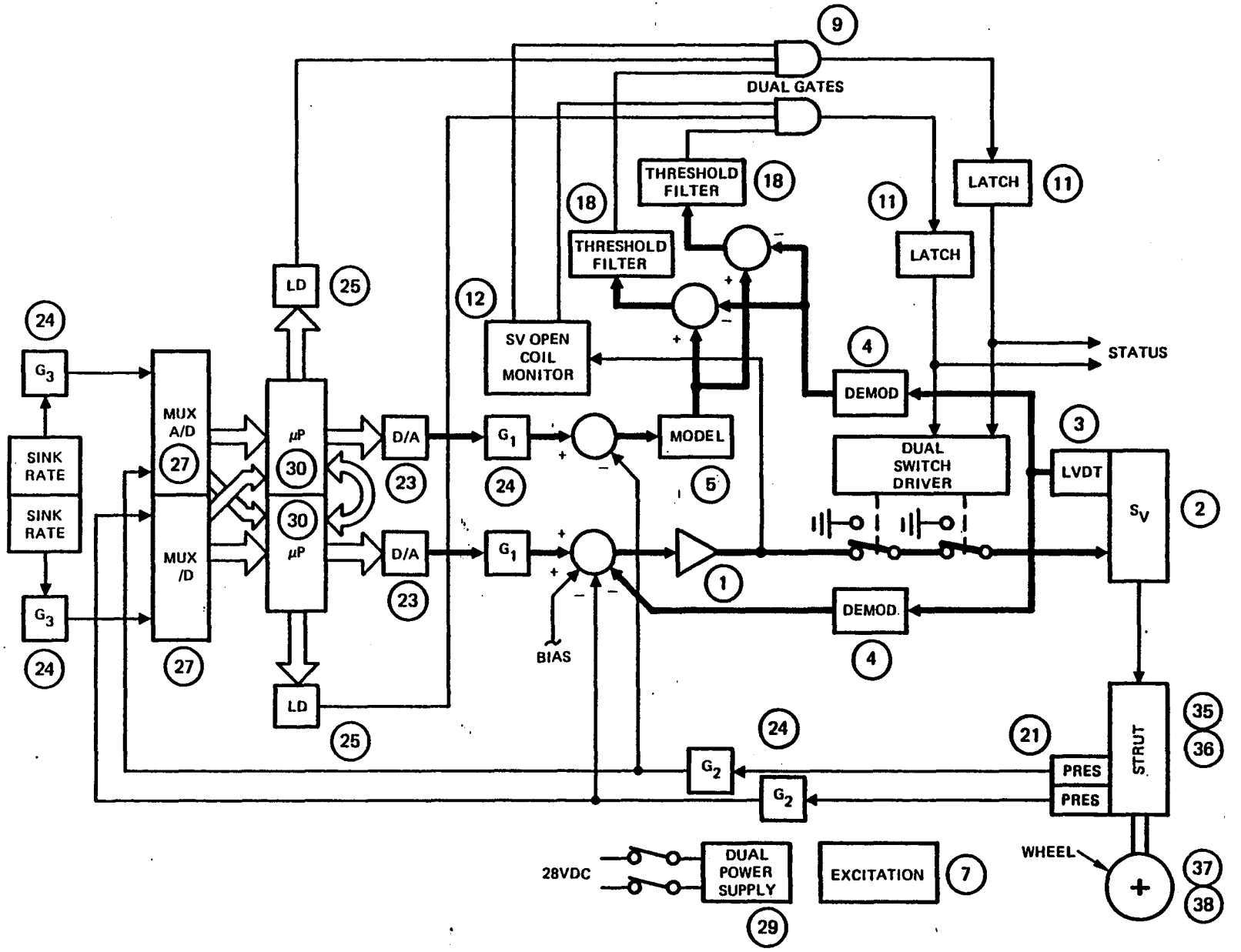

FIGURE 4-20. SYSTEM SCHEMATIC

TABLE 4-1. RELIABILITY TRADE STUDY

BASELINE PRODUCTION A-10		HR TEXTRON ACTIVE CATASTOPIC FAILURE		ITEMS
FR** X10-6	MTBF*** (HRS)	FR X10-6	MTBF (HR)	
526.51	1899.29	526.51	1899.29	NOSE L/G
1318.12	758.66	1318.12	758.66	TIRE NOSE L/G
1214.83	823.00	1214.83	823.00	MAIN L/G
2852.64	350.55	–	–	TIRE L/G
–	–	2852.64	350.55	HFT (MAIN L/G)
–	–			
–	–	1.65	606060	ACTIVE
5912.10	169.14	5913.75	169.0	NET

**FR = FAILURE RATE
***MTBF = MEAN TIME BETWEEN FAILURES

TABLE 4-2
COMPONENT FAILURE RATES

ITEM NO.	COMPONENT	FAILURE RATE ($x10^{-6}$/HR)	NO. REQ'D	TOTAL ($x10^{-6}$/HR)
1	SERVO AMP	.175	1	.175
2	SERVOVALVE	10.0	1	10.
3	LVDT/SV	.0112	1	.0112
4	DEMOD	.48	2	.96
5	MODEL	.876	1	.876
7	EXCITATION	.10	2	.20
9	GATE	.304	2	.608
11	LATCH	.30	2	.60
12	MONITOR	.304	1	.304
18	COMPARATOR	.264	2	.528
19	SW DRIVER	.13	2	.26
21	PRESS/SENSOR	.416	2	.832
23	D/A	1.084	2	2.168
24	FILTER	.144	6	.864
25	LOGIC DRIVER	.42	4	1.68
27	MULTIPLEXER	8.00	2	16.0
29	POWER SUPPLY	.40	2	.80
30	MICROPROCESSOR	200.	2	400.00
35	NOSE L/G	526.51	1	526.51
36	MAIN L/G	607.42	2	1214.83
37	TIRE NOSE	1318.12	1	1318.12
38	TIRE MAIN (HFT)	1426.32	2	2852.64

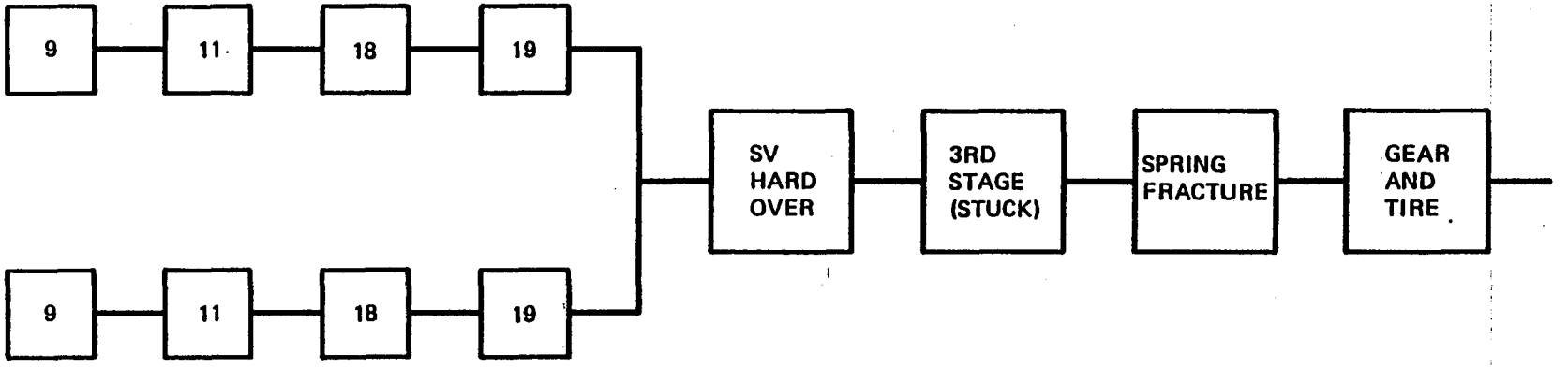

NOTE:

1. ALL OTHER FAILURES ARE DETECTED & SYSTEM REVERTS TO PASSIVE.
2. FOR A JET PIPE SERVOVALVE THE FAILURE RATE FOR A HARD OVER FAILURE (MAX. ΔP AT CYLINDER PORTS) IS ASSUMED TO BE 5% OF THE TOTAL FAILURE RATE.

FIGURE 4-21. RELIABILITY BLOCK DIAGRAM

5.0 DYNAMIC ANALYSIS OF THE ORIGINAL ACTIVE CONTROL LANDING GEAR CONCEPT

5.1 Introduction

This section presents the dynamic analyses that were performed for the development of an electrohydraulic active control system for the A-10 landing gear. The main objective of these analyses was to develop a loop compensation network for the active control landing gear concept applied to the A-10 aircraft and to evaluate the performance of the active control gear with respect to the passive (conventional) A-10 landing gear.

The active control concept addressed in this section essentially utilizes a high flow, high response electrohydraulic servovalve to meter fluid into or out of the landing gear shock strut cylinder from external hydraulic supply and return sources in order to minimize the transient forces transmitted to the wing/aircraft structure through the gear. This concept typically requires a hydraulic power source consisting of high flow pumps and/or accumulators.

Section 5.2 describes the analytical tools used in these studies, which are the linear and nonlinear vertical drop dynamic simulation models of the landing gear, without aircraft equations of motion included. Section 5.3 presents the correlation between the linear and nonlinear simulations, Section 5.4 presents the development of the loop compensation network and Section 5.5 presents transient results for specific landing impact cases and cases of rollout over runway disturbances, using the nonlinear vertical drop model, for both the passive gear and the active control gear.

5.2 Concept Description

As previously described, the ACLG replaces the fixed volume of hydraulic fluid in the hydraulic side of the strut with a variable volume, controlled by a servovalve in a closed loop configuration. The servovalve allows fluid to be removed from the strut when the sensed wing/gear interface force is excessive and to be supplied to the strut when the sensed forces are too low. Thus the servoloop attempts to maintain the wing/gear interface force at the level appropriate for the particular phase of the landing regime.

5.3 Dynamic Simulation Math Models

The main analytical tools used in these studies are the linear (s-domain) and nonlinear (time domain) dynamic simulation models of the landing gear, which simulate motion in the vertical axis only. Aircraft multi-dimensional equations of motion are not included. However, the overall aircraft weight minus lift (per gear) in the vertical axis is simulated as an input.

5.3.1. Nonlinear Model

The nonlinear model is developed from the time-dependent algebraic and differential equations of the system. The response of the system to input disturbances is obtained by integrating the differential equations with respect to time. Controller laws (including switching logic) and all other identifiable nonlinear attributes of the system of significance are simulated. Thus, the nonlinear model represents a more accurate simulation of the actual physical case than the linear model. This however, comes at the expense of considerably longer computational times. The

nonlinear model accepts input variations in airplane lift, ground level, and command limit force (for vertical drop impact transients, however, the controller automatically sets the command limit force subsequent to initiation of active control). A detailed description of the equations and controller logic comprising the nonlinear model is as follows.

Dynamic Equations

Figure 5-1 shows a schematic of the active control landing gear system (without loop closure and controller electronics) for reference in writing the dynamic equations. A force balance on the airplane mass including the upper portion of the landing gear shock strut gives

$$MU \frac{d^2XWG}{dt^2} = P1(A1-AP) + P2 \cdot AP - P3 \cdot A3 - MU \cdot g + FL \pm f \qquad (1)$$

A force balance on the lower portion of the shock strut (piston and tire) gives

$$ML \frac{d^2XA}{dt^2} = - P1(A1-AH) - P2 \cdot AH + P3 \cdot A3 - ML \cdot g + FA \pm f \qquad (2)$$

where the tire force is

$$FA = \begin{cases} KTIRE(XA - XG)^{ATIRE} & \text{for } XA > XG \\ 0 & \text{for } XA < XG \end{cases} \qquad (3)$$

The force transmitted through the wing/gear interface structure is of interest, and is determined by performing a force balance on the airplane mass not including the upper portion of the shock strut. Referring to Figure 5-2,

$$M \frac{d^2XWG}{dt^2} = FWG + FL - M \cdot g = FACC \tag{4}$$

The wing/gear interface force (FWG) is calculated from this equation, where $\ddot{XWG}$ is obtained from equation (1).

The pressure-volume relationships for the oil and gas in the shock strut are derived in the following manner. Referring to Figure 5-1, conservation of mass applied to the oil in the upper chamber (volume V1) gives

$$\frac{V1}{\beta} \frac{dP1}{dt} = - QO \pm QPV - (A1 + AP) \frac{dXS}{dt} \tag{5}$$

where

$$V1 = V1_i + A1 \cdot XS + VPIN \tag{6}$$

and where VPIN is described later.
For the oil in the rebound chamber (volume V3), conservation of mass gives

$$\frac{V3}{\beta} \frac{dP3}{dt} = QO23 + A3 \frac{dXS}{dt} \tag{7}$$

where

$$V3 = V3_i - A3 \cdot XS \tag{8}$$

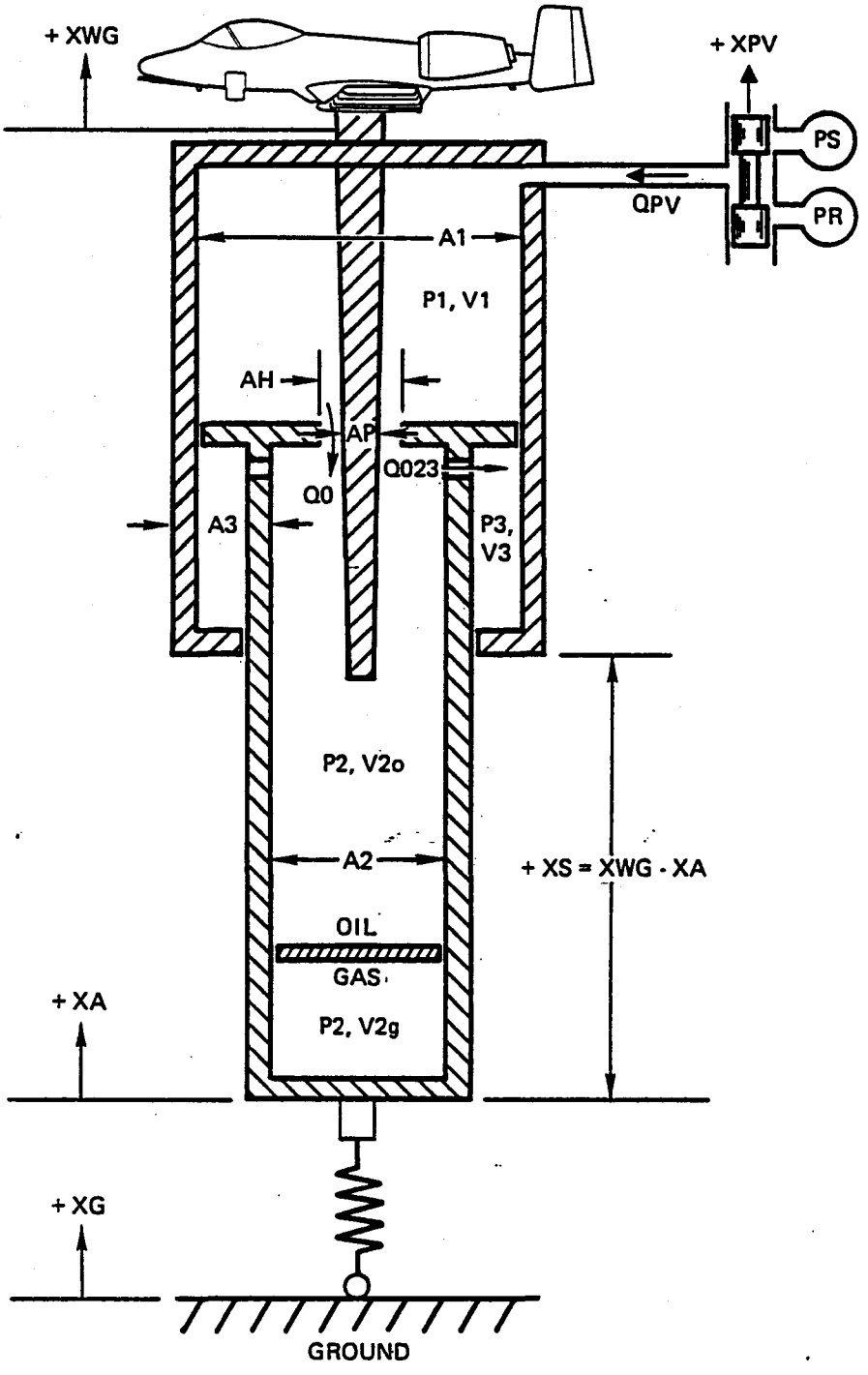

FIGURE 5-1. SCHEMATIC OF ACTIVE CONTROL LANDING GEAR SYSTEM

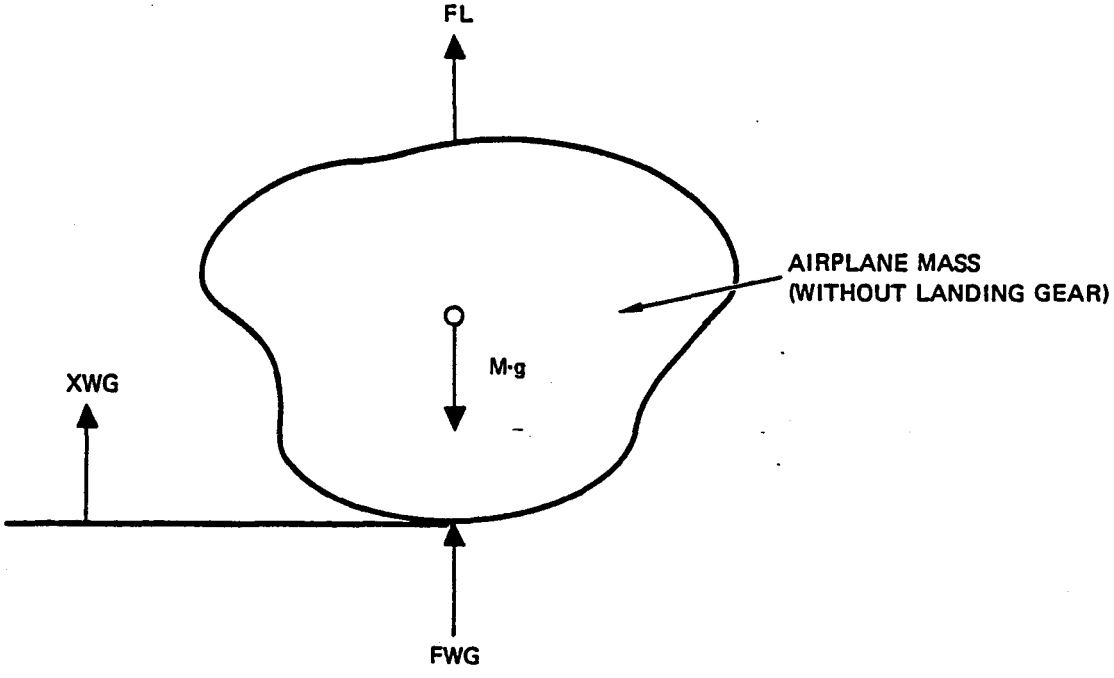

FIGURE 5-2. FORCES ACTING ON THE AIRPLANE MASS

To avoid ending up with a differential equation for the rebound pressure P3, which typically occupies a relatively small oil volume, the compressibility effect in equation (7) is neglected, thus, equation (7) becomes

$$QO23 = - A3 \frac{dXS}{dt} \tag{9}$$

For the oil portion in the lower strut (volume V2o), conservation of mass gives

$$\frac{V2o}{\beta} \frac{dP2}{dt} = QO - QO23 + \frac{dV2g}{dt} - AP \frac{dXS}{dt} \tag{10}$$

where

$$V2o = V2_i - V2g - VPIN - A3 \cdot \bar{XS} \tag{11}$$

Note that the volume V2o is written to include the volume of oil in the rebound chamber. This is to compensate for the fact that the oil compressibility in the rebound chamber was neglected in equations (9). The term VPIN represents the volume of oil displaced in the lower chamber (from the fully-extended strut condition) by the metering pin or tube which protrudes through the hole in the shock strut plate, as a function of the stroke. For gears with tapered metering pins (as shown in Figure 5-1), where the pin cross sectional area at the hole is a function of stroke,

$$VPIN = - \int_{o}^{XS} AP \cdot dXS \tag{12}$$

Note that the fully extended reference condition is defined at XS = 0. The minus sign is due to the fact that xs becomes more negative as the strut collapses. The equation thus produces

positive values for VPIN, as desired. For gears with constant area metering tubes (as in the A-10 landing gear), VPIN is simply equal to - AP . XS.

For the gas portion in the lower cylinder, assuming an isentropic process,

$$P2 \cdot V2g^{\gamma} = \text{constant} \tag{13}$$

Thus,

$$\frac{dP2}{P2} + \gamma \frac{dV2g}{V2g} = 0$$

$$dV2g = -\frac{1}{\gamma} \frac{V2g}{P2} dP2 \tag{14}$$

where

$$V2g = V2g_i (P2_i/P2)^{1/\gamma} \tag{15}$$

Substituting equations (9) and (14) into equation (10):

$$\left(\frac{V2o}{\beta} + \frac{1}{\gamma} \frac{V2g}{P2}\right) \frac{dP2}{dt} = QO + (A3 - AP) \frac{dXS}{dt} \tag{16}$$

The pressures P1 and P2 are determined from the differential equations (5) and (16), respectively. Since oil compressibility in volume V3 is neglected, the pressure P3 is determined algebraically as follows: From the orifice flow equation,

$$QO23 = CO23(P2-P3)/\sqrt{|P2-P3|} \tag{17}$$

or,

$$P3 = P2 - \frac{Q023 \quad Q023}{C023^2} \tag{18}$$

The flow rate through the metering orifice is

$$QO = CO(P1-P2)/\sqrt{|P1-P2|} \tag{19}$$

Figure 5-3 shows a schematic of the inner servo loop. It consists of a servoamplifier driving a two-stage electro-hydraulic servovalve which drives a power valve with electrical position feedback to the servoamplifier input. Power valve displacement is thus proportional to command voltage. The two-stage servovalve consists of a first stage electrical torque motor-driven flapper nozzle valve driving a second stage four-way spool valve, which meters hydraulic fluid to the power valve.

As indicated in Figure 5-3, the dynamics of the two stage servovalve are simulated by relating input torque motor current to output spool position using a second order differential equation, which has been broken down so that the nonlinear effect of second stage saturation is simulated by limiting spool displacement, and first stage flapper saturation is simulated by limiting second stage spool velocity. The effects of a static null bias in spool position and servovalve hysteresis are also simulated. The dynamics of the power valve are simulated by integrating second stage servovalve flow to get power valve position. Thus, pressure dynamics are ignored in the inner loop simulation.

The power valve is a three-way spool/sleeve valve which meters supply and return pressure oil to and from the landing gear upper cylinder.

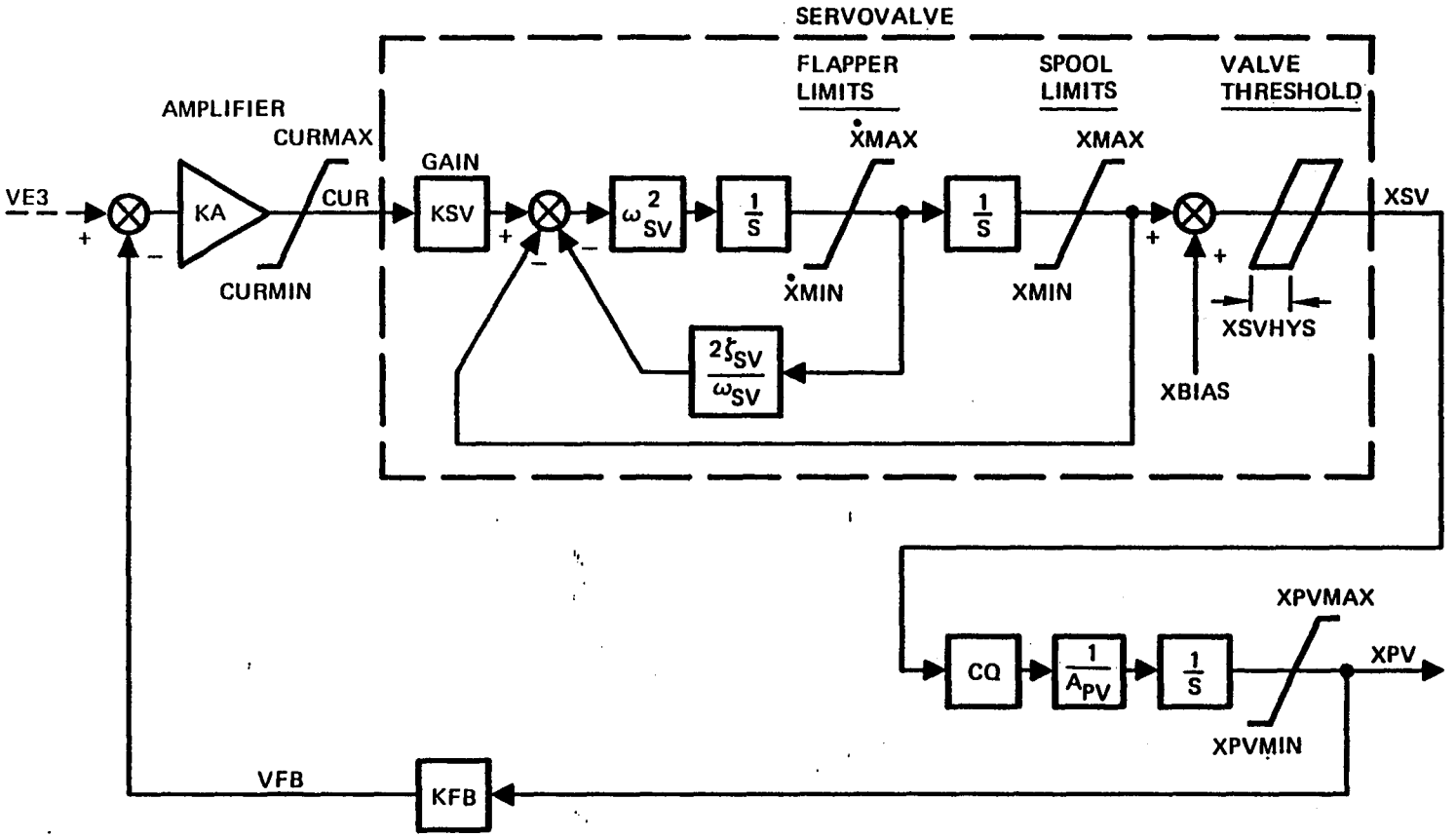

FIGURE 5-3. INNER LOOP SCHEMATIC OF TWO STAGE SERVOVALVE DRIVING A POWER VALVE WITH ELECTRIC POSITION FEEDBACK

The flows through the power valve are illustrated in Figure 5-4. They are calculated in the nonlinear simulation as a function of spool displacement, the cylinder pressures, the supply and return pressures, fluid properties, and the spool valve geometry (i.e., window widths, window lengths, spool/sleeve clearance, spool diameter, overlap and/or underlap lengths). The method utilizes sharp-edge orifice equations and equations for flow between concentric cylinders, with entrance region effects taken into account. Reynolds number effects (i.e., laminar, transitional, and turbulent flow considerations) are accounted for.

Figure 5-5 shows a schematic of the outer loop closure, which consists of a force loop and a strut stroke loop. Forward path compensation is also indicated in the figure. The force loop closure is comprised of a command limit force signal and a feedback force signal obtained from an accelerometer mounted on the upper mass (airplane). The strut stroke loop closure is comprised of a strut stroke command signal and a feedback signal obtained from a LVDT mounted on the landing gear strut. The strut stroke loop is a very low bandwidth loop and merely serves the purpose of preventing low frequency drift in strut stroke during airplane rollout.

Controller Logic

The main function of the electronic controller is to control the command limit force input to the active control servo loop. For initial landing impacts, the controller does this automatically by monitoring the kinetic energy to be dissipated in the system along with the available work potential of the

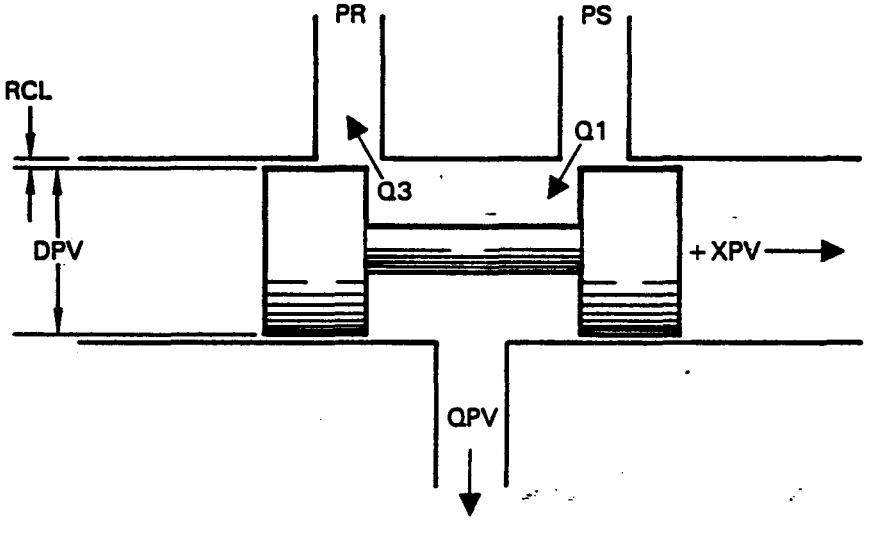

FIGURE 5-4. POWER VALVE

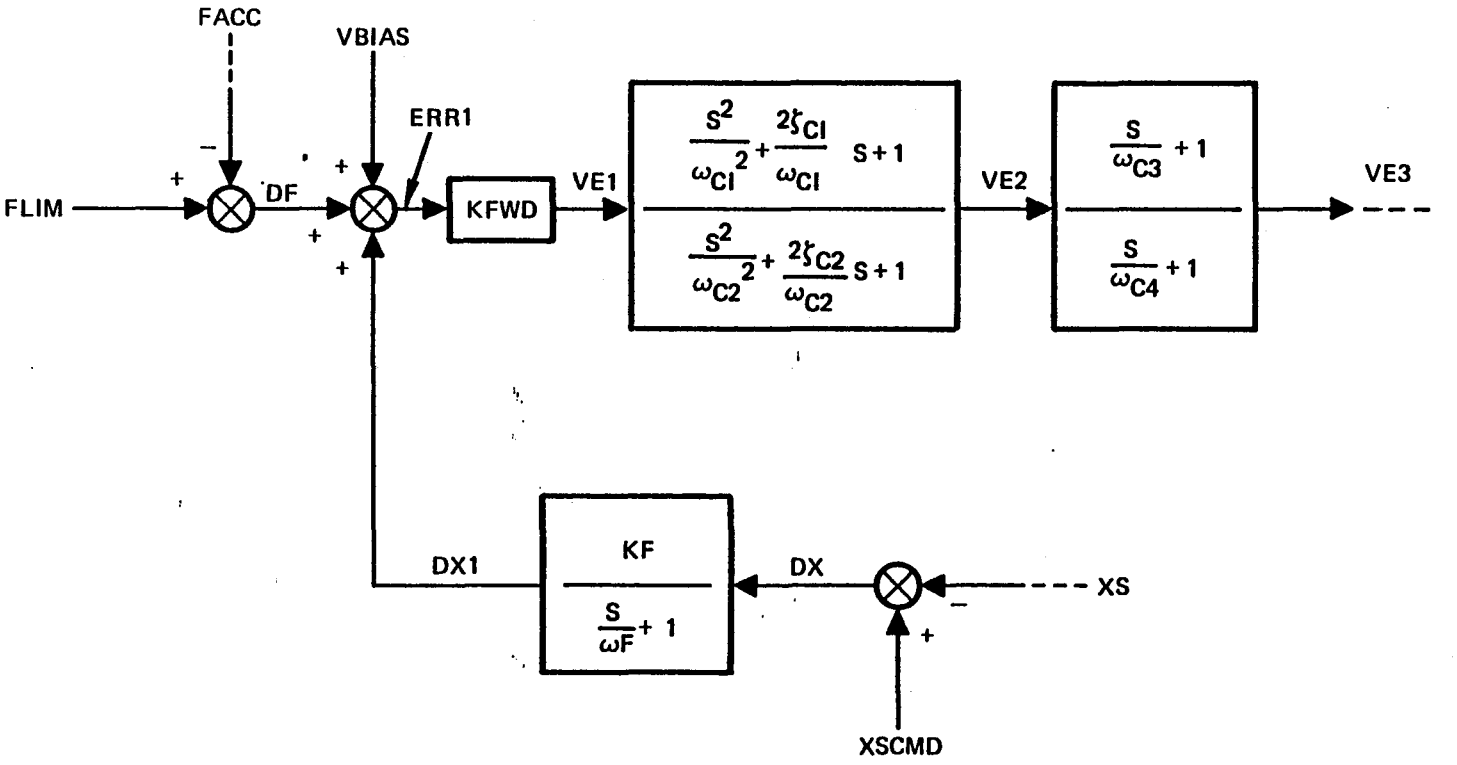

FIGURE 5-5. OUTER LOOP CLOSURE AND COMPENSATION SCHEMATIC

shock strut. The controller sets the limit force accordingly so that the work potential is sufficient to absorb the remaining kinetic energy, thus preventing bottoming of the strut, precluding structural damage.

A landing impact is characterized by four phases as far as the controller is concerned:

a. An initial passive phase which exists from the instant of impact until the time when the controller determines that the active control servo loop should be turned on,

b. The "impact phase", which starts the instant the servo loop is turned on and during which the limit force is set to a constant value,

c. The "transition phase", during which the command limit force is linearly decreased from its impact value to its rollout phase value, and

d. The "rollout phase", which occurs after all the initial kinetic energy has been absorbed, and during which the command limit force remains constant at a value of zero.

The rollout phase remains in effect as long as the aircraft is significantly in motion so that the effect of runway disturbances will continue to be actively controlled.

The controller has available as inputs the upper mass accelerometer signal, from which changes in upper mass velocity, and hence kinetic energy, can be obtained, and the shock strut potentiometer signal, from which the remaining stroke, and hence work potential, of the gear can be determined. At the start of an initial landing impact, the system is in a passive gear mode; that is, the servo loop is turned off with the power valve isolated from the strut. The controller continually calculates the current system kinetic energy and the total remaining shock strut work potential from the equations

$$\text{KINETIC ENERGY} = 1/2\ M \cdot \dot{XWG}^2 \tag{20}$$

$$\text{WORK POTENTIAL} = FWG \cdot {}_{\Delta}XS \tag{21}$$

where ${}_{\Delta}XS$ is the remaining stroke of the shock strut. FWG in equation (21) can be determined by solving the differential equation (4). M is the mass of the airplane per gear. When the work potential exceeds the kinetic energy, the controller initiates active control of the servo loop and calculates the impact phase command limit force from the equation

$$FLIM_{im} = 1/2M \cdot \dot{XWG}^2 / {}_{\Delta}XS \tag{22}$$

which results from equating the work potential with the kinetic energy. The controller at this time also computes the upper mass

velocity that will exist at the start of the transition phase from the equation

$$V_{tr} = \frac{FLIM_{im}^2}{2 \cdot M \cdot R_s} \tag{23}$$

where R_s is the predetermined linear slope of the limit force with respect to time during transition. Equation (23) results from equating the impulse to the change in momentum for the transition phase.

5.3.2 Linear Model

The linear model simulates the dynamics of the active control landing gear system in the frequency domain for small perturbations about a condition where the airplane mass (per gear) is at rest on top of the gear with the gear in contact with the ground and with the lower cylinder hydraulic pressure at a value halfway between the hydraulic supply and return pressures. The input disturbance variables are command limit force, airplane lift, and ground level. Also, the pressure variable P3 is assumed to be equal to P2 at all times. The linear model is a valuable tool since it allows rapid evaluation of system modifications or the effect of variation in system parameters in the areas of system stability and frequency response. The equations which comprise the linear model are as follows:

From equations (1) and (2), the linearized equations of motion for the upper and lower masses are, respectively,

$$XWG = \frac{(A1 - AP)P1 - (A3 - AP)P2}{MU \cdot S^2} \tag{24}$$

$$XA = \frac{-(A1 - AH)P1 + (A3 - AH)P2 + KT \cdot XG}{ML \cdot S^2 + KT} \tag{25}$$

In deriving these equations, the pressure P3 has been assumed to be equal to P2.

The flow through the metering orifice is linearized as follows:

$$QO = CO \sqrt{P1 - P2}$$

$$d(QO) = [CO/(2\sqrt{P_1 - P2})] \cdot [d(P1) - d(P2)]$$

$$\text{or } d(QO) = CPO[d(P1) - d(P2)] \tag{26}$$

where $$CPO = \frac{\partial QO}{\partial (P1 - P2)} = CO/(2\sqrt{P1 - P2}) \tag{27}$$

The flows through the three-way power valve are linearized as follows. Referring to Figure 5-4, for +XPV, the flow to the load is approximately equal to the flow Q1. Thus

$$QPV = Q1 = CPV \cdot XPV \sqrt{PS - P1}$$

Linearizing,

$$d(QPV) = \frac{\partial QPV}{\partial XPV} d(XPV) + \frac{\partial QPV}{\partial P1} d(P1)$$

$$= CPV \sqrt{PS - P1}\, d(XPV) - \frac{CPV \cdot XPV}{2\sqrt{PS - P1}} d(P1)$$

Linearizing about a condition where the cylinder pressure is midway between the supply and return pressures (i.e., P1 = (PS + PR)/2 , the previous equation can be expressed as

$$d(QPV) = CQPV\, d(XPV) - CPPV\, d(P1) \tag{28}$$

where $$CQPV = \frac{\partial QPV}{\partial XPV} = CPV \sqrt{(PS - PR)/2} \tag{29}$$

and $$CPPV = -\frac{\partial QPV}{\partial P1} = CQPV/PGPV \tag{30}$$

where PGPV is the slope of the power valve cylinder pressure versus stroke curve in the null region.

For -XPV it can be shown that equations (28), (29), and (30) still apply. Thus, they are valid for all XPV. This is true only because the flows were linearized about the condition where P1 is midway between PS and PR.

Linearizing the strut cylinder pressure equations (equations (5) and (16)) and eliminating the linearized metering orifice and power valve flows using equations (26) and (28), results in

$$P1 = \frac{CQPV \cdot XPV + CPO \cdot P2 - A1 \cdot S \cdot XS}{\frac{V1}{\beta} S + (CPPV + CPO)} \tag{31}$$

$$P2 = \frac{CPO \cdot P1 + A3 \cdot S \cdot XS}{\left(\frac{V2o}{\beta} + \frac{1}{\gamma}\frac{V2g}{P2}\right) S + CPO} \tag{32}$$

The dynamics of the two-stage servovalve are simulated by relating input torque motor current with output spool postion using a second order linear differential equation. Thus,

$$\frac{XSV}{i} = \frac{KSV}{\frac{S^2}{\omega sv^2} + \frac{2\xi sv}{\omega sv} S + 1} \tag{33}$$

The dynamics of the power valve are simulated by integrating second stage servovalve flow to get power valve position. Thus,

$$XPV = \frac{CQSV}{APV}\frac{1}{S} XSV \tag{34}$$

Equations (24), (25), (31), (32), (33), and (34), along with the appropriate loop closure and compensation relationships discussed in the nonlinear model section, comprise the linear model. A block diagram of the linear model is shown in Figure 5-6. The compensation discussed in Section 5.5 is included in the block diagram.

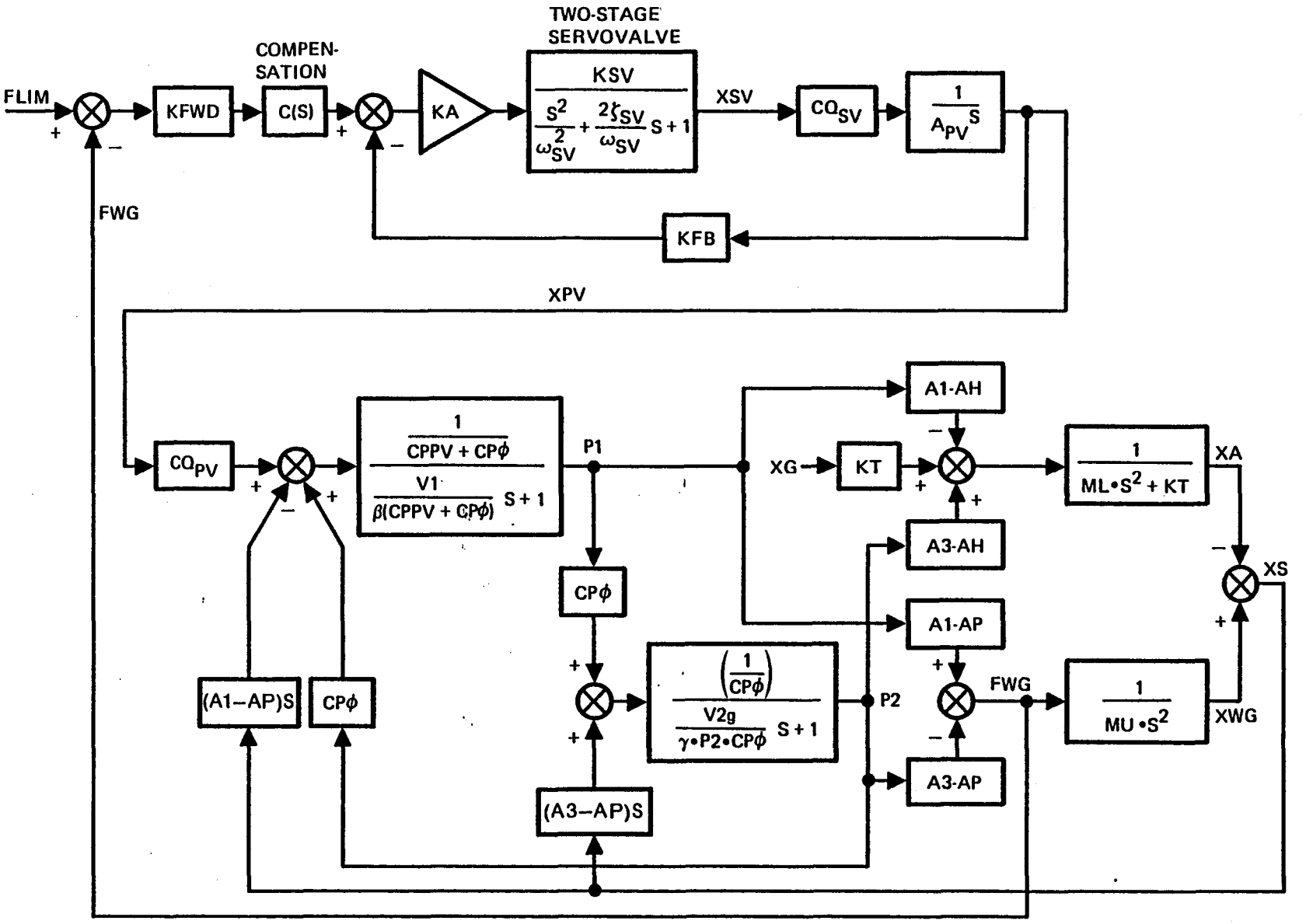

FIGURE 5-6. LINEAR MODEL BLOCK DIAGRAM

5.4 Correlation of Linear and Nonlinear Models

Since both the linear and nonlinear models were utilized in the development of the loop compensation, the first task was to correlate the linear model with the more precise nonlinear model to ensure that it would give at least reasonably credible results. Figures 5-7 and 5-8 show frequency response results obtained from the linear and nonlinear models, without compensation. The loop is opened at the point of wing/gear force feedback, and the strut position feedback loop is not included. The input is command limit force and the output is the wing/gear force response. The nonlinear runs were made with zero lift and for command amplitudes of ±4448. N (±1000. pounds), and the amplitude and phase angle at each frequency were computed from a Fourier analysis of the resultant input and output waveforms. The linear model results were obtained using a linearized orifice coefficient for the shock strut orifice (CP_o) of 0.9 $in^3/sec/psi$. This value seemed to give the best overall correlation between the linear and nonlinear models. Note that the agreement is reasonably good out to a frequency of about 150 Hertz. Figures 5-9 and 5-10 show open loop Nyquist diagrams for these same results, for the linear and nonlinear models, respectively.

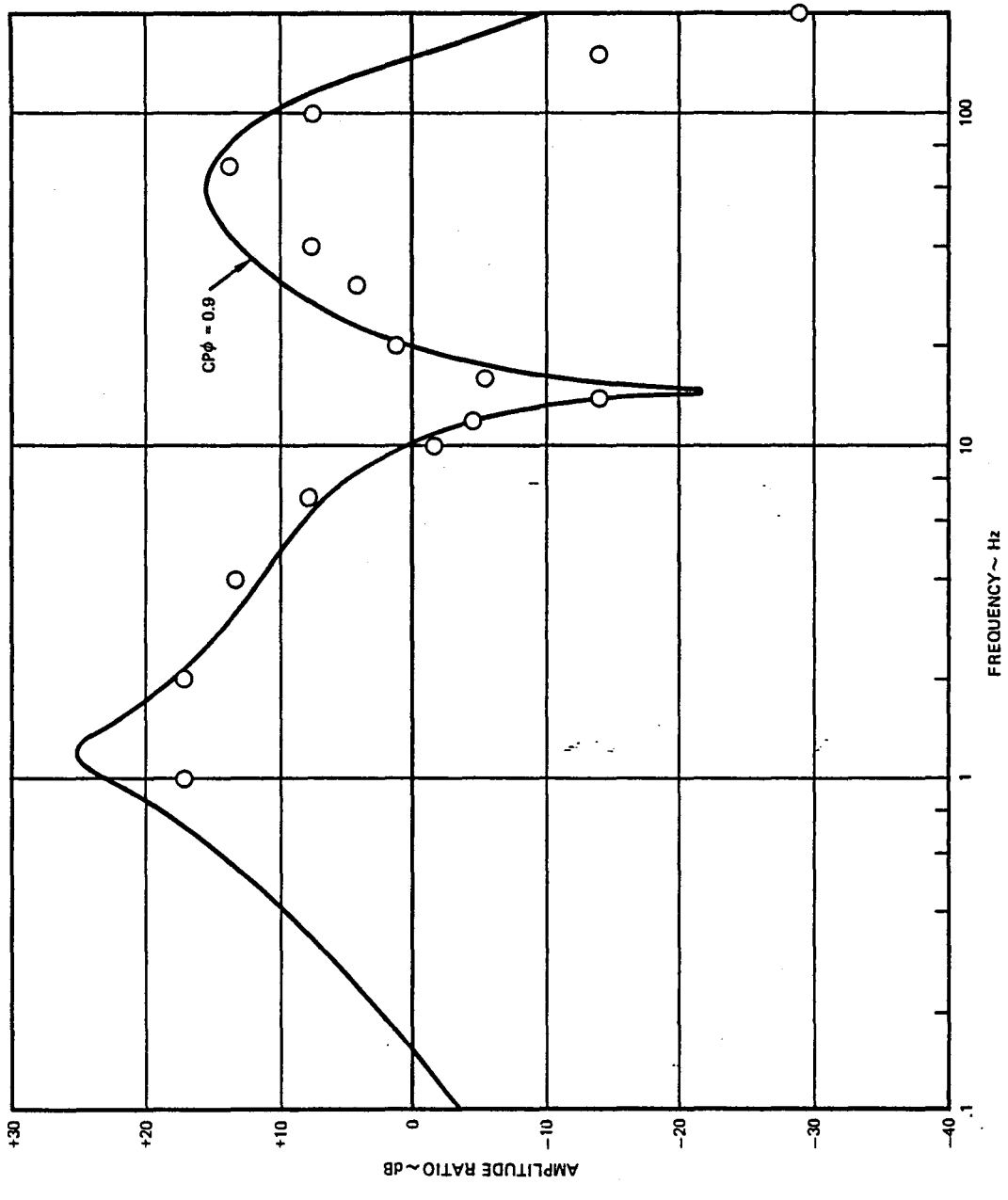

FIGURE 5-7. OPEN–LOOP, FREQUENCY RESPONSE, NO COMPENSATION

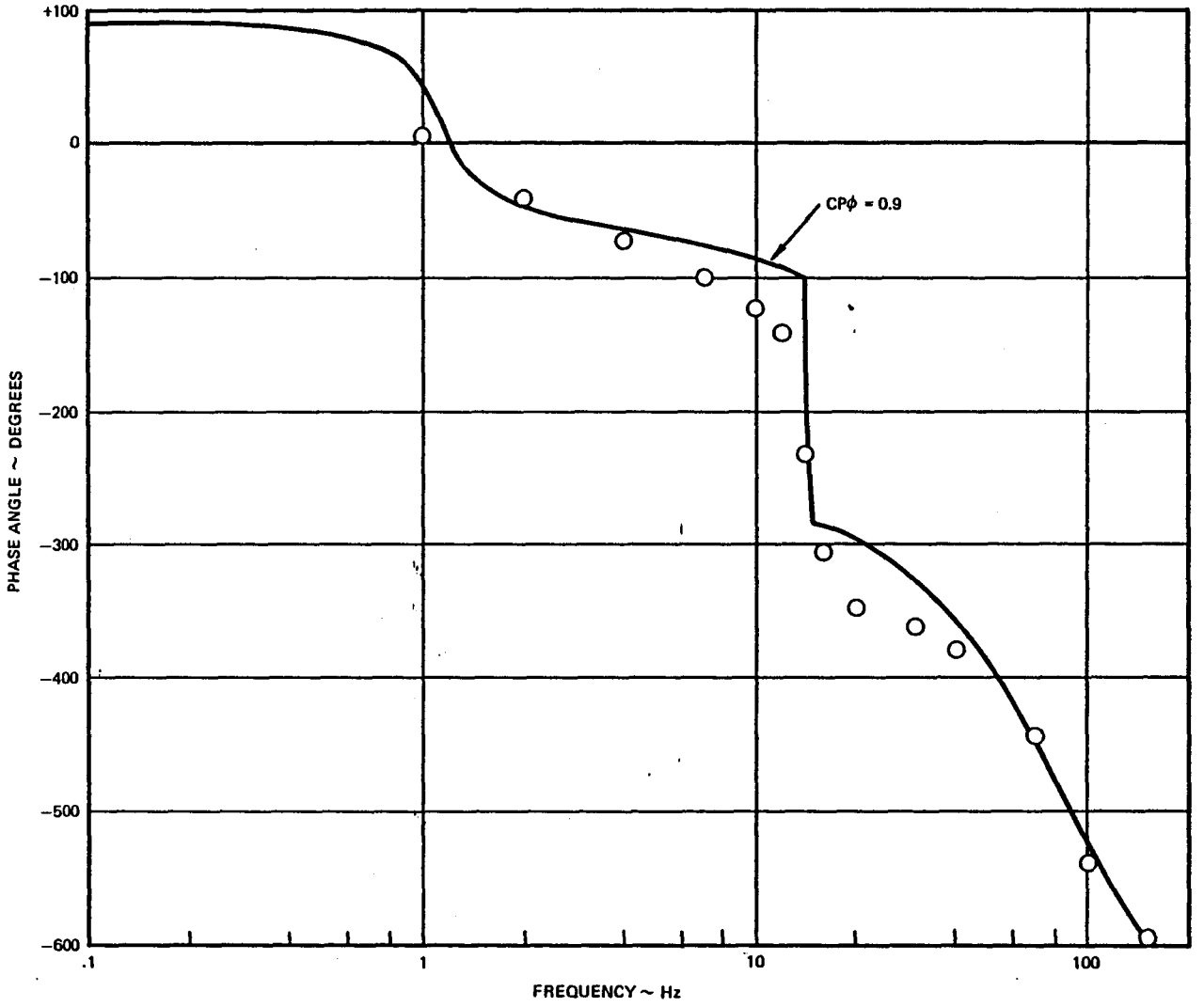

FIGURE 5-8. OPEN–LOOP, FREQUENCY RESPONSE, NO COMPENSATION

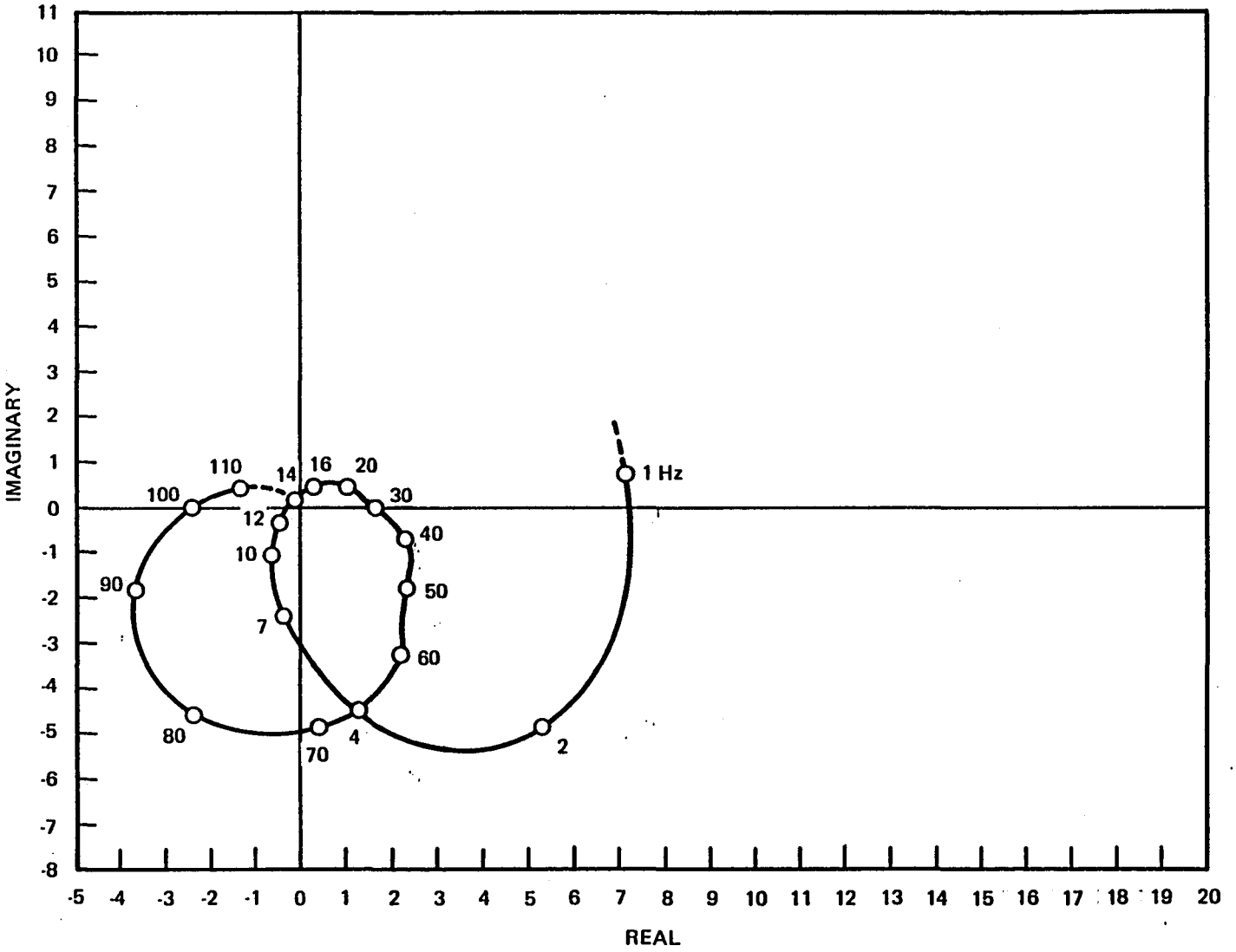

FIGURE 5-9. OPEN LOOP NYQUIST DIAGRAM (FACC/FLIM) FROM NONLINEAR MODEL, WITHOUT COMPENSATION.

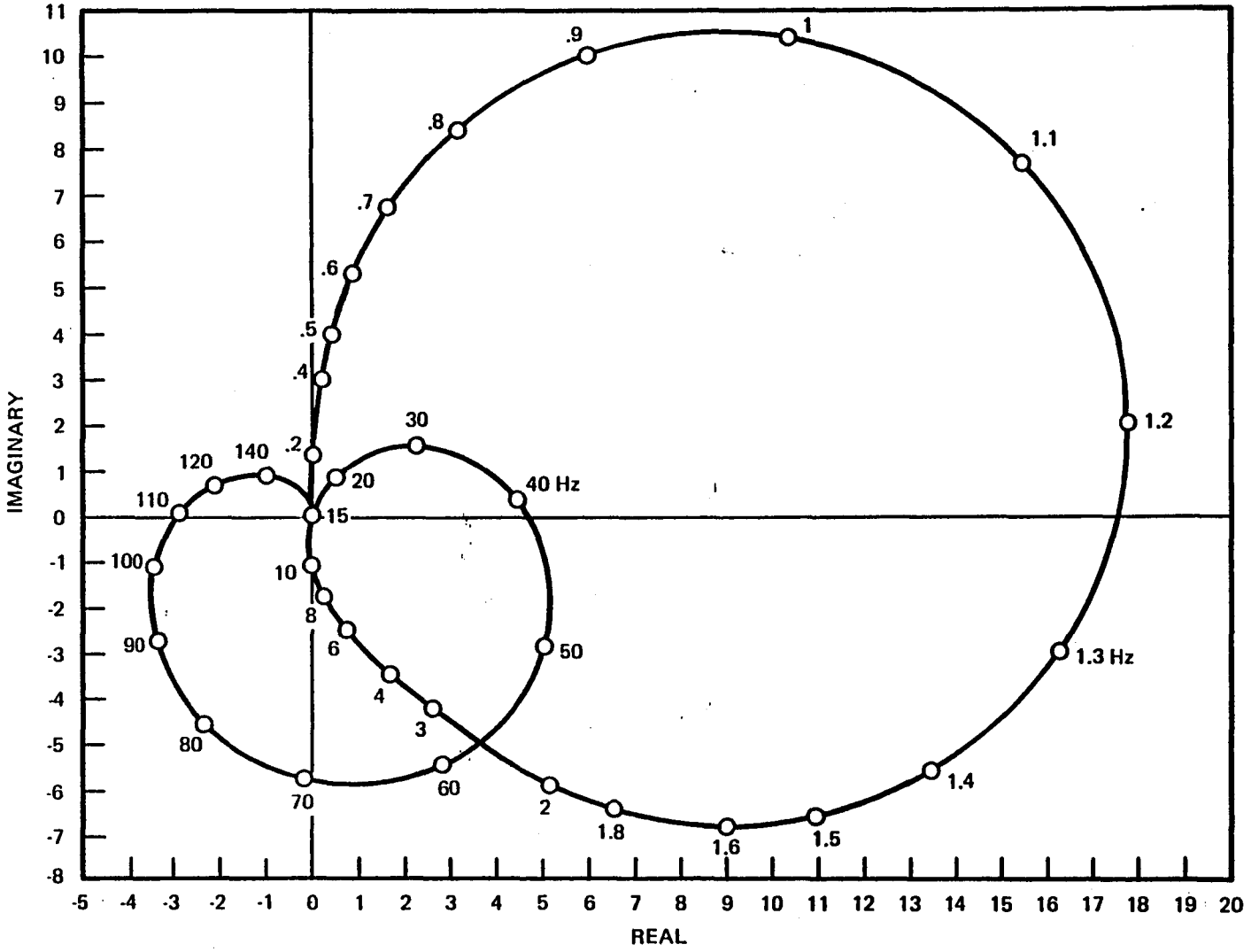

FIGURE 5-10. OPEN LOOP NYQUIST DIAGRAM (FACC/FLIM) FROM LINEAR MODEL, WITHOUT COMPENSATION.

5.5 Loop Compensation

The open-loop Nyquist diagrams of the uncompensated system presented in the previous section indicate that the system is unstable around 100 Hertz. Thus, compensation is deemed necessary. The compensation that was developed for this system is implemented in the forward path of the control loop, and has the following transfer function.

$$T(S) = \left[\frac{\frac{S^2}{628.^2} + \frac{2(.100)}{628.}S+1}{\frac{S^2}{628.^2} + \frac{2(5.00)}{628.}S+1}\right] \cdot \frac{\frac{S}{129.7}+1}{\frac{S}{1297.}+1} \qquad (3\text{-}1)$$

It consists of a notch filter at 100 Hertz and a first-order 20 dB lead/lag network. The frequency response of the compensation is shown in Figures 5-11 and 5-12 and the Nyquist plot including compensation is shown in Figure 5-13.

To understand the effect of each part of the compensation network on system dynamics, open-loop Nyquist diagrams obtained from the linear model are presented with successive portions of the compensation network incorporated. Figure 5-9 (from the previous section) shows the uncompensated Nyquist diagram. Figure 5-14 shows the effect of including the compensation notch only. The system is now stable, but rather low damped at a frequency around 65 Hertz. The lead/lag network was included to add phase lead in this frequency range. The Nyquist diagram with the notch and lead/lag incorporated is shown in Figure 5-15.

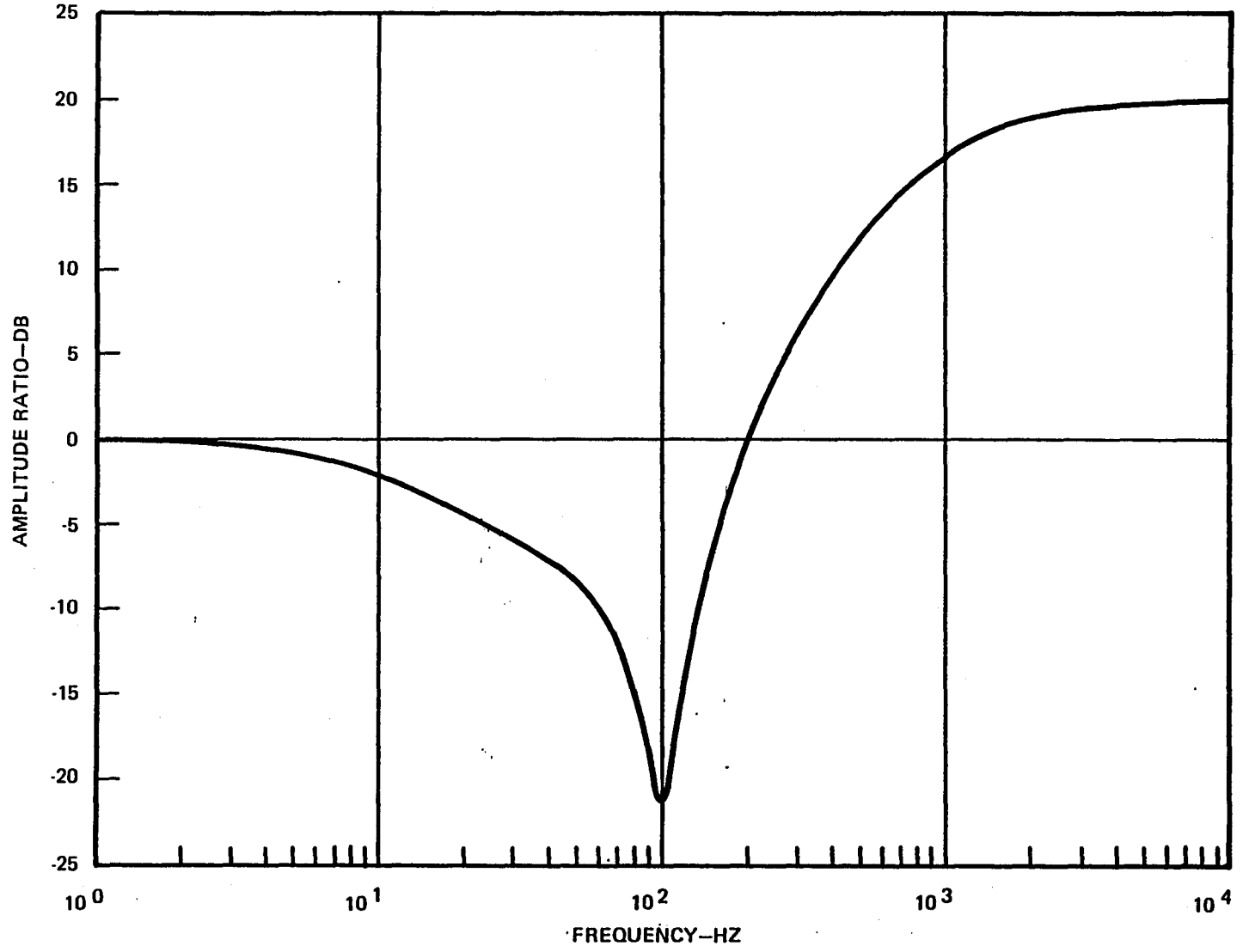

FIGURE 5-11. FREQUENCY RESPONSE OF COMPENSATION (AMPLITUDE)

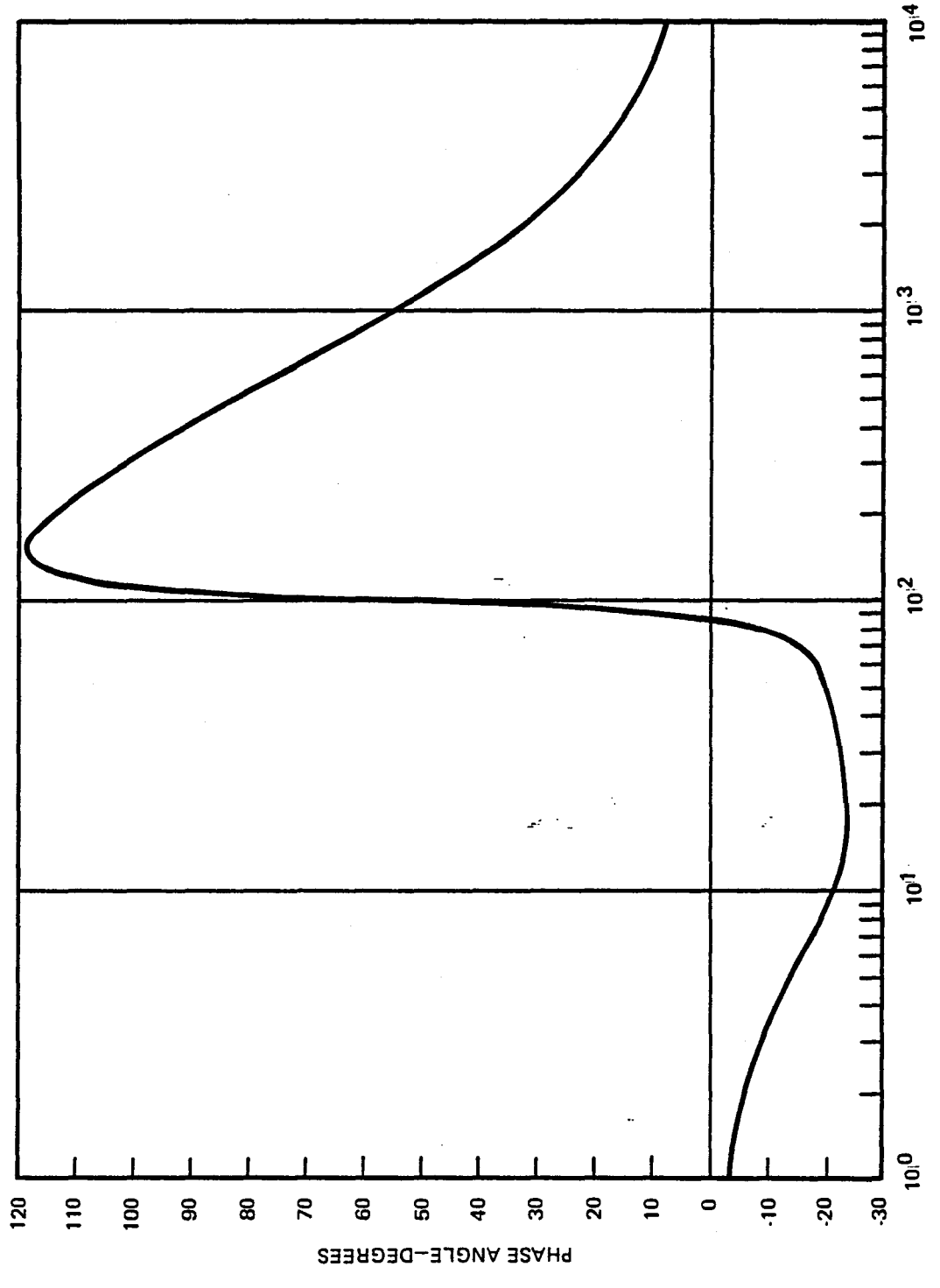

FIGURE 5-12. FREQUENCY RESPONSE OF COMPENSATION (PHASE)

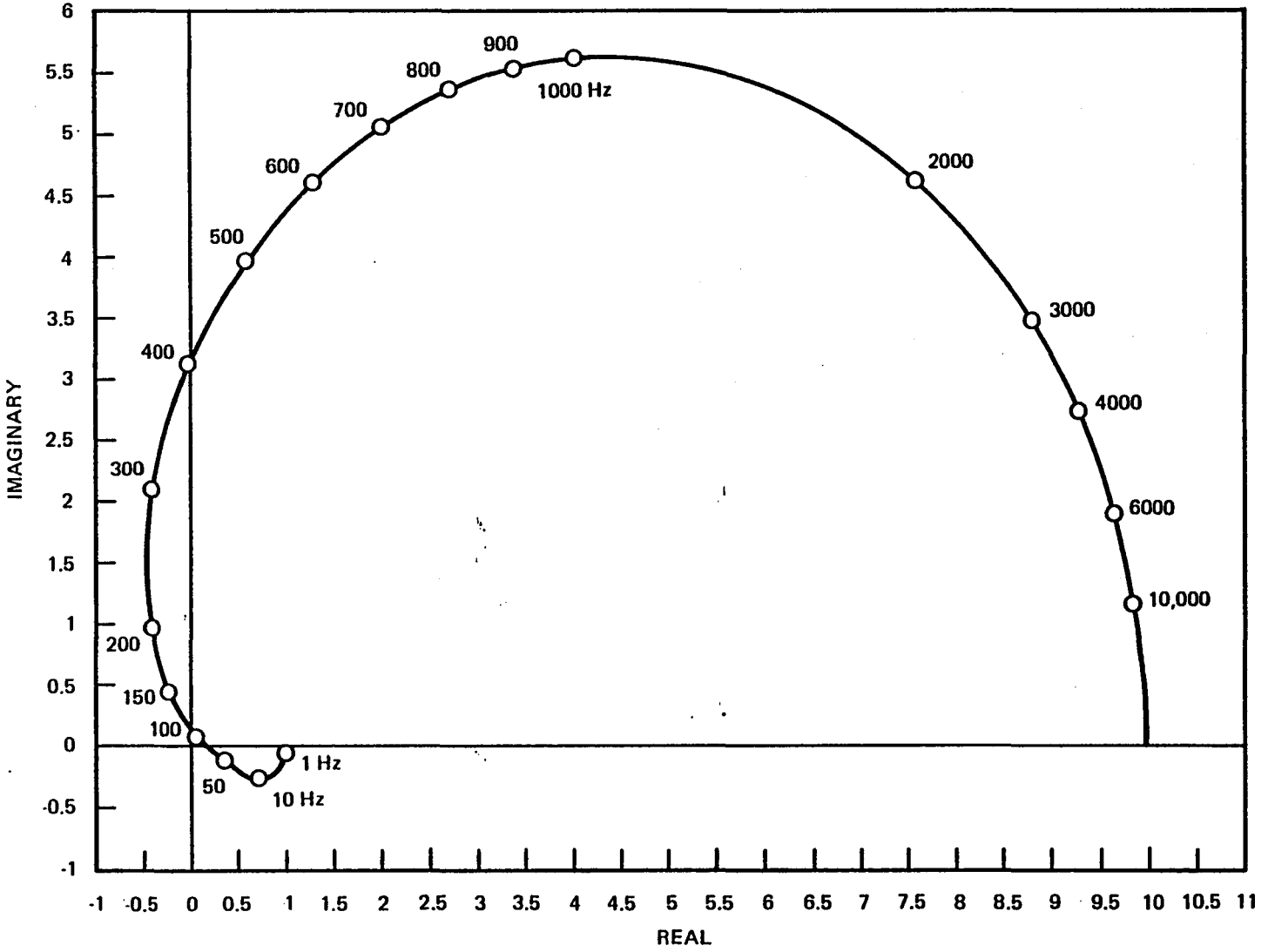

FIGURE 5-13. NYQUIST PLOT OF COMPENSATION

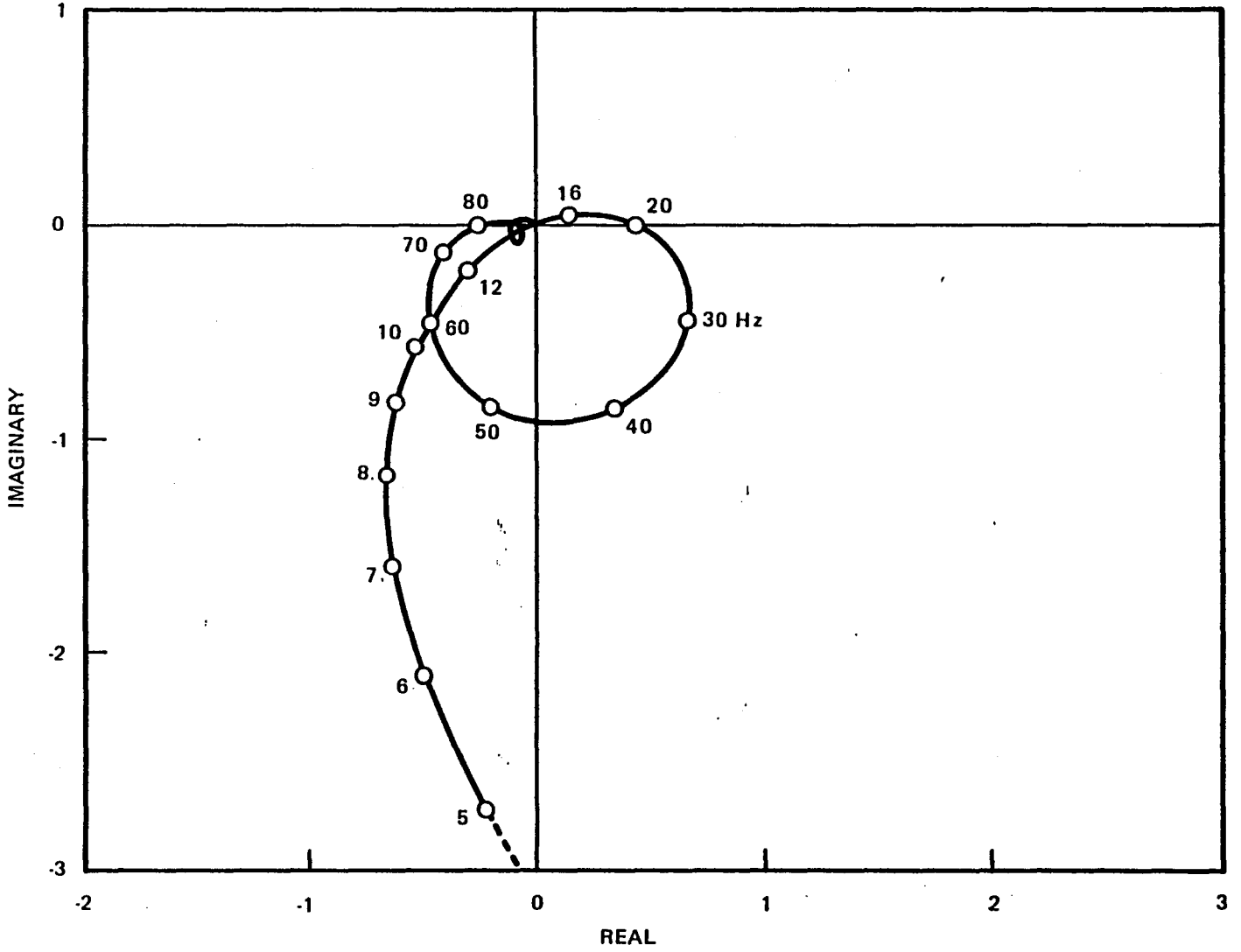

FIGURE 5-14. SYSTEM NYQUIST PLOT (FACC/FLIM) (COMPENSATION CONSISTS OF NOTCH ONLY)

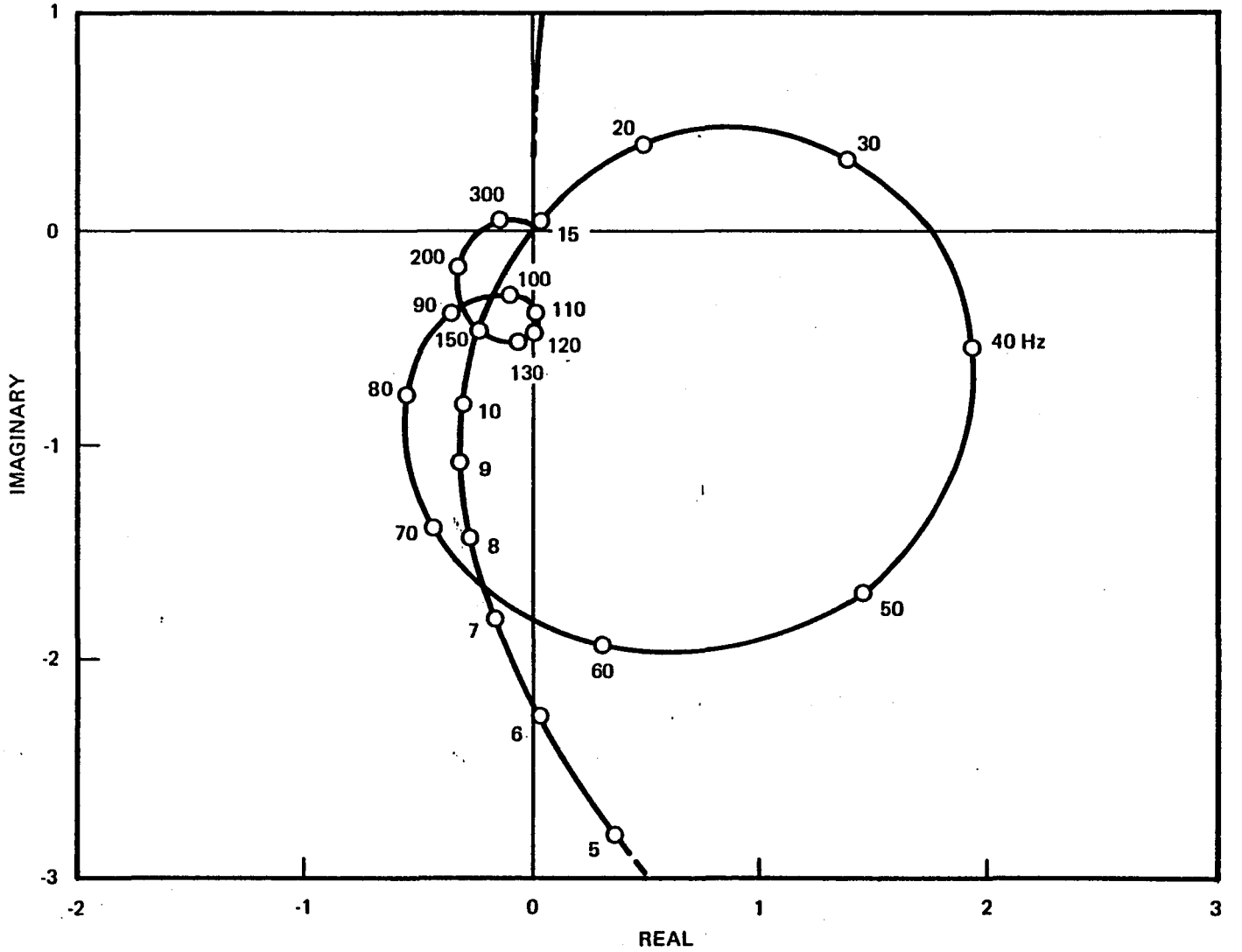

FIGURE 5-15. SYSTEM NYQUIST PLOT (FACC/FLIM) (COMPENSATION CONSISTS OF NOTCH & LEAD/LAG)

The effect of each part of the compensation network on system dynamics was also evaluated using the nonlinear model on a typical vertical drop case. The conditions of the case are (1) the sink rate prior to impact is 2.54 m/sec (100 in/sec); (2) the lift is equal to airplane weight at initial impact, then linearly reduced to 10 percent of the airplane weight over the next 1 second, then held constant at 10 percent thereafter; and (3) the ground level is held constant.

Figure 5-16 shows the resultant force transients when the compensation consists of the notch only. The results show that the notch basically stabilizes the system; however, note the presence of the 65 Hertz oscillations. Figure 5-17 shows the results for the same case except with the entire compensation (notch and lead/lag) incorporated. Note that the lead/lag is effective in eliminating the 65 Hertz oscillations. However, higher frequency (89 Hertz) oscillations now appear in a different portion of the transient. Since the oscillations are low amplitude, short lived, and occur only during the most active portion of the transient, this result was considered acceptable and the lead/lag network effectively reduces the oscillatory behavior of the system at the higher frequencies.

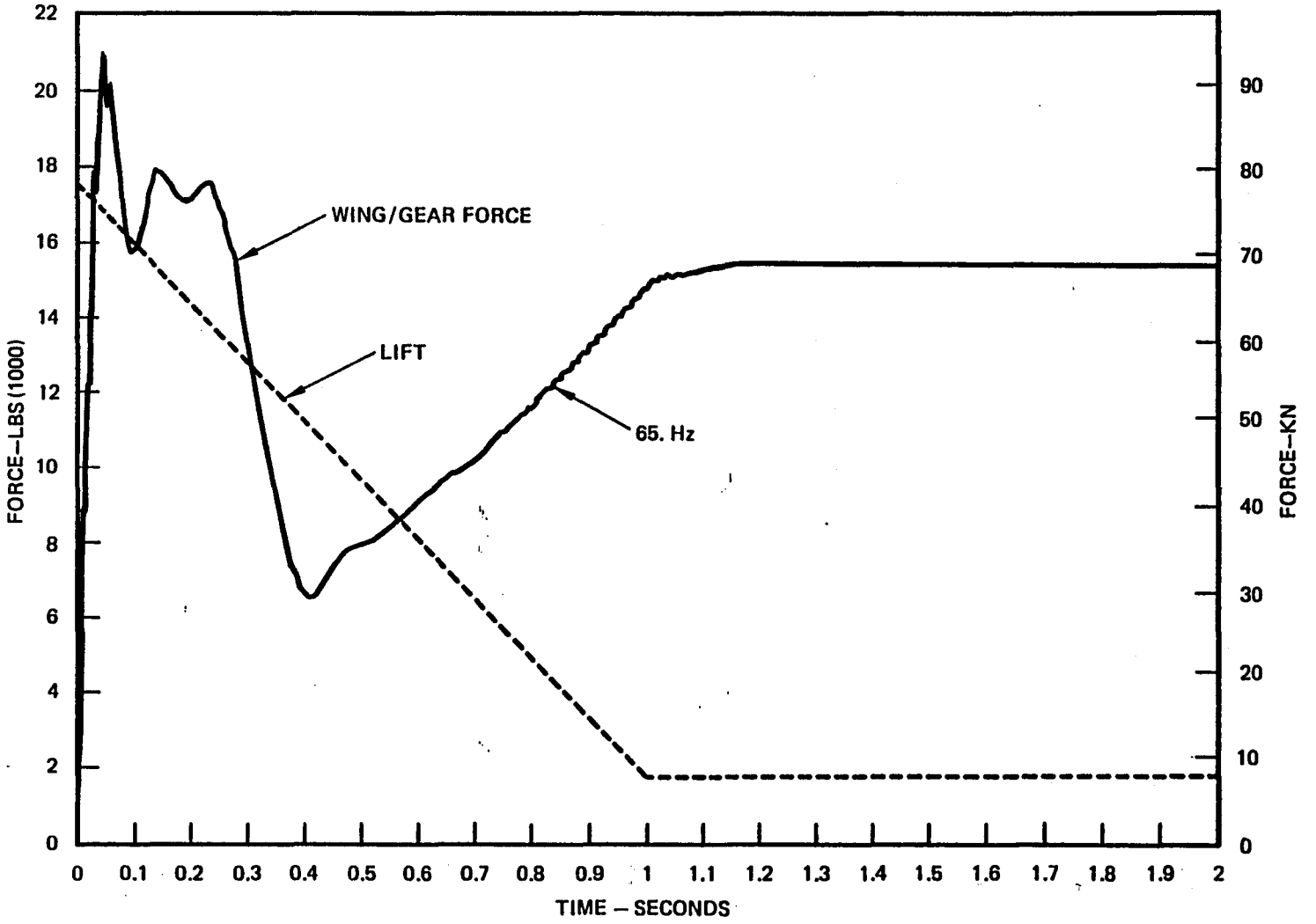

FIGURE 5-16. IMPACT LANDING, ACTIVE GEAR (COMPENSATION CONSISTS OF NOTCH ONLY)

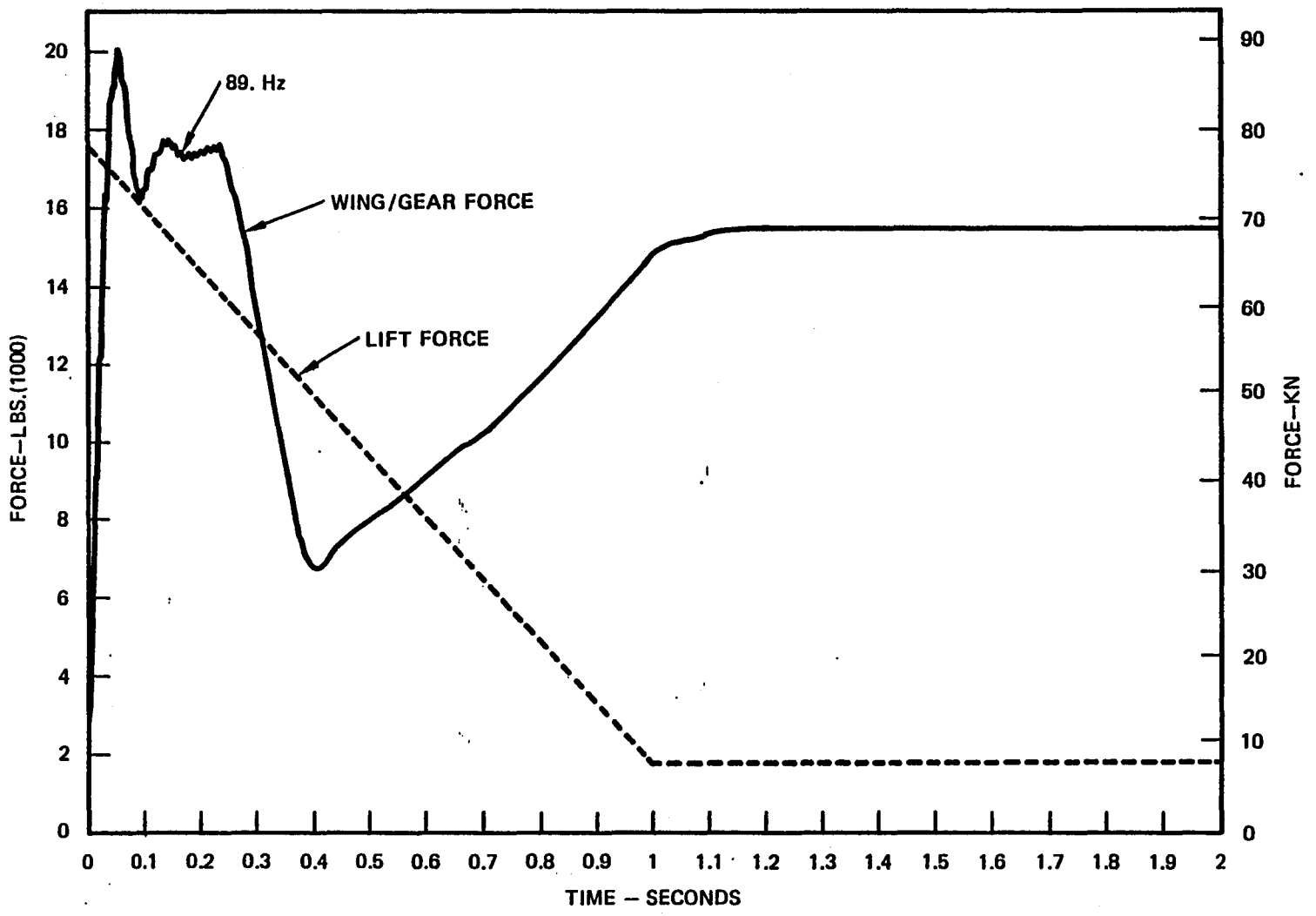

FIGURE 5-17. IMPACT LANDING, ACTIVE GEAR (COMPENSATION CONSISTS OF NOTCH AND LEAD/LAG)

5.6 Transient Response Results

The nonlinear model was used to simulate vertical drop landings and rollouts over runway disturbances using active control on the A-10 landing gear. In all cases the passive gear was also simulated in order to evaluate the effectiveness of active control in reducing the loads transmitted through the wing/gear interface.

5.6.1 Landing Impacts

The conditions for the vertical drop case are as follows:

a. The sink rate prior to impact is 2.54 m/sec (100 in/sec).

b. The lift equals airplane weight (per gear) prior to and up to the point of impact, then lift is linearly reduced to 10 percent of airplane weight during the first second after impact, and lift is held constant at ten percent thereafter.

c. The ground level remains constant.

Command limit force is set automatically by the controller. Figures 5-18 through 5-20 show the resultant transients for the passive gear. Figures 5-21 through 5-25 show the results for the active gear. Comparing Figure 5-18 and 5-21, active control reduces the peak force 32 percent below the passive gear case. Figure 5-22 shows how closely the accelerometer force followed the commanded limit force throughout

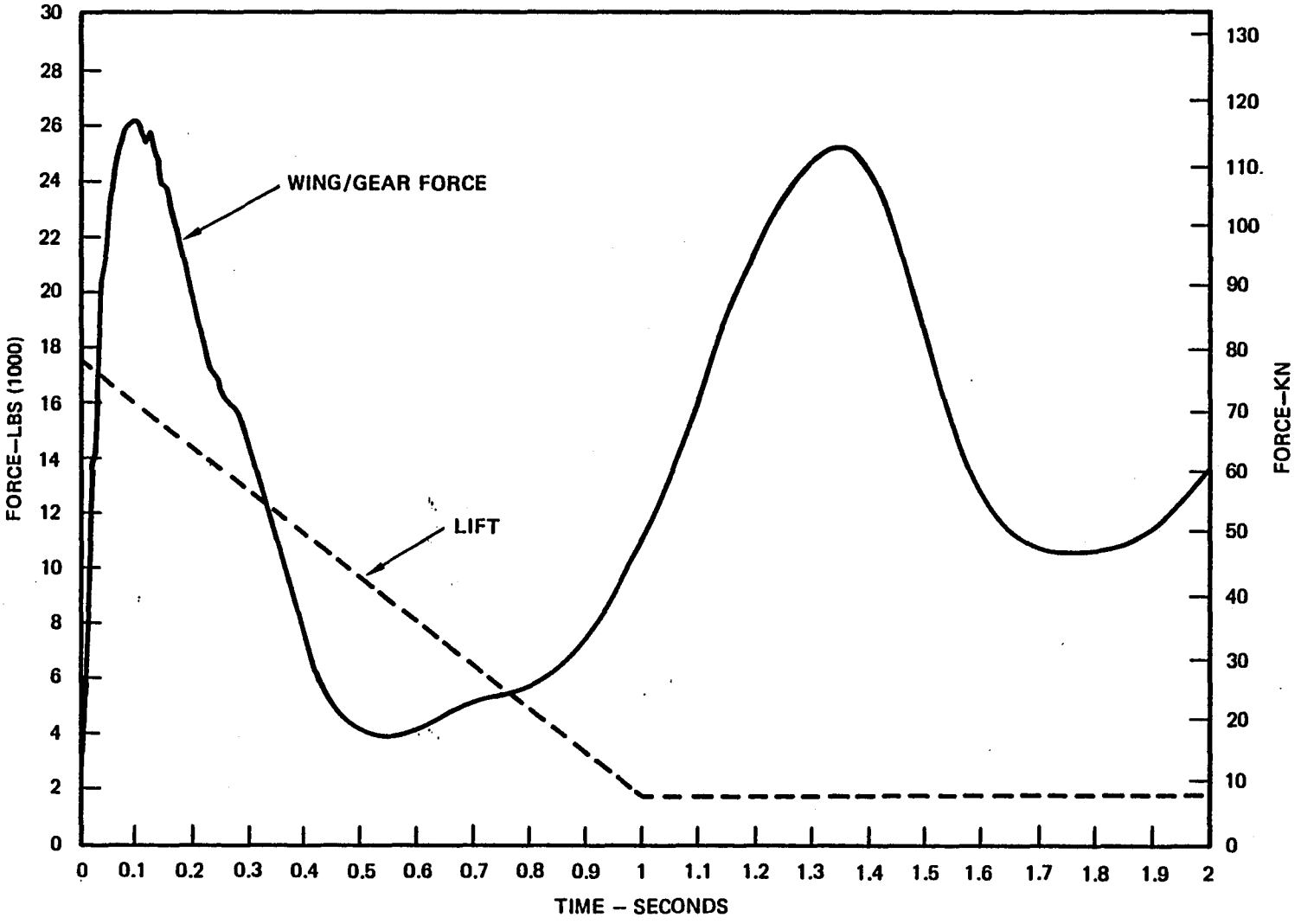

FIGURE 5-18. IMPACT LANDING, PASSIVE GEAR

06

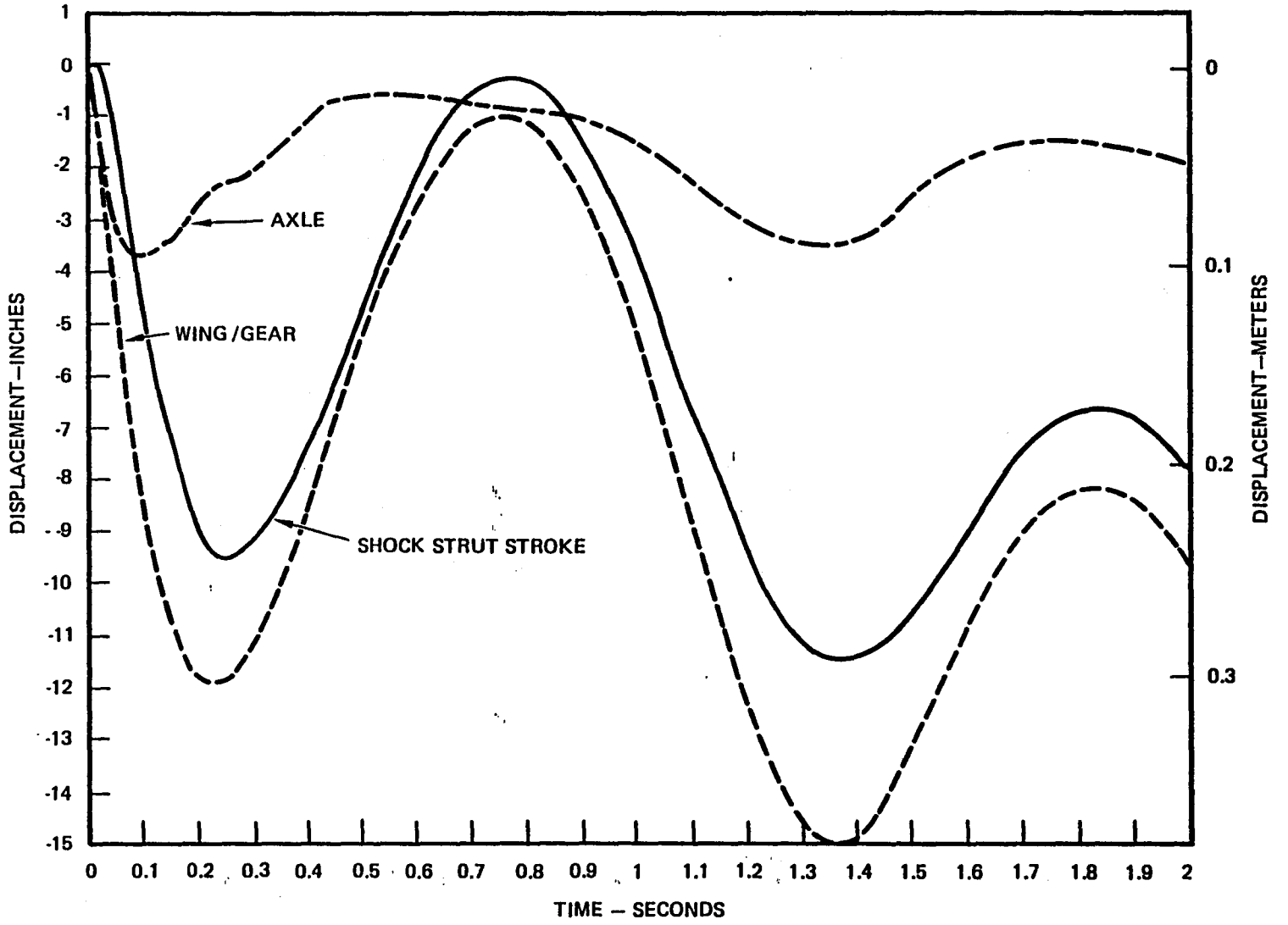

FIGURE 5-19. IMPACT LANDING, PASSIVE GEAR

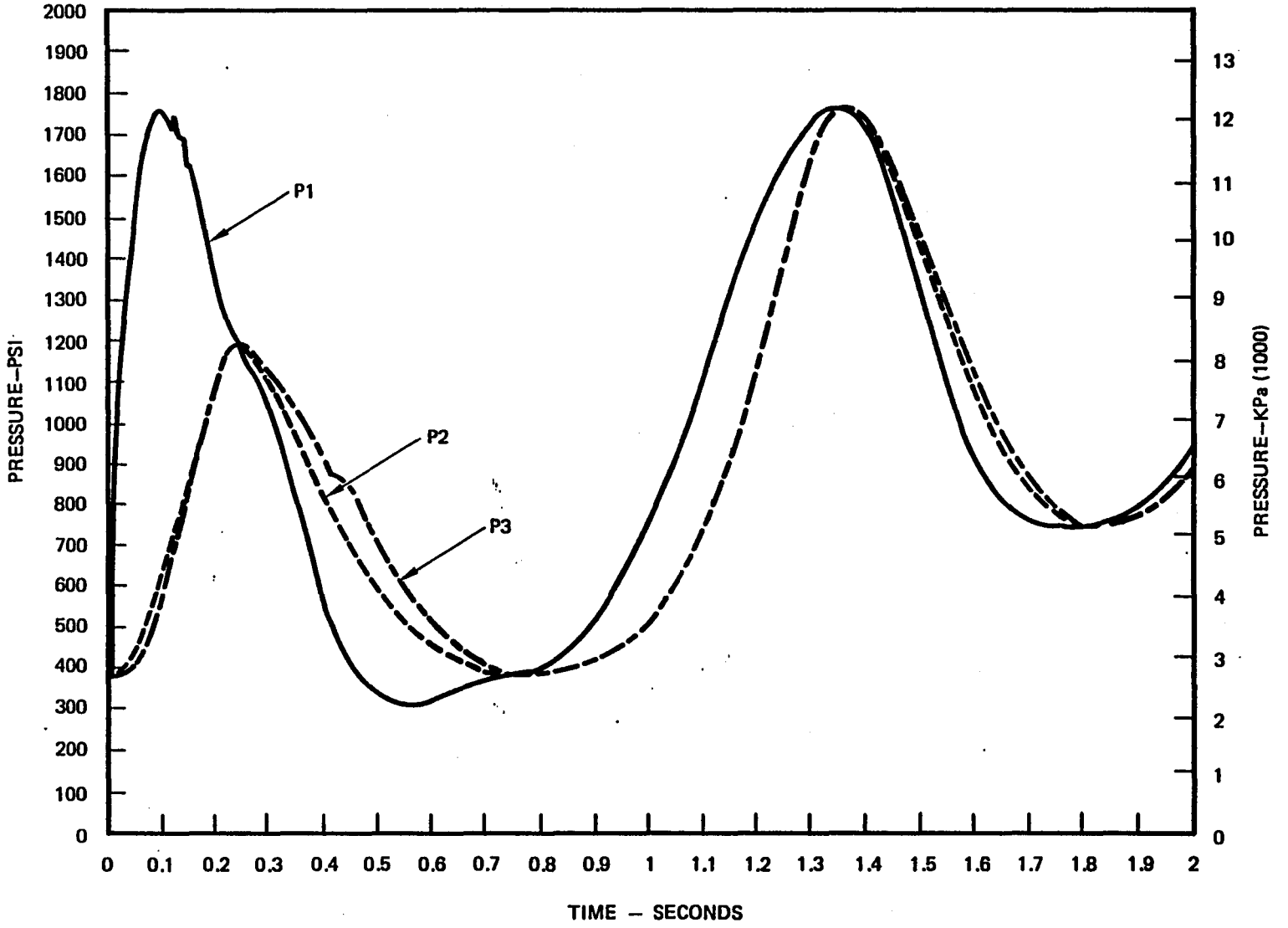

FIGURE 5-20. IMPACT LANDING, PASSIVE GEAR

92

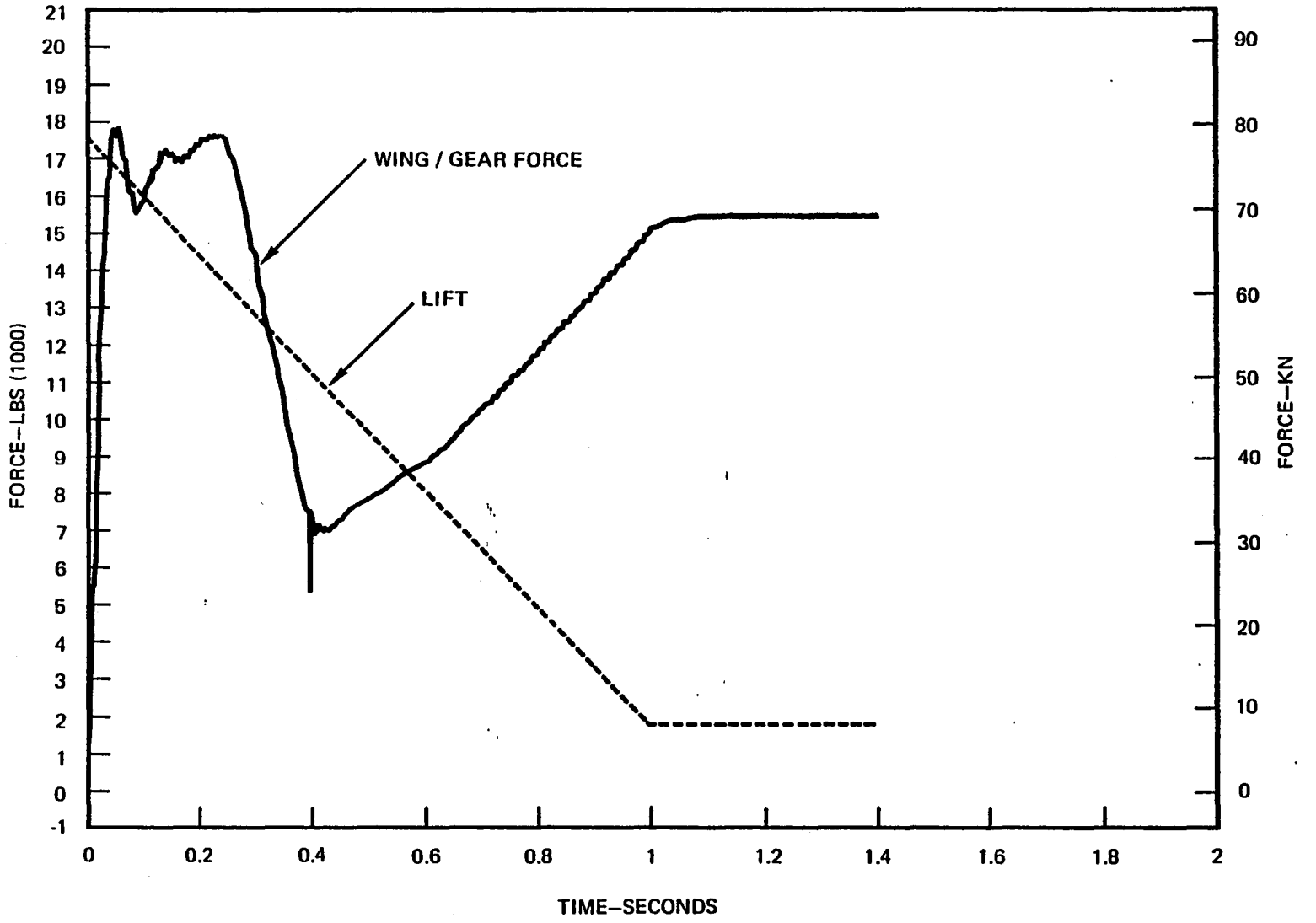

FIGURE 5-21. IMPACT LANDING, ACTIVE GEAR

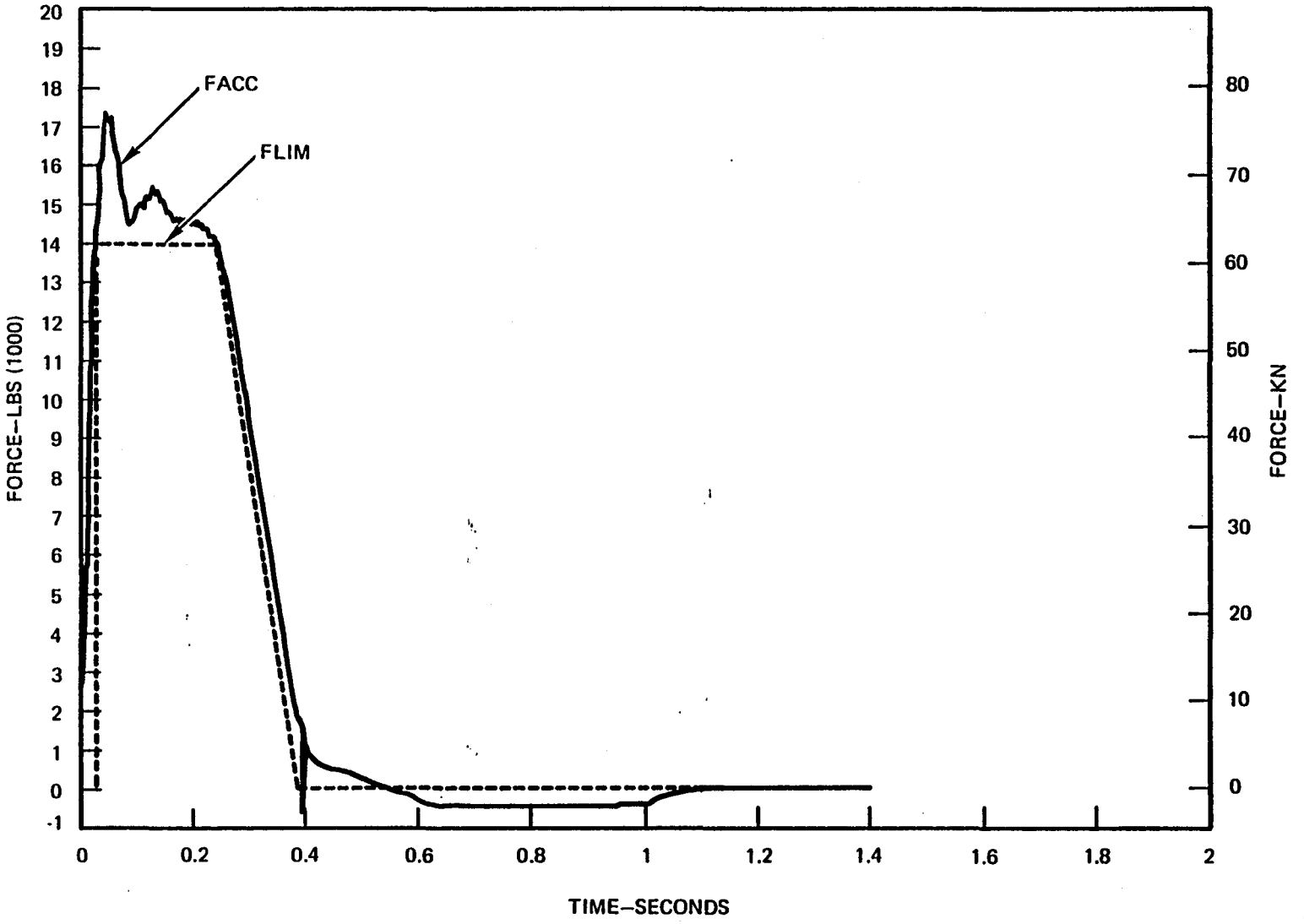

FIGURE 5-22. IMPACT LANDING, ACTIVE GEAR

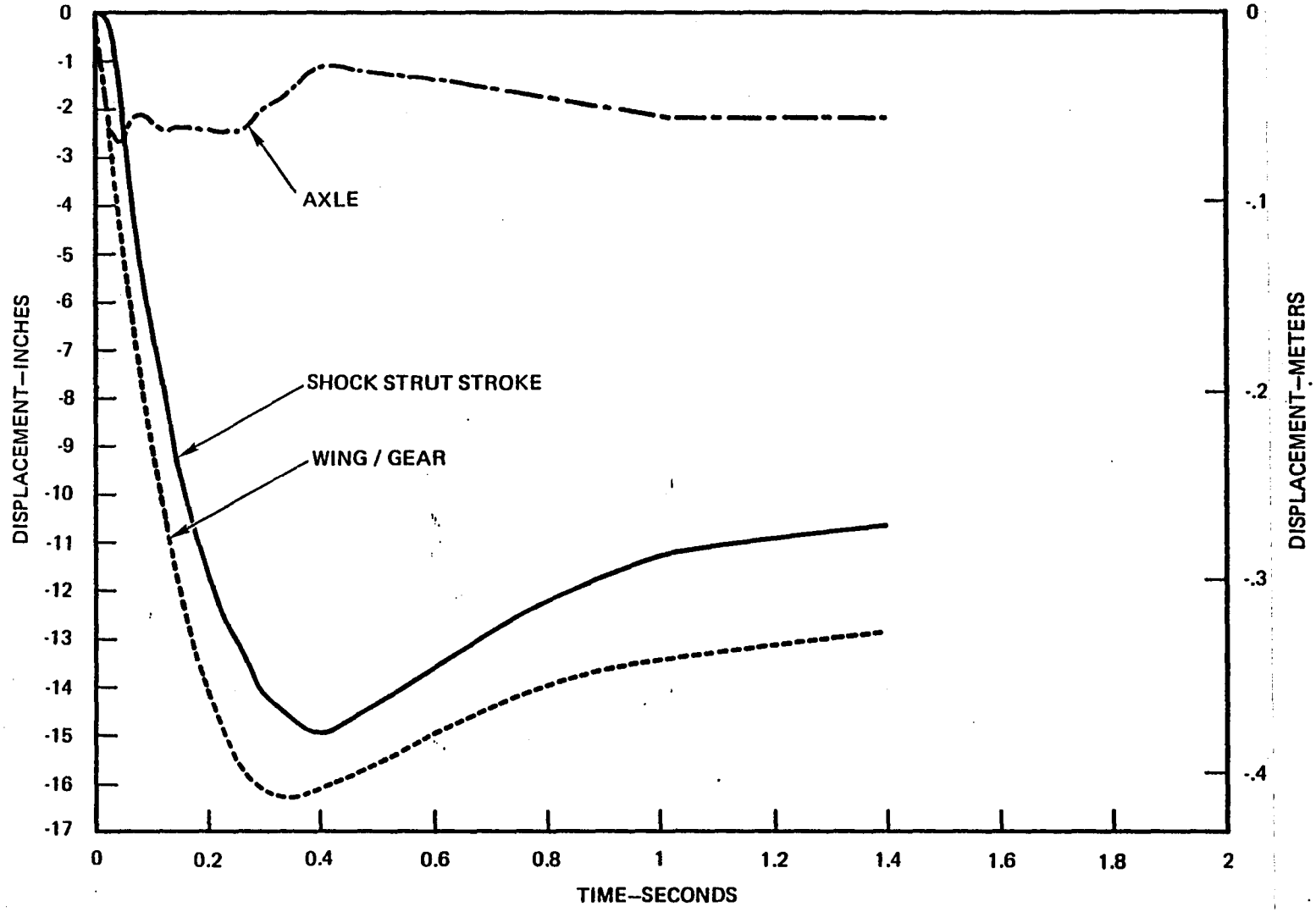

FIGURE 5-23. IMPACT LANDING, ACTIVE GEAR

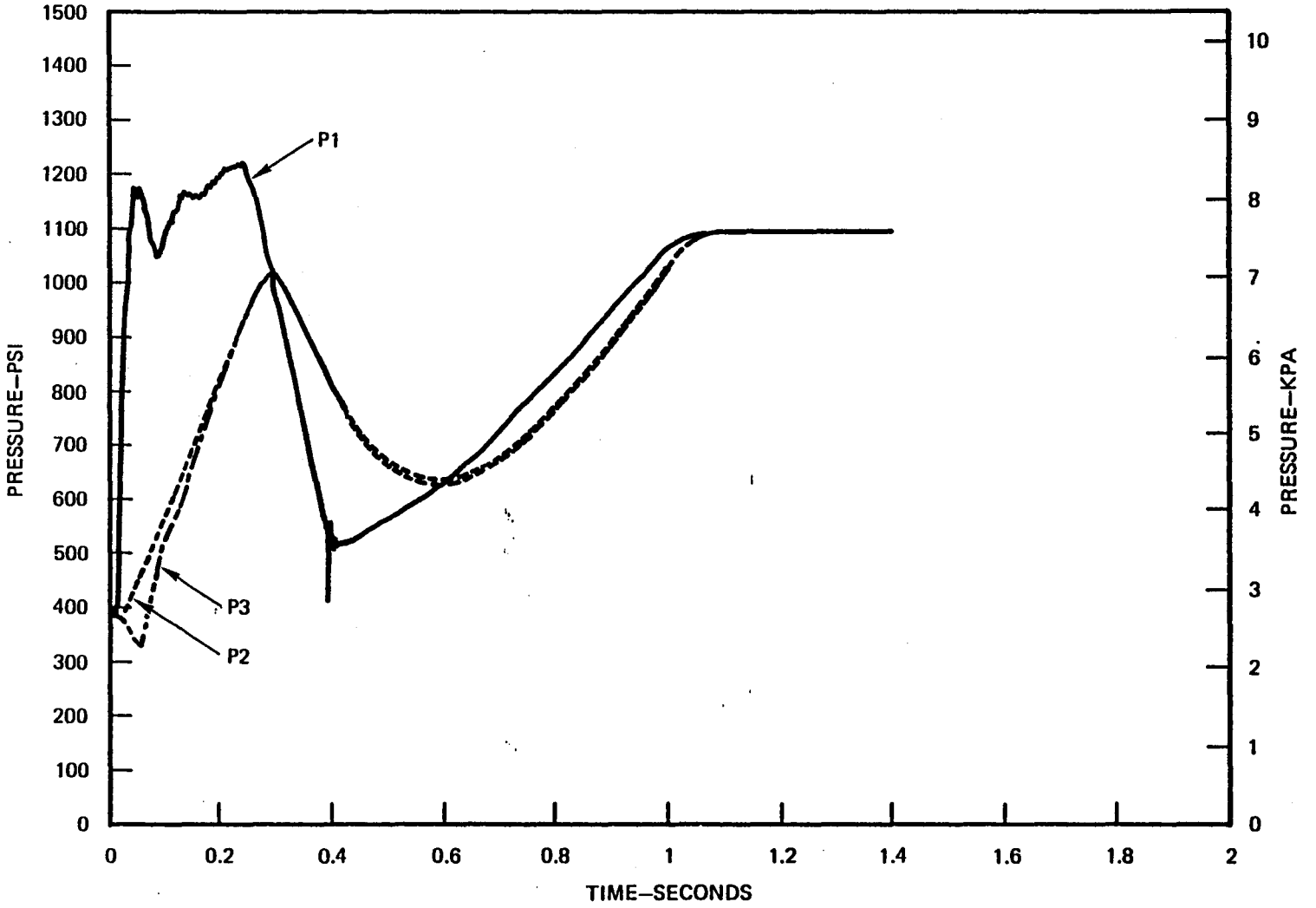

FIGURE 5-24. IMPACT LANDING, ACTIVE GEAR

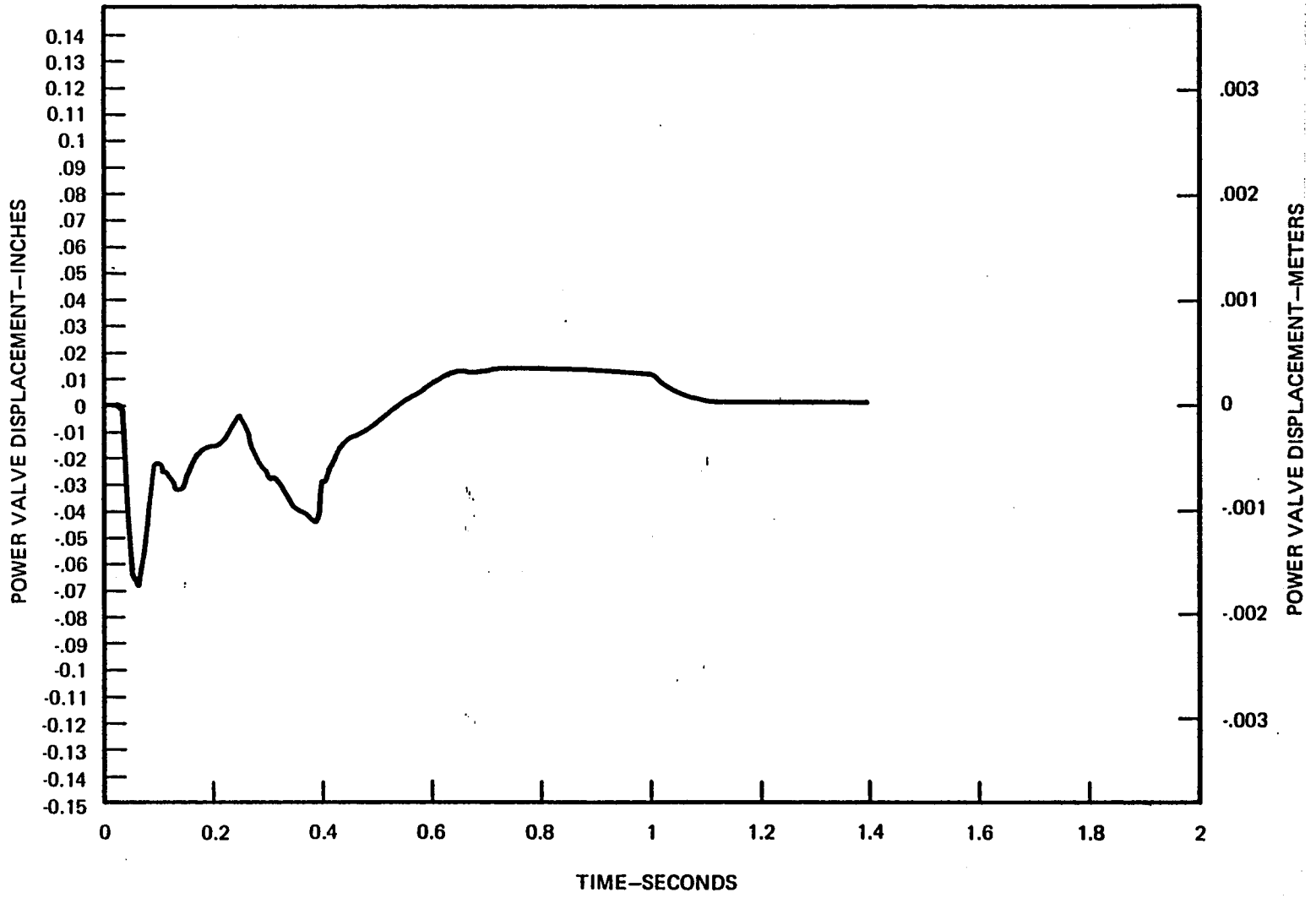

FIGURE 5-25. IMPACT LANDING, ACTIVE GEAR

the transient for the active case. Figures 5-19 and 5-23, which show the shock strut stroke and the vertical displacements of the ground, landing gear axle, and wing/gear interface warrant some explanation. All displacements are positive in the up direction, and are referenced to the condition where the gear is fully extended and barely in contact with the ground with zero tire compression. Thus, at the point of impact (at time = 0) all the variables are zero. When the axle displacement is below the ground level (which is constant), the tire is in compression; when it is above, the landing gear is off the ground. Also, when the wing gear interface displacement is the same as the axle displacement, the gear is fully extended. For both of these cases, note that the tire is always in contact with the ground after the initial impact, and after the strut initially starts stroking it never fully extends again. Also note that the active gear uses significantly more stroke than the passive gear, as expected. Figures 5-20 and 5-24 show the strut pressure transients. The pressures are significantly reduced in both cylinders as a result of active control. Finally, Figure 5-25 shows the valve third stage spool displacement for the active control case.

5.6.2 Runway Disturbances

Simulation of aircraft rollout over a runway disturbance (subsequent to an impact landing) was accomplished using the nonlinear vertical drop model. Initial conditions are calculated assuming the aircraft is in contact with the ground and the landing gear has reached an equilibrium condition in supporting the aircraft weight minus its lift. Assuming some horizontal speed for the aircraft, actual physical changes in ground level can be represented as transient changes which can be input to the

nonlinear model. For this case a Class I repaired bomb crater constituted the runway disturbance. A diagram of the bomb crater is shown in Figure 5-26. The horizontal speed of the aircraft was assumed to be 51.8 m/sec (170 ft/sec). The command limit force is set to zero with a force deadband of zero throughout the transient, consistent with the assumption that the disturbance occurs during rollout, subsequent to an impact landing. The lift is set to 10 percent of the aircraft weight (per gear) throughout the transient. Figures 5-27 through 5-29 show the results for the passive case and Figures 5-30 through 5-34 show the results for the active case. Active control reduces the peak wing/gear force 43 percent below the passive gear case. Note also from Figures 5-28 and 5-32 that the passive gear leaves the ground significantly (from t = .31 to t = .44 sec), while the active gear remains in contact with the ground.

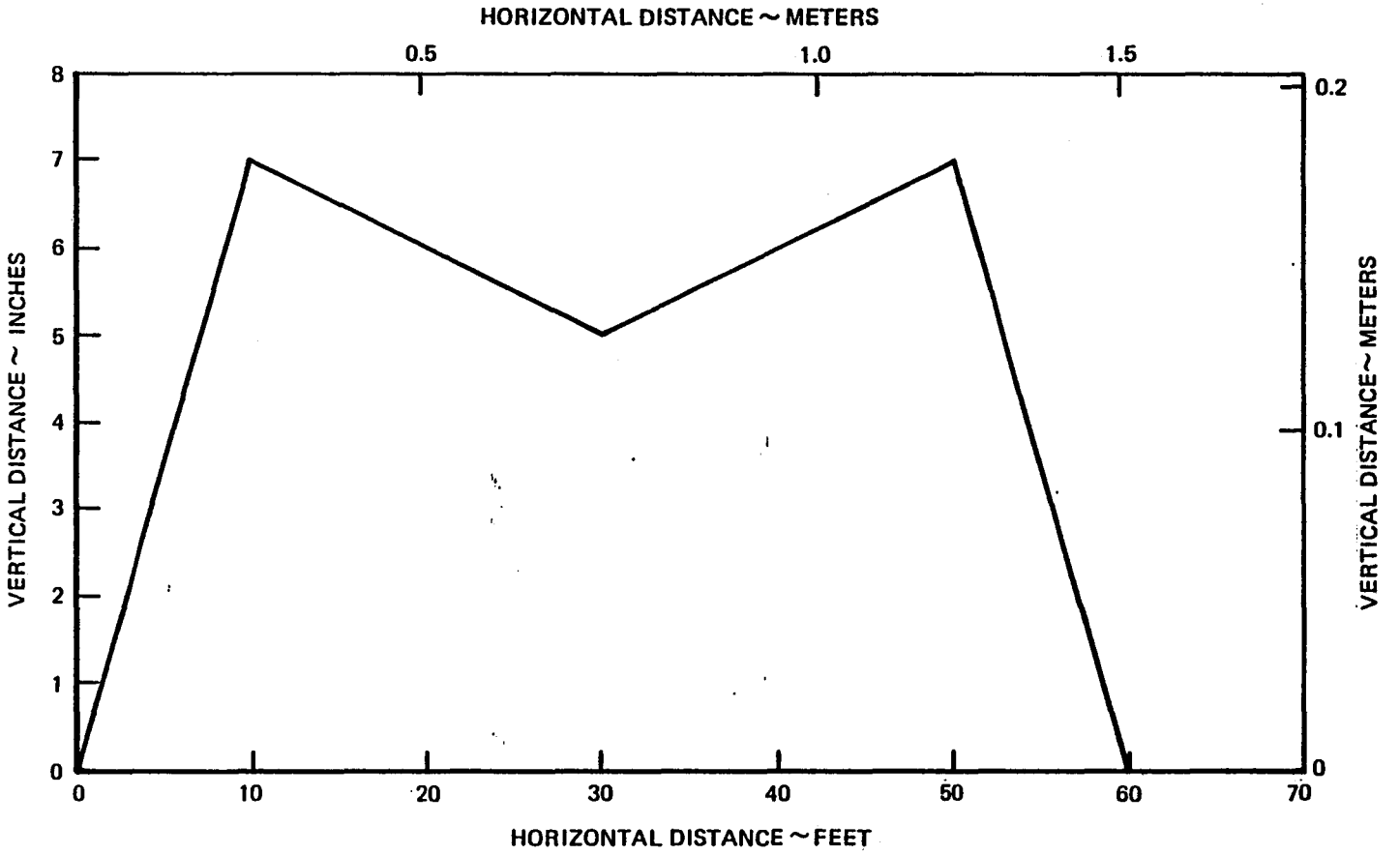

FIGURE 5-26. RUNWAY DISTURBANCE

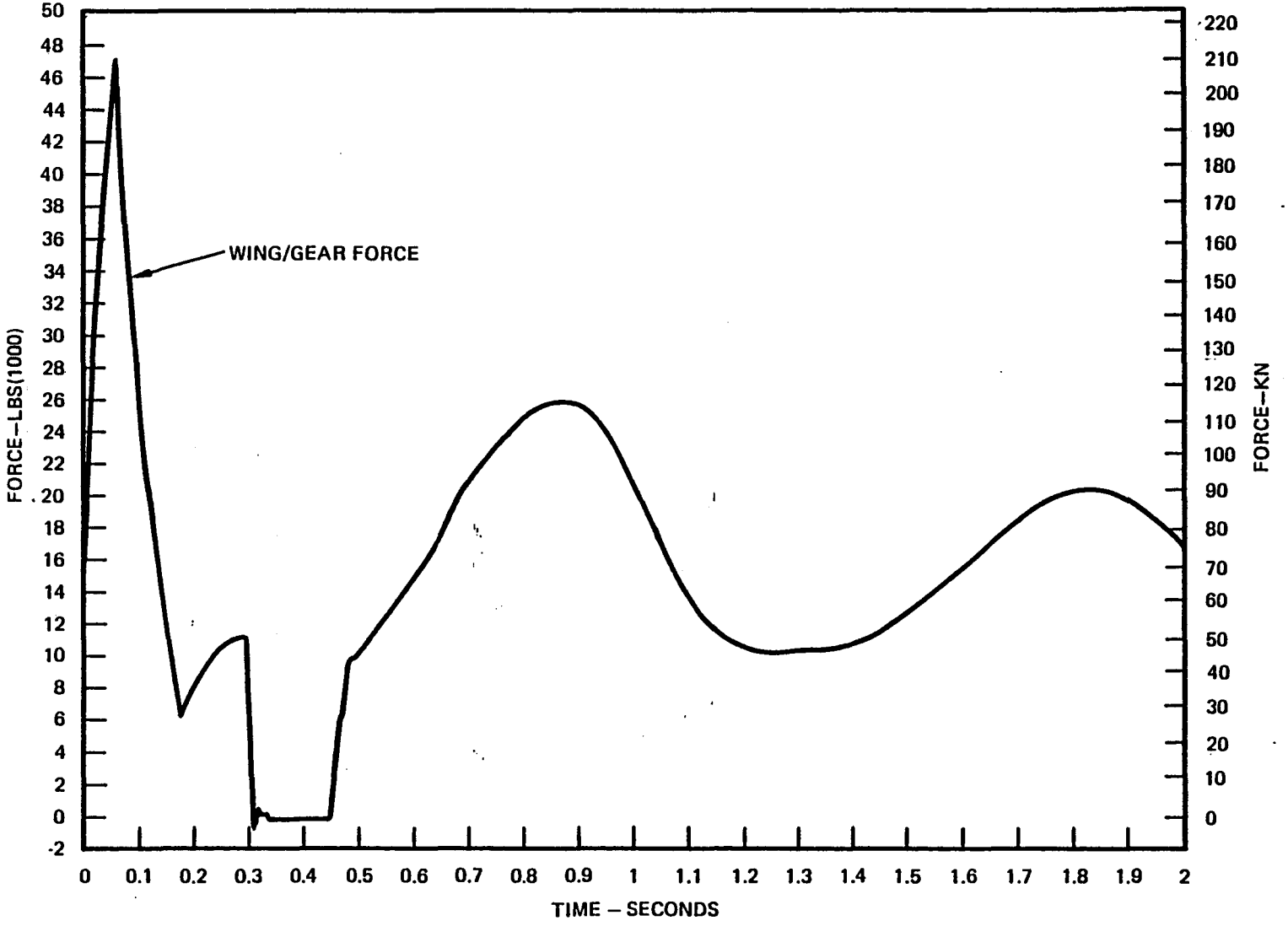

FIGURE 5-27. RUNWAY DISTURBANCE, PASSIVE GEAR

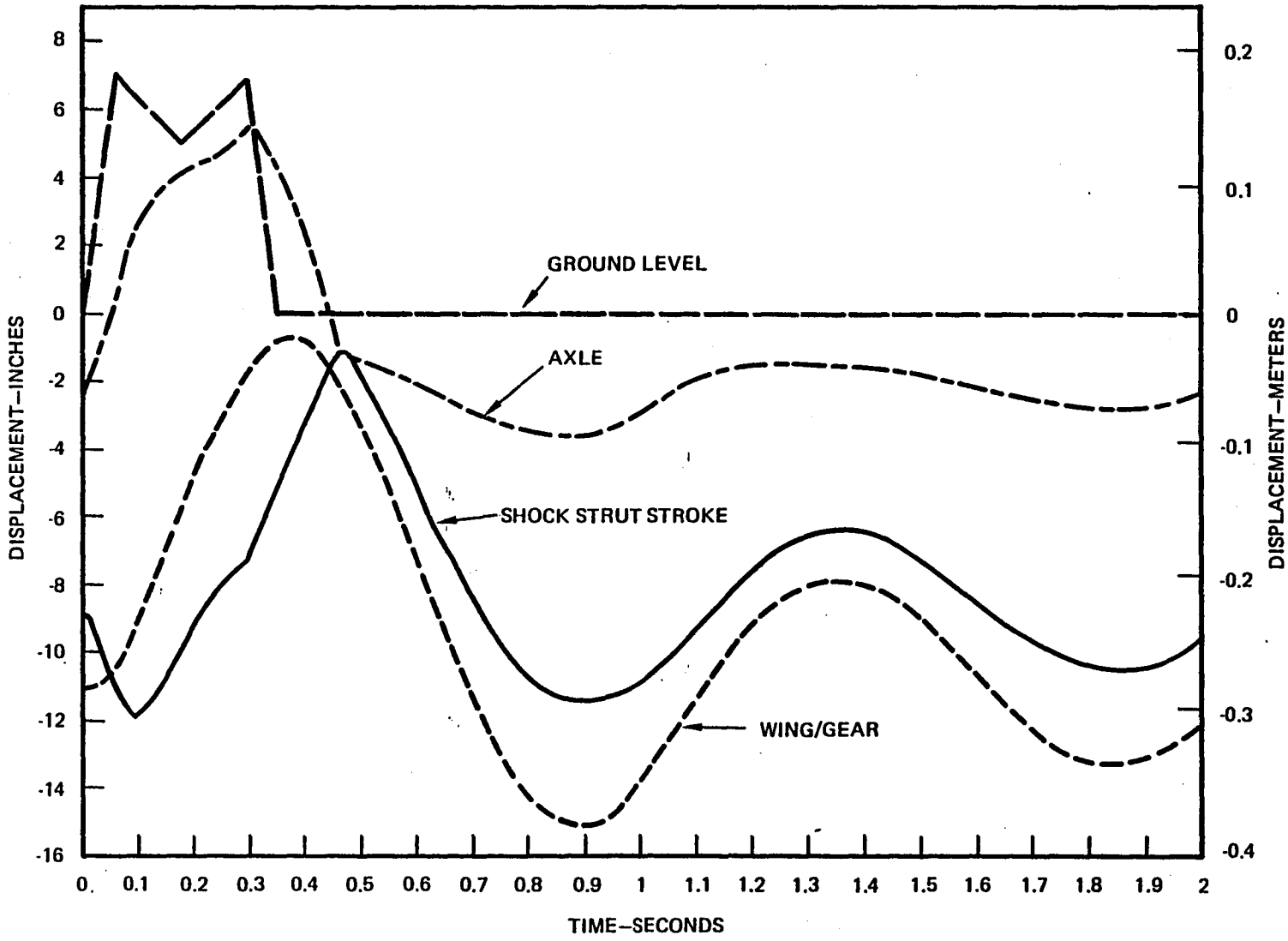

FIGURE 5-28. RUNWAY DISTURBANCE, PASSIVE GEAR

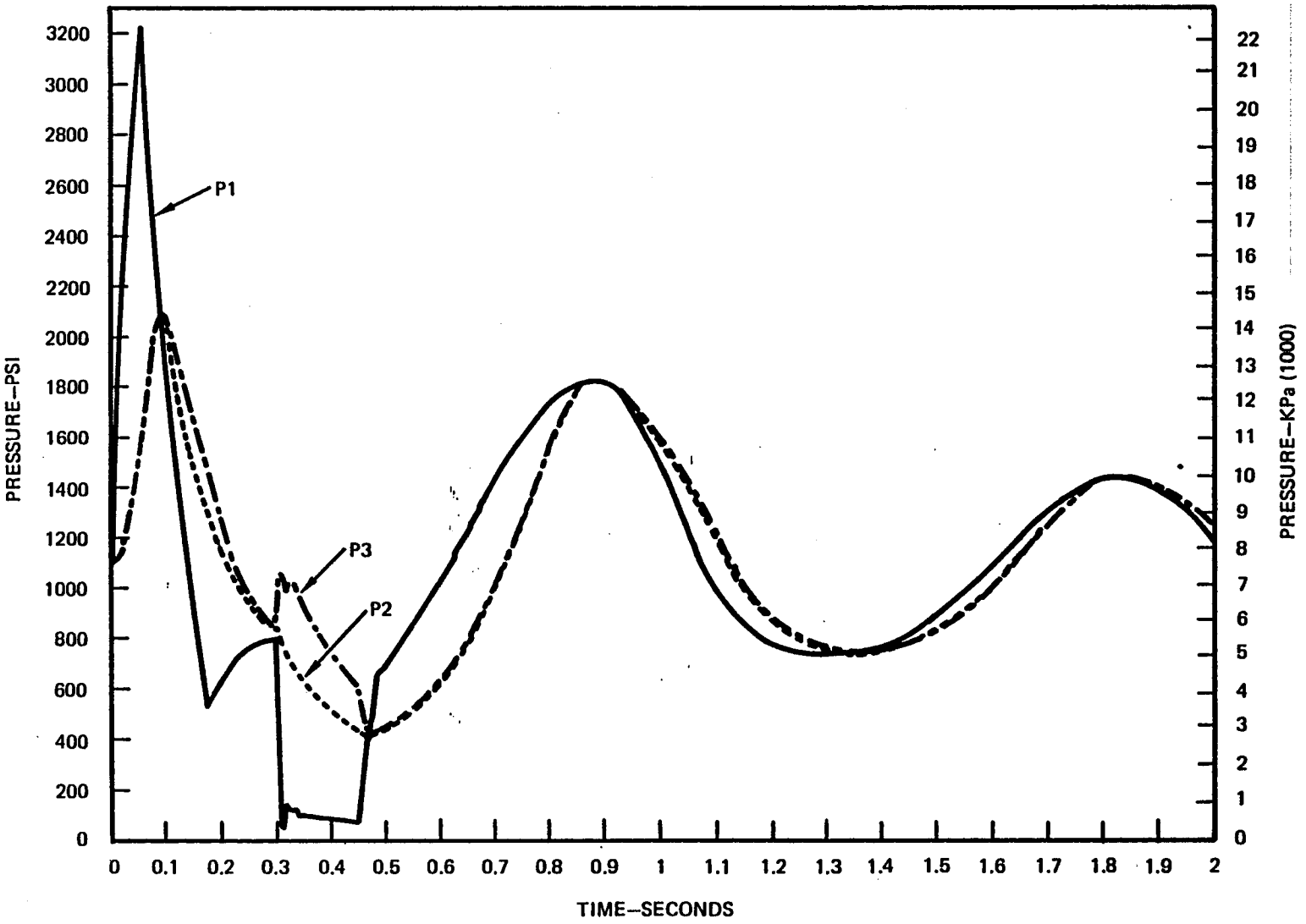

FIGURE 5-29. RUNWAY DISTURBANCE, PASSIVE GEAR.

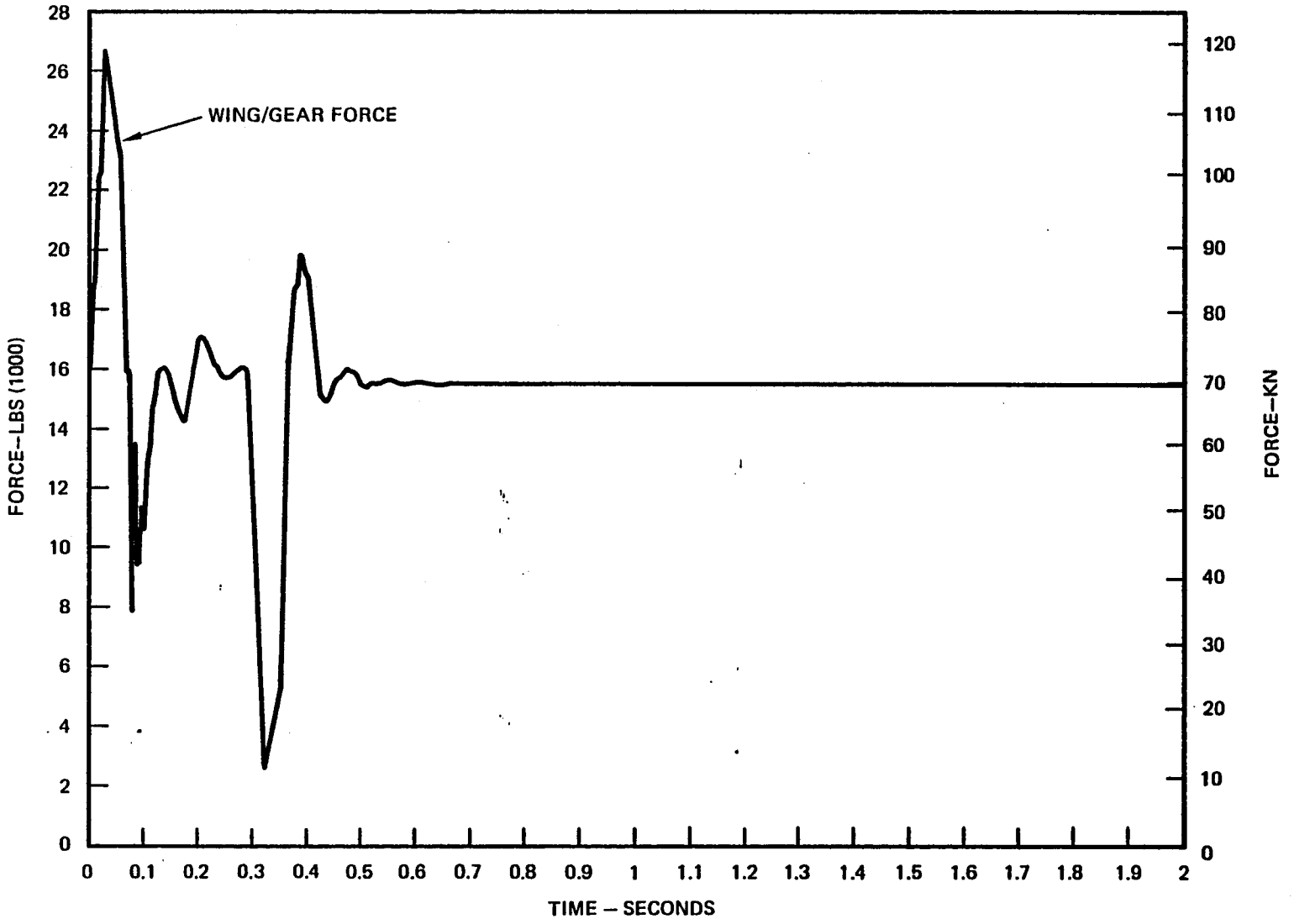

FIGURE 5-30. RUNWAY DISTURBANCE, ACTIVE GEAR.

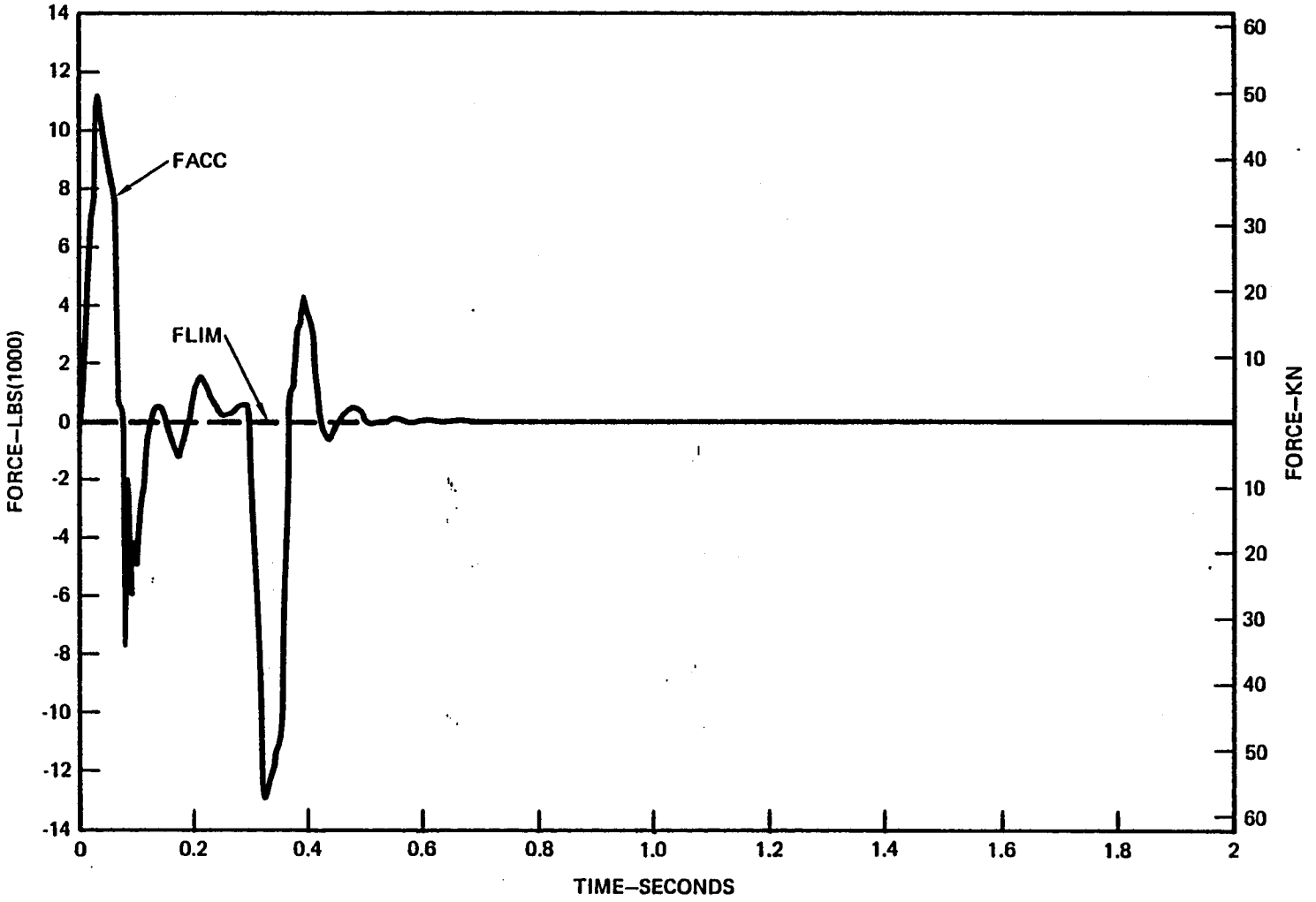

FIGURE 5-31. RUNWAY DISTURBANCE, ACTIVE GEAR.

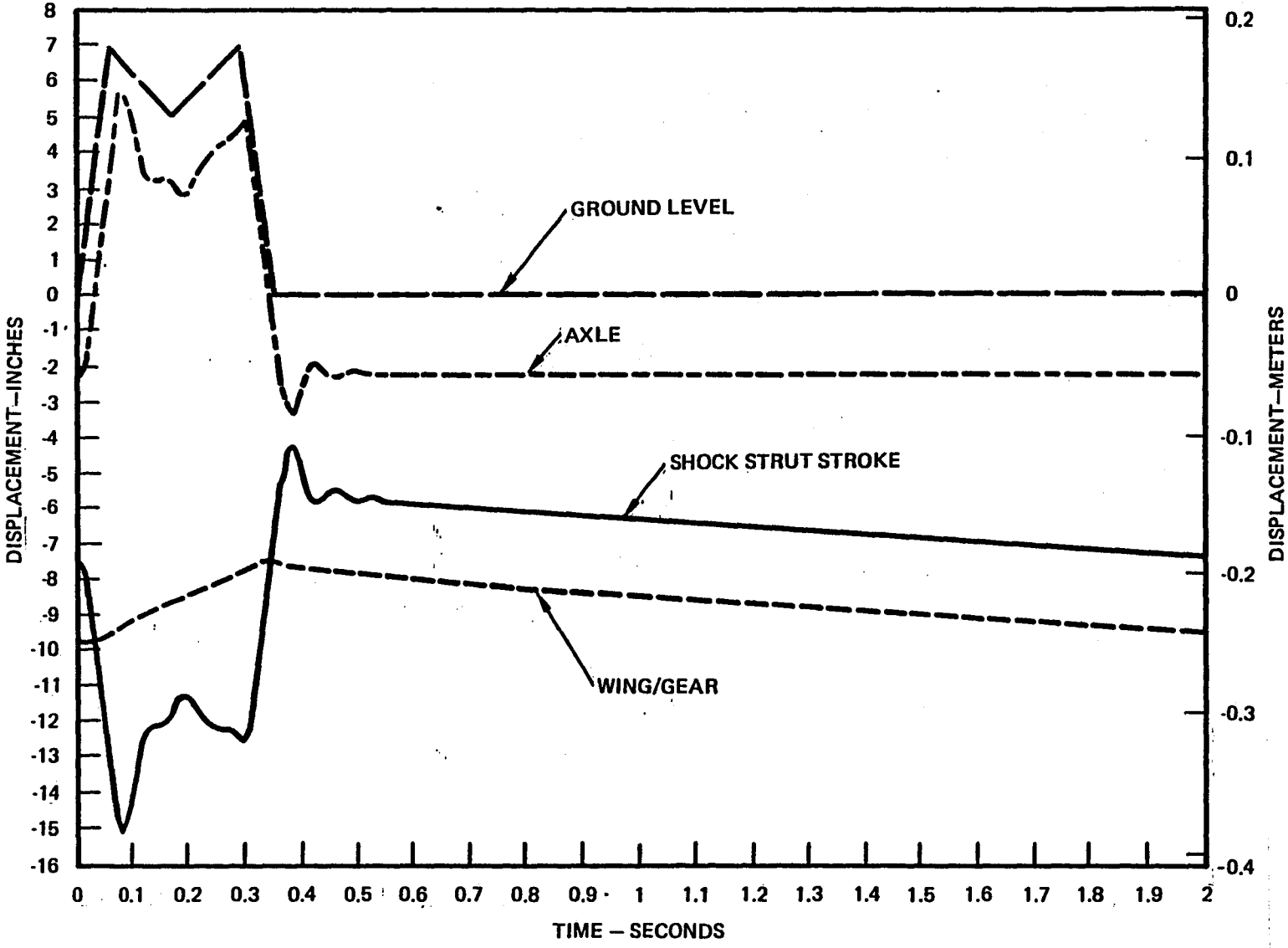

FIGURE 5-32. RUNWAY DISTURBANCE, ACTIVE GEAR

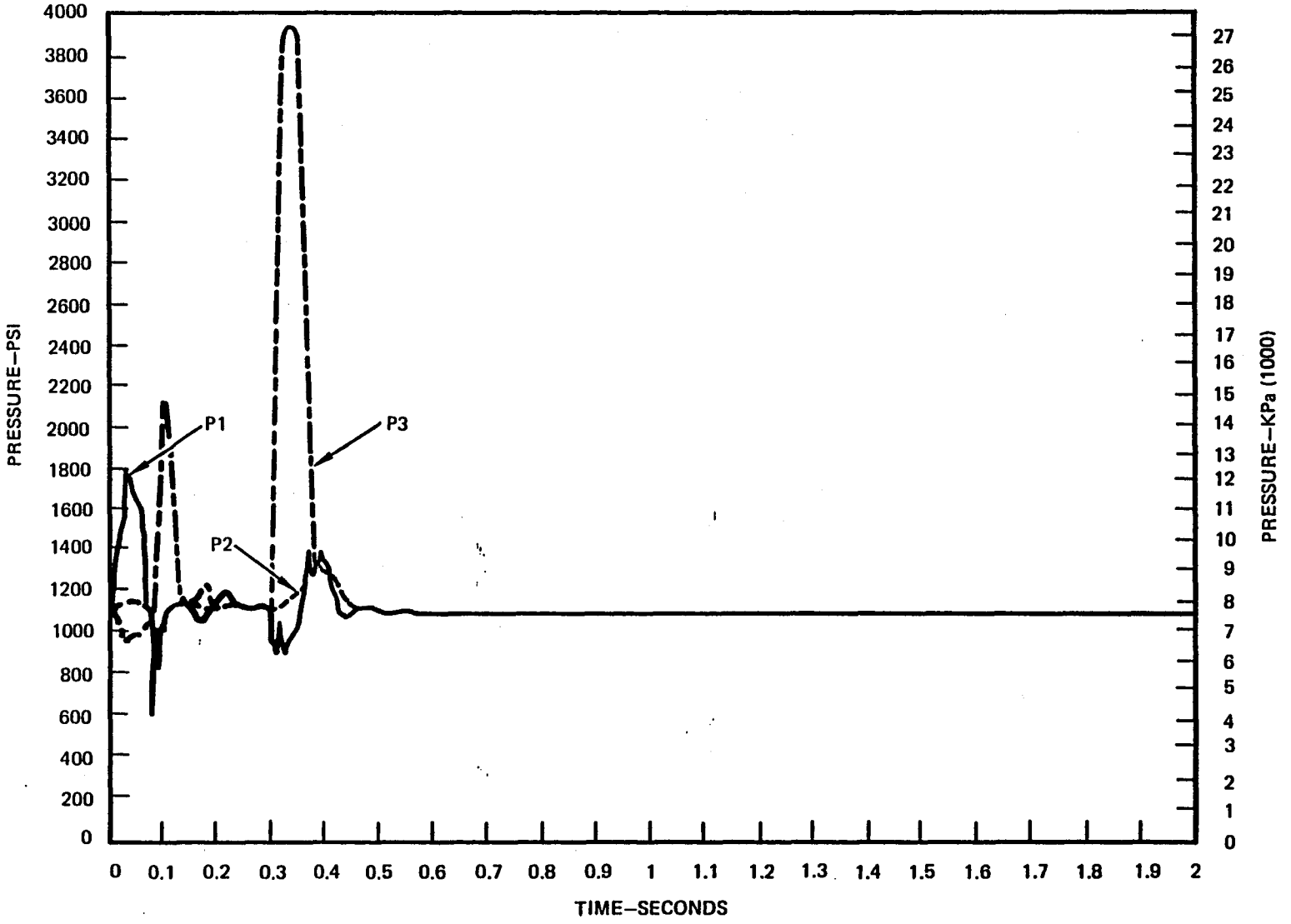

FIGURE 5-33. RUNWAY DISTURBANCE, ACTIVE GEAR.

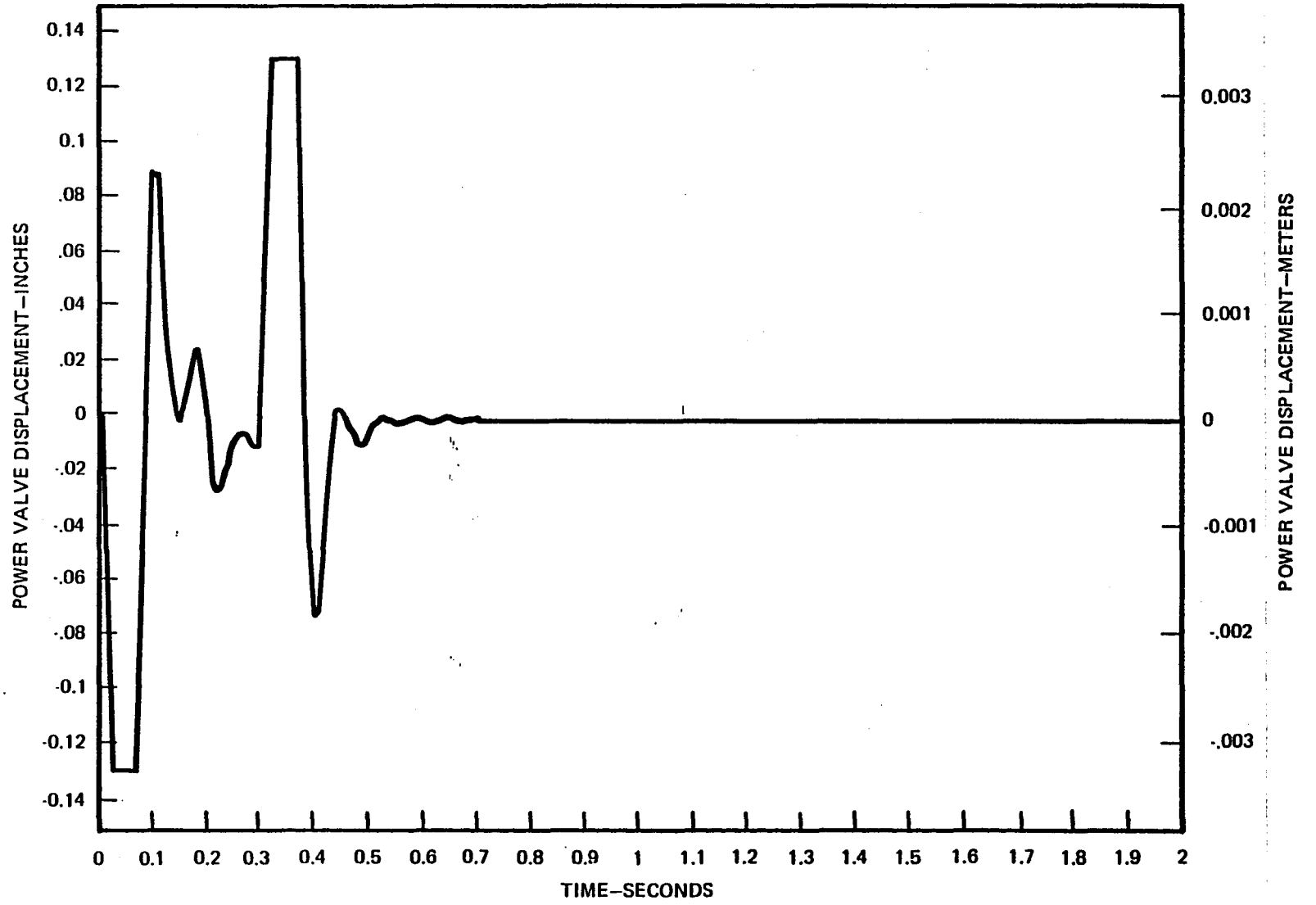

FIGURE 5-34. RUNWAY DISTURBANCE, ACTIVE GEAR.

5.7 Failure Detection and Redundancy Management

The objective of redundancy management is to assure that all failures will be detected and the system will revert to the passive mode. There is no attempt to have component redundancy to increase the reliability in the active mode.

The failure detection objective is accomplished by having three detection points as shown in Figure 5-35. The three detection points are as follows:

a. Dual cross monitoring microprocessors.
b. Model of the servovalve.
c. Servovalve open coil monitor.

The dual microprocessors constitute the only place where cross comparison exists. The microprocessors are synchronized and have a continuous bit-by-bit comparison, and any difference will cause a failure signal through the logic driver (LD) to the dual gates. This will initiate the reversion to the passive mode. The microprocessors also perform the failure detection function for the sensors. The sensors are all dual and each sensor feeds into the separate multiplexer (MUX) analog to digital (A/D) blocks. The MUX A/D's transmit the sensor information to both microprocessors. Each microprocessor processes the signal, determining if the sensor has failed and also calculates the average value between the dual sensors. The average value is used in calculating the command. Again, a failure signal to the dual gates will cause the system to revert to the passive mode.

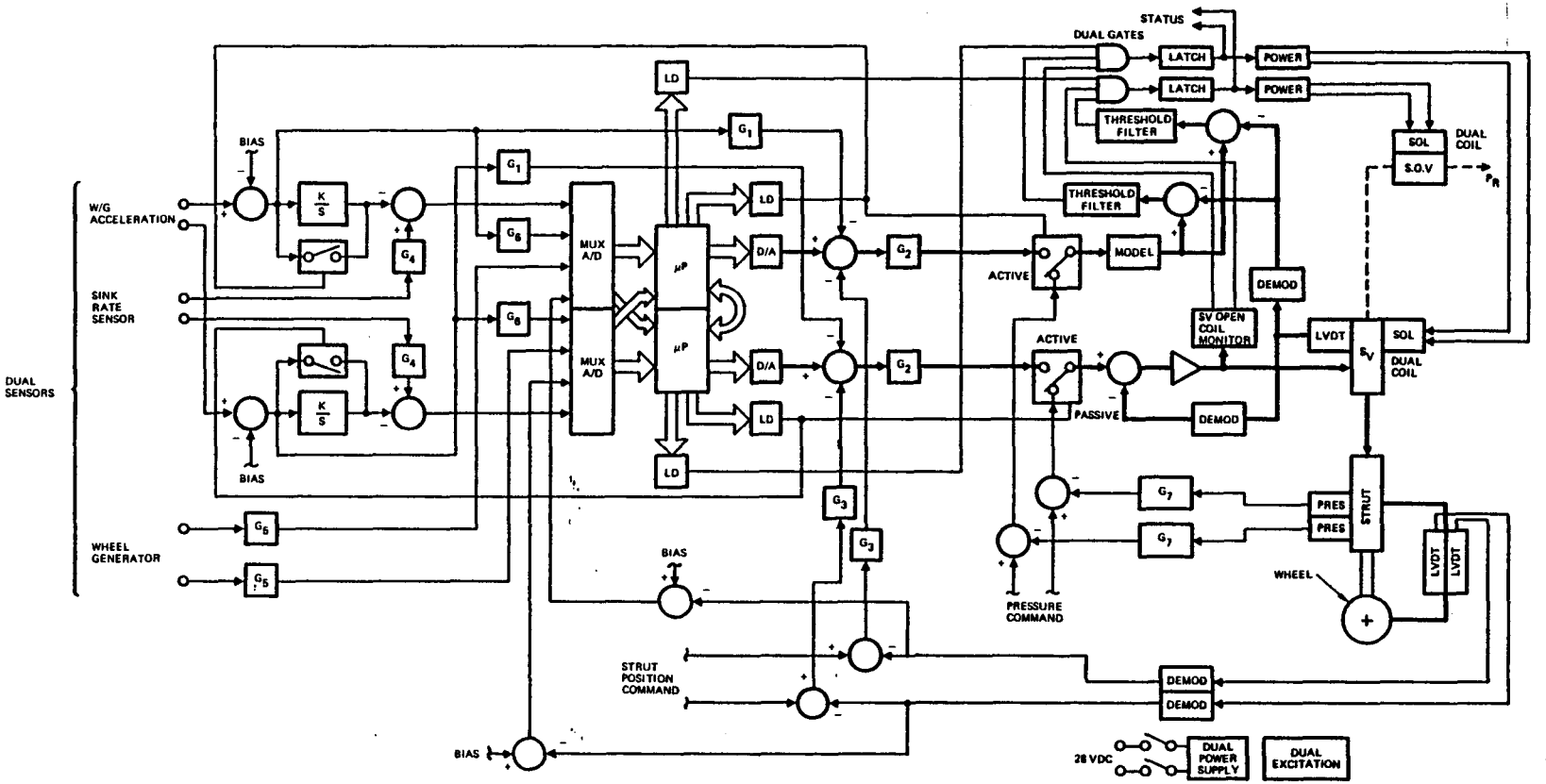

FIGURE 5-35. CONTROLLER, ORIGINAL CONCEPT

From the dual microprocessors two parallel paths exist. One path is through the servoamp to the servovalve which controls the actuator (strut). The second path is to the model. The model emulates the servoamp and the servovalve to the third stage position. The servovalve third stage has an LVDT to provide a signal proportional to its position. This signal is used in the feedback loop but is also used to compare with the output of the model. Any failure of any component between the microprocessor and the servovalve LVDT will cause a disagreement between the model and the demodulated LVDT signal and a failure signal will be generated. A threshold and a filter are used to prevent nuisance trips.

The servovalve open coil monitor is used to detect a servovalve coil failure. During the pre-touchdown mode, the servovalve is approximately at the zero current position. A failure of the coil would not cause a significant change in servovalve position and the model would not detect the failure, therefore the open coil monitor is used. An open coil will be detected and a failure signal generated. This failure signal causes reversion to the passive mode and provides an indication to the flight crew.

The power supply and LVDT excitation are also dual. A failure of the power supply will be detected by the model. An excitation failure will cause the dual strut position LVDT to disagree and the microprocessor will detect the failure.

The reversion to the passive mode is accomplished by the use of two solenoids. One solenoid, as shown in Figure 5-35, operates the normally closed shut-off valve in the return line. De-energizing this valve will result in full pressure at the

strut. The second solenoid valve is part of the three stage servovalve. This solenoid controls an isolation valve located between the second and third stages and when it is de-energized the isolation valve moves to allow return pressure to be applied to both ends of the third stage spool. The centering springs on this spool will therefore center the spool and block the cylinder port (to the strut). This action isolates the strut cylinder from the accumulators and the supply pressure. Both solenoids have dual coils.

The passive mechanism is such that each solenoid is driven by one of the dual gates. On a dual failure where one of the failures is in the gate circuit, only one of the solenoids will operate (de-energize), giving some degree of passive operation. If only the shut off valve solenoid operates, the system will be passive, but the upstream volume will be greatly increased by the accumulators. If only the solenoid valve on the servovalve operates, the passive mode will be affected by the servovalve spool leakage. This will allow the pressure in the strut to reach a value half way between supply and return.

6.0 APPLICATION PROGRAM

The following constitutes a program plan statement of work and schedule for application of active control landing gears to the A-10 aircraft. The tasks that must be accomplished to design, develop, and demonstrate the active control landing gears are delineated in the program plan shown in Figure 6-1. Due to its advantages of implementation, only the alternate concept will be discussed.

6.1 Statement of Work

This section delineates the tasks that must be accomplished to design, develop, and demonstrate the nose and main active control landing gears.

6.1.1 ACLG System Sizing Analysis

6.1.1.1 Control Laws

Utilizing a linear model, establish the control laws and system gains for the nose and main active control landing gear system.

6.1.1.2 Nonlinear Analysis

Conduct nonlinear analyses to verify and modify, as necessary, the control laws and control system gains.

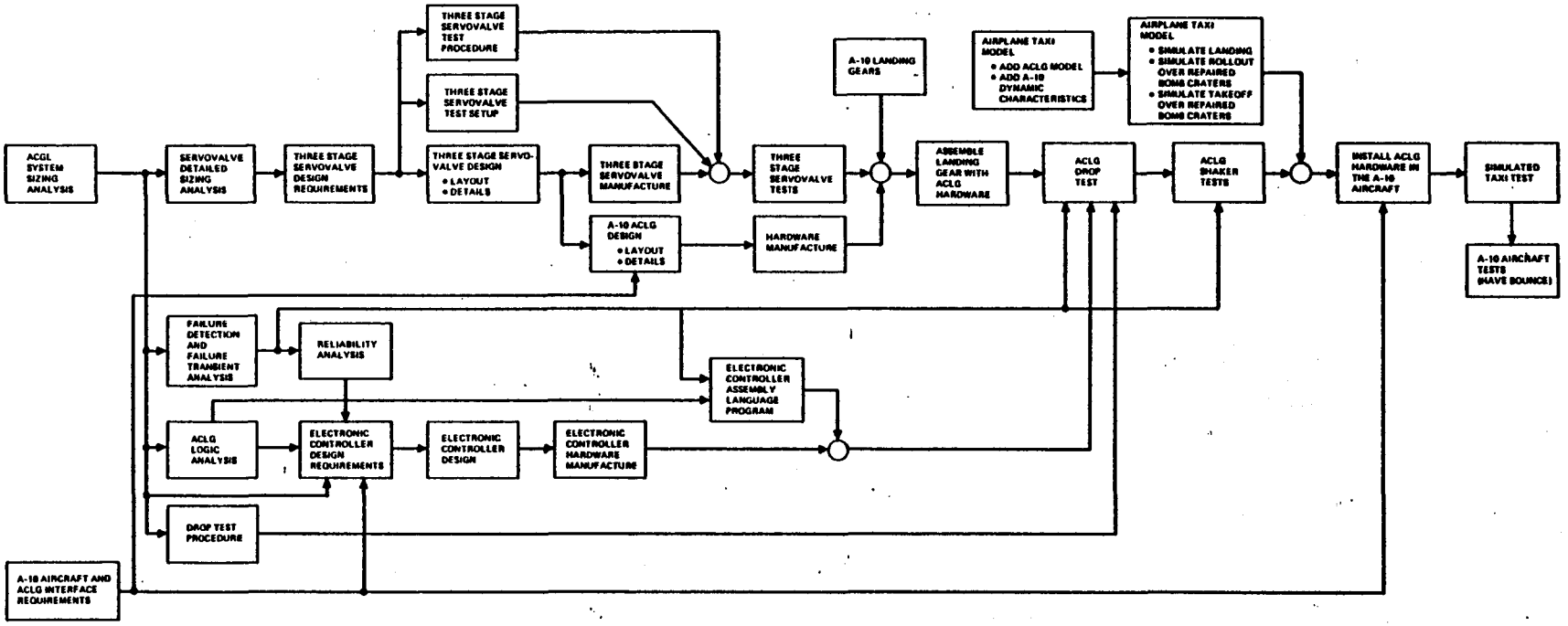

FIGURE 6-1. A-10 ACLG PROGRAM PLAN

6.1.1.3 Simulated Drop Tests

Conduct simulated vertical drop test analysis to determine the effectiveness of the nose and main ACLG in reducing the wing/gear forces.

6.1.1.4 Simulated Landings and Takeoffs

Conduct simulated landing and takeoff analyses to determine the effectiveness of the nose and main ACLG in reducing the wing/gear forces when traversing over repaired bomb craters.

6.1.2 System Analysis

6.1.2.1 ACLG Logic Analysis

Conduct simulated landing impact and rollout over repaired bomb crater parametric analyses to determine the optimum pressure limit commands for landing impact and rollout.

Determine the logic required to effect transition from the landing impact operational mode to the landing rollout mode if further study indicates that the optimum pressure for one mode differs from that of the other.

6.1.2.2. Redundancy Management Analysis

Develop a redundancy management model and determine the degree of redundancy required to achieve the desired reliability.

Conduct simulated landing impact and rollout analyses and introduce various failures to determine the effectiveness of the failure detection scheme.

6.1.2.3 A-10 Aircraft Taxi Analysis

Incorporate the ACLG model and the A-10 dynamic characteristics into the airplane taxi model

Make computer runs to simulate the following:

Landing impact
Rollout over repaired bomb craters
Takeoff over repaired bomb craters

6.1.3 Three Stage Servovalve Design and Development

6.1.3.1 Servovalve Detailed Sizing Analysis

Conduct detailed sizing analysis to determine the design requirements for the two stage servovalve and the third stage valve.

6.1.3.2 Three Stage Servovalve Design and Development

Design and manufacture the third stage valve.

Assemble the three stage servovalve package and conduct design verification tests.

6.1.4 Nose and Main ACLG Design and Fabrication

Prepare a layout showing the installation of the system into the strut. (See Figure 6-2.)

Prepare detailed drawings for the third stage valve, the strut cylinder, the gas/oil piston and the head-end of the metering tube.

Manufacture the above mentioned hardware.

Assemble the landing gears with the ACLG hardware and conduct acceptance tests.

6.1.5 Electronic Controller Design and Development

Design, manufacture, assemble and test the electronic controller.

Develop the software for the microprocessor in the controller.

6.1.6 ACLG Drop Tests

Prepare a drop test procedure.

Conduct drop test on the nose and main ACLG systems to verify their performance.

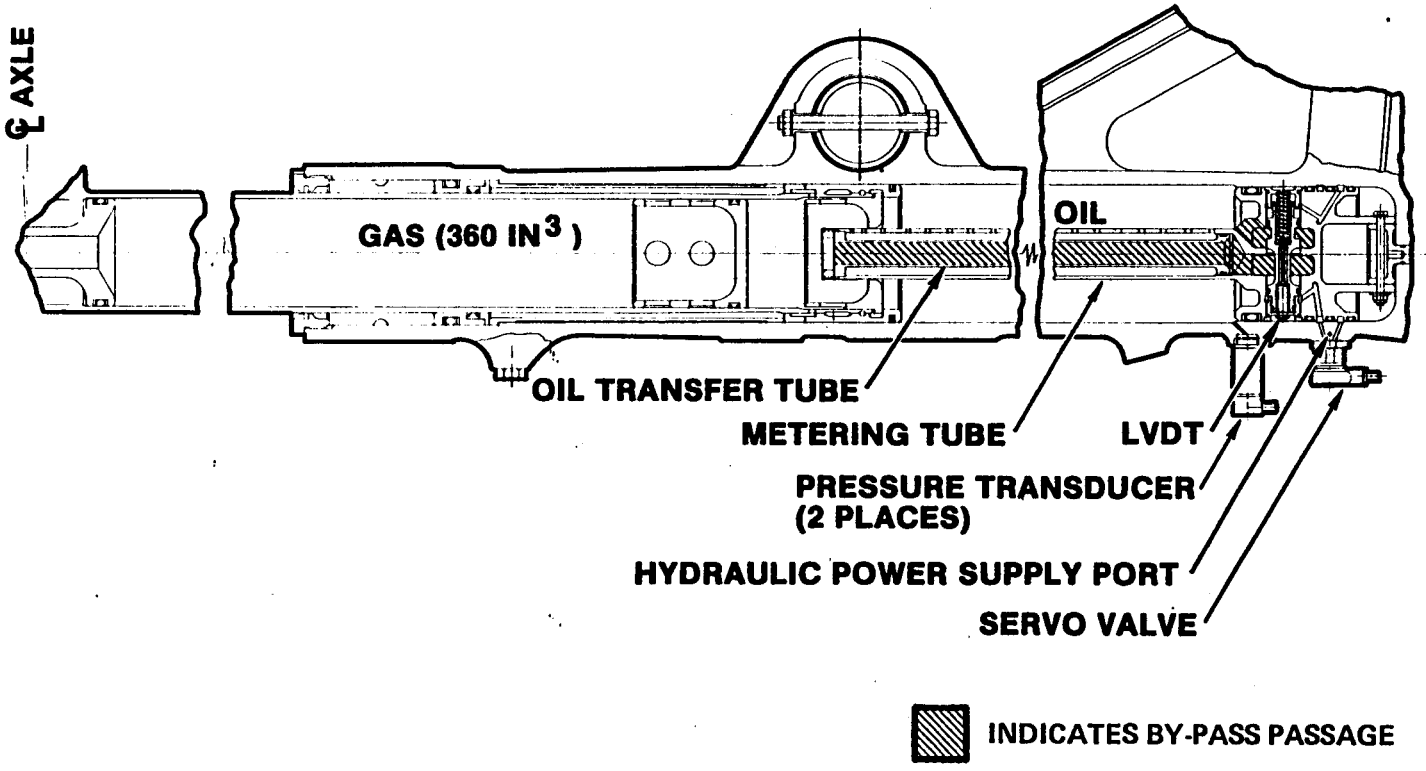

FIGURE 6-2. ACTIVE LANDING GEAR (ALTERNATE CONCEPT)

6.1.7 ACLG Shaker Test

Prepare a shaker test procedure.

Conduct shaker tests on the nose and main ACLG systems inputing step and sinusodial force inputs.

6.1.8 Simulated Taxi Tests

Install the ACLG hardware in the A-10 aircraft.

With the aircraft mounted on the AGILE test fixture run simulated takeoff and landing tests.

6.1.9 A-10 Aircraft Taxi Test

With the nose and main ACLG systems installed on the A-10 aircraft run the have bounce test.

6.2 Schedule

The program schedule to accomplish the Paragraph 6.0 statement of work is shown in Figure 6-3. All effort encompasses a 24 month period of time including formal documentation.

FIGURE 6-3 A-10 ACLG PROGRAM SCHEDULE

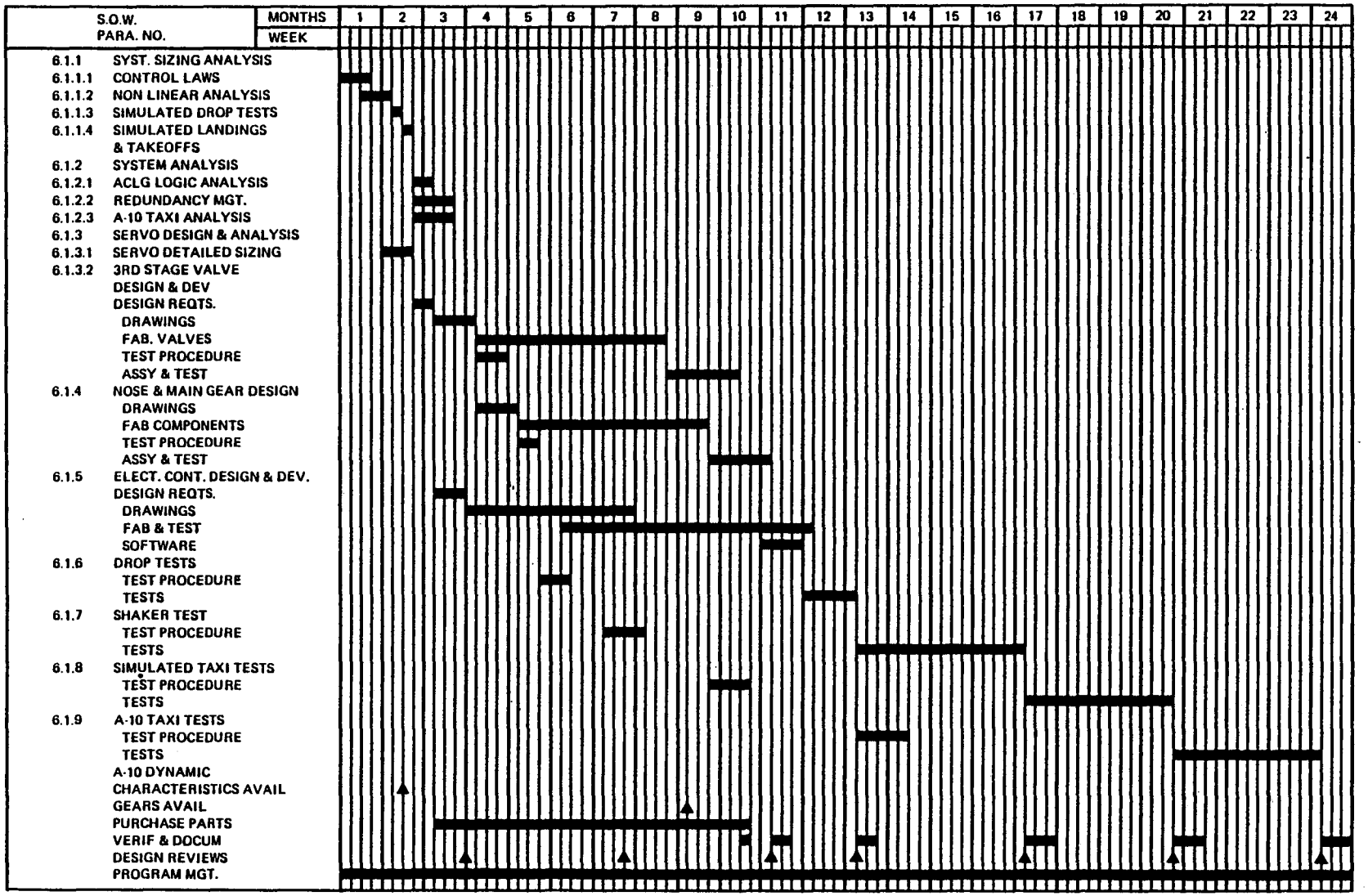

7.0 CONCLUSIONS

System sizing and dynamic performance analyses have been conducted on two concepts of an active control landing gear and applied to the A-10 aircraft. Servocontrol loops and signal shaping have been defined. The results of the analysis show that the active control landing gear can significantly reduce the loads transmitted to the aircraft for both landing impact cases and rollout over irregular runways. For the landing impact cases analyzed, the original concept reduced the peak forces by 32% and the alternate concept reduced them by 12%. In the case of the alternate concept the performance can probably be improved by scheduling the command pressure as a function of sink speed. For the case of rollout over a repaired bomb crater, the original concept reduced the peak forces by 43% and the alternate concept achieved a 36% reduction.

It can be concluded that both concepts are effective in reducing the peak loads for landing impact and rollout over runway irregularities. However, the alternate concept appears to be a much more practical implementation since it is simpler, smaller, lighter, less expensive and less demanding on the aircraft hydraulic system. The alternate concept can be implemented with no impact on the aircraft's aerodynamic and mission performance, and minimal impact on the aircraft's reliability and maintainability.

A program plan, statement of work, and schedule were developed for implementing the alternate concept nose and main active control landing gear system on the A-10 aircraft. The implementation program can be accomplished in 24 months.

8.0 REFERENCES

1. McGehee, John R. and Carden, Huey D.: A Mathematical Model of an Active Control Landing Gear for Load Control During Impact and Rollout. NASA TN D-8080, Feb., 1976.

2. Ross, Irving and Edson, Ralph: An Electronic Control for an Electrohydraulic Active Control Aircraft Landing Gear. NASA Contractor Report 3113, April, 1979.

3. Ross, Irving and Edson, Ralph: An Electronic Control for an Electrohydraulic Active Control Landing Gear for the F-4 Aircraft. NASA Contractor Report 3552, April, 1982.

1. Report No.	2. Government Accession No.	3. Recipient's Catalog No.
NASA 166104		

4. Title and Subtitle	5. Report Date
APPLICATION OF ACTIVE CONTROL LANDING GEAR TECHNOLOGY TO THE A-10 AIRCRAFT	June 1983
	6. Performing Organization Code

7. Author(s)	8. Performing Organization Report No.
Irving Ross & Ralph Edson	
	10. Work Unit No.

9. Performing Organization Name and Address	11. Contract or Grant No.
HR Textron Inc. 25200 W. Rye Canyon Road Valencia, CA 91355	NAS1-17068
	13. Type of Report and Period Covered
12. Sponsoring Agency Name and Address	Contractor Report
National Aeronautics and Space Administration Washington, D.C. 20546	14. Sponsoring Agency Code

15. Supplementary Notes

Langley Technical Monitor: John R. McGehee
Final Report

16. Abstract

HR Textron Inc., under NASA Contract NAS1-17068, has defined control laws and system gains for the application of an active control landing gear to the A-10 aircraft. Two different concepts are presented. One concept, called the Original Concept, reduces the wing/gear force by 32% on landing impact and by 43% on rollout over a Class E repaired bomb crater. The other concept, called the Alternate Concept, reduces the wing/gear force by 12% on landing impact and by 39% on rollout over a similar repaired bomb crater.

17. Key Words (Suggested by Author(s))	18. Distribution Statement
Aircraft Landing Gear Electronic Controls Active Controls Impact Loads	Unclassified - Unlimited

19. Security Classif. (of this report)	20. Security Classif. (of this page)	21. No. of Pages	22. Price
Unclassified	Unclassified	122	

For sale by the National Technical Information Service, Springfield, Virginia 22161

End of Document